

**The Transient Liquid
Phase Sintering of
Aluminium Based Alloys**

By

Roger Lumley

The following is the PhD thesis of the author, produced in its final format in February 1998 at the University of Queensland, Australia. Four copies were originally produced. Wherever possible, the same images have been used as in the original text, or have been redrawn for digital reproduction. Micrographs have been scanned from the original grayscale photographs. Where use of the original image has not been possible, details are included as footnotes. The reader is advised that this manuscript is as close as possible to the original publication, and, as a result, literature in this field published after February 1998 is not reviewed, discussed or included. For subsequent information on the topic of this manuscript, the reader is directed to publications citing the papers associated with this thesis.

Table of Contents

	Page
Table of Contents	3
List of Associated Publications	9
Abstract	10
Chapter 1. Introduction	11
Chapter 2. Literature Review	13
<i>2.1 Introduction</i>	13
<i>2.2 Powder Characterisation</i>	13
<i>2.3 Powder Fabrication</i>	13
<i>2.4 Powder Compaction</i>	15
<i>2.4.1 Uniaxial Compaction</i>	15
<i>2.5 Sintering</i>	16
<i>2.5.1 Sintering in the Absence of a Liquid Phase</i>	17
<i>2.5.2 Sintering in the Presence of a Liquid Phase</i>	18
<i>2.5.3 Primary Mechanisms of Liquid Phase Sintering - Rearrangement and Shape Change</i>	21
<i>2.5.3.1 Primary Rearrangement</i>	22
<i>2.5.3.2 Secondary Rearrangement</i>	22
<i>2.5.3.2(a) Contact Flattening</i>	23
<i>2.5.3.2(b) Ostwald Ripening</i>	24
<i>2.5.3.2(c) Pore Elimination</i>	24

2.5.3.2(d) <i>Coalescence</i>	25
2.5.3.2(e) <i>Directional Particle Growth</i>	26
2.5.3.2(f) <i>Particle Disintegration</i>	29
2.5.3.2(g) <i>Summary of Mechanisms</i>	29
2.5.3.3 <i>Melt Penetration and Boundary Migration</i>	29
2.5.3.3(a) <i>Diffusion Induced Grain Boundary Migration</i>	31
2.5.3.3(b) <i>Liquid Film Migration</i>	32
2.5.4 <i>Supersolidus Sintering</i>	33
2.5.5 <i>Transient Liquid Phase Sintering</i>	33
2.5.5.1 <i>Non-Powder Metallurgy Utilisation of Transient Liquid Phases</i>	34
2.6 <i>The Microstructural Evolution of Liquid Phase Sintered Materials</i>	35
2.7 <i>The Sintering of Fe-Cu Compacts</i>	37
2.8 <i>Aluminium Powder Metallurgy</i>	39
2.8.1 <i>Utilisation of Aluminium Powder Metallurgy Components</i>	39
2.8.2 <i>The Sintering of Aluminium Liquid Phase Sintered Materials</i>	40
2.8.2.1 <i>Sintering of Aluminium Based on Tin Additions</i>	40
2.8.2.2 <i>Sintering of Aluminium Based on Silicon Additions</i>	41
2.8.2.3 <i>Sintering of Aluminium Based on Magnesium Additions</i>	42
2.8.2.4 <i>Sintering of Aluminium Based on Copper Additions</i>	42
2.8.2.5 <i>Sintering of Aluminium Based on Zinc Additions</i>	43
2.8.2.6 <i>Metal Matrix Composites Based on Aluminium Powder Metallurgy Alloys</i>	45
2.8.2.7 <i>The Effect and Use of Atmospheres in Liquid Phase Sintered Aluminium</i>	46
2.8.2.8 <i>The Effect and Use of Lubricants in Powder Metallurgy</i>	46
2.9 <i>Summary</i>	47

Chapter 3. Experimental Methods	48
3.1 <i>Specimen Preparation</i>	48
3.2 <i>Particle Size Effect</i>	48
3.3 <i>Effect of Composition</i>	48
3.4 <i>Sintering</i>	48
3.5 <i>Atmospheres</i>	51
3.6 <i>Characterisation Techniques</i>	52
3.7 <i>Heat Treatment</i>	54
3.8 <i>Mechanical Properties</i>	54
3.9 <i>The Effect of Gravity</i>	54
3.10 <i>The Effect of Cooling Rate</i>	54
Chapter 4. Results	55
4.1 <i>The Effect of Zn on Sintering Al</i>	55
4.2 <i>The Effect of Cu on Sintering Al</i>	56
4.3 <i>The Effect of Mg on Sintering Al</i>	56
4.3.1 <i>The Role of Mg in oxide disruption</i>	57
4.4 <i>The particle size effect in binary systems</i>	60
4.4.1 <i>Al-Zn</i>	60
4.4.2 <i>Al-Cu</i>	64
4.4.3 <i>Al-Sn</i>	67
4.4.4 <i>Fe-Cu</i>	72
4.5 <i>The particle size effect in ternary and quaternary systems</i>	75
4.6 <i>The effect of composition in ternary and quaternary alloys</i>	79

<i>4.7 The effect of gravity on Al-8Zn-2.5Mg-1Cu</i>	86
<i>4.8 The effect of cooling rate</i>	86
<i>4.9 Summary of results</i>	90
Chapter 5. Discussion	91
<i>5.1 Introduction</i>	91
<i>5.2 Isothermal solidification</i>	91
<i>5.3 Wetting</i>	95
<i>5.4 The role of Mg in the break up of the oxide layer</i>	99
<i>5.5 The sintering of Al with Mg-microstructural development and sintering events</i>	102
<i>5.6 The effect of increasing chemical additions on mechanical properties in binary alloys</i>	104
<i>5.7 The particle size effect</i>	105
<i>5.7.1 Introduction</i>	105
<i>5.7.2 Sintering mechanisms and microstructural development for Al-Zn</i>	105
<i>5.7.2(a) Fine particles</i>	105
<i>5.7.2(b) Coarse particles</i>	106
<i>5.7.3 Sintering mechanisms and microstructural development for Al-Cu</i>	107
<i>5.7.3(a) Fine particles</i>	107
<i>5.7.3(b) Coarse particles</i>	107
<i>5.7.4 Sintering mechanisms and microstructural development for Fe-Cu</i>	111
<i>5.7.4(a) Fine particles</i>	111
<i>5.7.4(b) Coarse particles</i>	111

5.7.5	<i>Sintering mechanisms and microstructural development for Al-Sn</i>	111
5.7.6	<i>The relationship between solubility and particle size</i>	112
5.7.7	<i>The effect of additive particle size on mechanical properties (Al-4Cu)</i>	113
5.7.8	<i>Summary of the particle size effect in binary systems</i>	114
5.8	<i>The role of ternary additions of Mg and Cu on the particle size effect</i>	115
5.8.1	<i>Microstructural evolution and sintering mechanisms</i>	115
5.8.1.1	<i>Sintering mechanisms and microstructural development for Al-8Zn-2Mg</i>	115
5.8.1.2	<i>Sintering mechanisms and microstructural development for Al-8Zn-1Cu</i>	115
5.8.1.3	<i>Sintering mechanisms and microstructural development for Al-8Zn-3Cu</i>	116
5.8.1.4	<i>Sintering mechanisms and microstructural development for Al-4.5Cu-1.6Mg</i>	116
5.8.2	<i>Summary of Ternary Sintering Systems</i>	117
5.9	<i>The particle size effect in quaternary Al-8Zn-2.5Mg-1Cu</i>	117
5.9.1	<i>Microstructural evolution and sintering mechanisms for quaternary AlZnMgCu</i>	117
5.9.1.1	<i>The transient stage of the sintering cycle</i>	118
5.9.1.1(a)	<i>Fine additive zinc particles</i>	118
5.9.1.1(b)	<i>Coarse additive zinc particles</i>	118
5.9.1.1(c)	<i>Analysis of the transient stage of the sintering cycle</i>	119
5.9.1.2	<i>The persistent stage of the sintering cycle</i>	119
5.9.1.3	<i>The role of additive particle size ranges in Al-8Zn-2.5Mg-1Cu</i>	123
5.10	<i>Effect of composition in quaternary Al-8Zn-xMg-yCu alloys</i>	123
5.10.1	<i>The role of increasing additions of Mg</i>	123
5.10.2	<i>The role of increasing additions of Cu</i>	124

<i>5.10.3 The combined role of additions of Mg and Cu</i>	124
<i>5.11 The influence of gravity on quaternary Al-8Zn-2.5Mg-1Cu</i>	125
<i>5.12 The effect of slow cooling</i>	126
Chapter 6. Conclusion	127
Chapter 7. References	130

Associated Publications

1. R.N. Lumley and G.B Schaffer, The Effect of Solubility and Particle Size on Liquid Phase Sintering, , Scripta Materialia, Vol.35, #5, pp.589-595, 1996
2. R.N. Lumley and G.B Schaffer, The Particle Size Effect in Multicomponent Aluminium Alloys, Advances in Powder Metallurgy and Particulate Materials, Proceedings 1996 World Congress on Powder Metallurgy and Particulate Materials, MPIF, Vol.11, pp.185-196, 1996.
3. R.N. Lumley and G.B Schaffer, The Effect of Additive Particle Size on the Mechanical Properties of Sintered Aluminium-Copper alloys, Scripta Materialia, 39, (8), 1089-1094, 1998.
4. R.N. Lumley and G.B Schaffer, Anomalous Pore Morphologies in Liquid Phase Sintered Al-Zn Alloys, Metallurgical and Materials Transactions A, 30A, (6), 1682-1685, 1999.
5. R.N Lumley, T.B Sercombe and G.B Schaffer, Surface Oxide and the role of Magnesium During the Sintering of Aluminium, Metallurgical and Materials Transactions A, 30A, (2), 457-463, 1999.
6. G.B. Schaffer, T.B. Sercombe, R.N. Lumley, and S.H. Huo, Trace Element Effects in the Sintering of Aluminium Alloys, Proceedings of the Powder Metallurgy Aluminium and Light Alloys for Automotive Applications Conference, USA, p.11-18, 1998.
7. G.B. Schaffer, T.B. Sercombe, R.N. Lumley, and S.H. Huo, On the Design of Sintered Aluminium Alloys, Proceedings of the Powder Metallurgy Aluminium and Light Alloys for Automotive Applications Conference, USA, p.43-50, 1998.
8. G.B. Schaffer, T.B. Sercombe and R.N. Lumley Liquid Phase Sintering of Aluminium Alloys, Materials Chemistry and Physics, 67, pp.85-91., 2001.
9. R.N. Lumley and G.B. Schaffer, Precipitation Induced Densification in a Sintered Al-Zn-Mg-Cu alloy, Scripta Materialia, 55, pp.207-210, 2006.

Abstract

The aim of this thesis was to investigate the effect of composition and selected process variables on the sintering of aluminium alloys. The effect of additive particle size in binary, ternary and quaternary alloys containing zinc, copper and magnesium has been analysed. Aluminium alloys based on these systems were either fully or partially transient liquid phase sintering systems. Binary systems were compared to a fully persistent (Al-Sn) system and to a non-aluminium transient system (Fe-Cu). In systems having a transient aspect to sintering, a moderate to coarse additive particle size is beneficial to the sintering process. However, a very coarse particle size is detrimental to the sintered properties and an intermediate particle size is preferred. Additionally, a fine additive particle size and a very high heating rate resulted in optimisation of sintered properties.

Magnesium plays a critical role in the disruption of the alumina layer present on all aluminium particles. This occurs due to the solid state (partial) reduction of the alumina to spinel. However, Mg is generally deleterious to the sintering of Al at higher concentrations. This is due to the linearly decreasing densification (expansion) with Mg additions and the increased diffusivity of Zn in Al where Mg is present.

The phenomenon of isothermal solidification has been proposed as a mechanism of bonding in transient liquid phase sintering. The effect of gravity and of cooling rates have been studied and characterised. Microstructures which form in zinc containing systems have some similar characteristics to those reported to form under microgravity conditions in the W-Ni system. This is due to the relatively high vapour pressure of zinc at the sintering temperature.

In higher order alloys containing copper, there is an improved sintering response due to enhanced liquid flow and improved wetting. The means by which liquid phases wet aluminium surfaces in the absence of a reducing agent has been examined and a mechanism proposed. The wetting of aluminium appears to be governed by the solubility of the base in the liquid phase, the solubility of the additive elements in the base and the diffusivity of the additive in the base.

Chapter 1. Introduction

The sintering of particulate materials is a widely used industrial process. A common characteristic of all forms of sintering is atomic motion at elevated temperature resulting in the formation of interparticle bonds. During liquid phase sintering a liquid (additive) co-exists with a solid (base) phase. This liquid phase enhances mass transfer which results in an improved sintering response and increased material strength. During sintering, the alloying elements form a liquid phase and this flows between the matrix particles, filling voids and promoting densification. If the additive phase has appreciable solubility in the base, the liquid is subsequently absorbed into the matrix. This is termed transient liquid phase sintering.

The properties of sintered aluminium materials are often poor. Current commercial (sintered) aluminium powder metallurgy (P/M) alloys are those based on the 6061 and 2041 wrought alloys, being elemental powder blends of Al-Mg-Si-Cu and Al-Cu-Mg-Si respectively. These alloys attain maximum strengths of approximately 75% of their wrought equivalents. 7xxx series alloys based on additions of Zn, Mg and Cu have previously been available commercially, but have since been discontinued due to the inconsistent and often poor properties developed (usually <50% of their wrought equivalents). Since the compositions of Al P/M alloys are usually based on wrought alloys, their alloying additions may not be entirely appropriate for sintering processes. Because many of the aluminium systems have a transient aspect to the sintering cycle, the materials are highly process sensitive.

One of the greatest problems with aluminium powders is the stable oxide phase present, and its inability to be easily reduced during sintering. These limitations have largely limited the utilisation of Al P/M alloys by industry. However, new applications may result if adequate properties could be developed for aluminium based alloys. Currently the majority of P/M components manufactured by press and sinter operations are ferrous. If appropriate aluminium alloys were developed, these could replace many of the parts currently manufactured from iron. Alloys based on the high strength 7000 series (Al-Zn-Mg-Cu) offer the opportunity to fulfil these criteria, if the processing variables can be optimised.

The aim of this project was to investigate the sintering of aluminium based alloys with additions of zinc, magnesium, and copper, singularly and in combination. This includes the effect of additive particle size, mutual solid solubility, and diffusivity on the predominant mechanisms of sintering in non-ideal systems and their comparison to other ideal (Al-Sn) and non-ideal (Fe-Cu) systems. Also examined is the effect of varying additive composition, heating rate, cooling rate and the role of gravity on dimensional stability. A crucial aspect of this study is understanding how liquid phases are able to wet aluminium particles in the presence of an oxide phase.

In the following chapter the literature relevant to this work will be critically reviewed (Chapter 2). The experimental methods employed during this research are presented in Chapter 3, followed by the results of this work (Chapter 4) and a discussion of the results (Chapter 5). Chapter 6 presents conclusions drawn from the findings of this thesis.

Chapter 2 Literature Review

2.1 Introduction

Powder metallurgy (P/M) is a processing approach which gives component producers the ability to fabricate novel materials or complex parts with close tolerances⁽¹⁾. This makes it an attractive process by which parts can be made economically in large volumes. The steps involved in transforming powders into consolidated products can be viewed from either a technological or scientific perspective and the great versatility of these methods allows novel solutions to processing and fabrication problems⁽¹⁾.

In essence, P/M takes metal powders of one or more elements with specific characteristics, converting them into a strong, precise high performance part⁽¹⁾. The applications of P/M are extensive. Areas as diverse as supercorroding materials, medical and automotive components are but a few of the realisations of P/M processing. Other uses of metal powders include applications in pyrotechnics, paint and food additives.

This literature review summarises the sintering of particulate materials, in particular the mass transport mechanisms involved and evaluates prior research in sintering science with specific reference to aluminium alloy systems. Aspects discussed include powder characterisation, sintering with and without a liquid phase, mass transport mechanisms and the driving forces involved. The microstructural development of liquid phase sintered alloys is also reviewed.

2.2 Powder Characteristics

The nature of the powders directly influences the forming procedures, the sintering treatments and the behaviour of the final component in service. The characteristics important to part fabrication and microstructural concerns are generally considered to be:

- 1) particle size and size distribution,
- 2) particle shape and variation with size,
- 3) surface characteristics (area, chemistry, etc.),
- 4) interparticle friction (during compaction),
- 5) flow and packing,
- 6) particle microstructure, and
- 7) composition, homogeneity and contamination.

Most of these factors are a function of the method of fabrication and post fabrication treatments. Typical particle shapes and qualitative descriptors are given in Figure 2.1.

2.3 Powder Fabrication

Knowing how powders are made is a good basis for understanding their characteristics. The method chosen for fabrication of a powder depends largely on the specific

properties of the material⁽¹⁾. The formation of a particulate material involves the application of energy to a material to create a new morphology with a greatly increased surface area⁽¹⁾. The selection of any fabrication method depends on understanding the process, its economics, the resulting powder characteristics and how those characteristics match the intended application. Detailed explanations of particulate fabrication methods are discussed thoroughly in several texts⁽¹⁻⁴⁾. Fabrication methods are summarised in Figure 2.2.

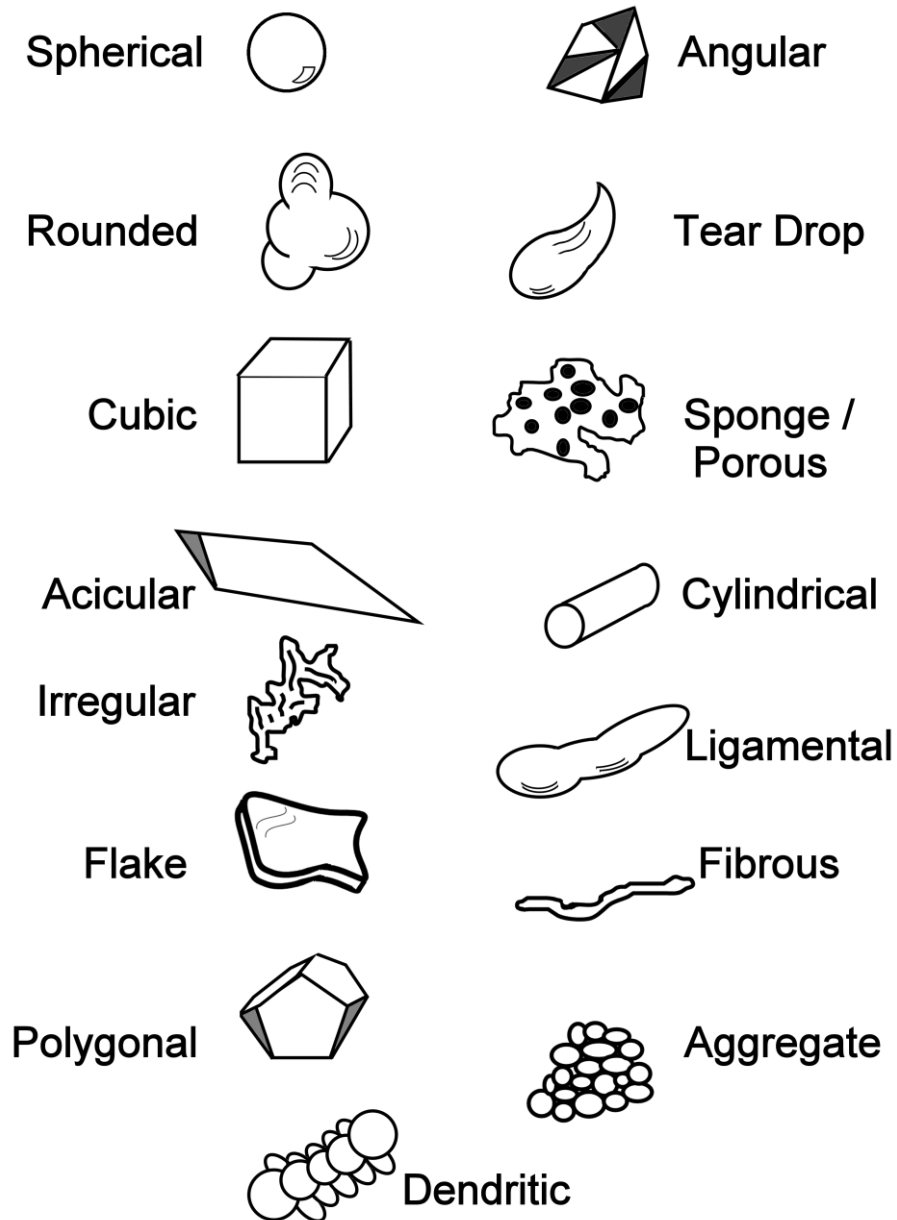


Figure 2.1 A collection of possible particle shapes and the suggested qualitative descriptors. After German⁽¹⁾.

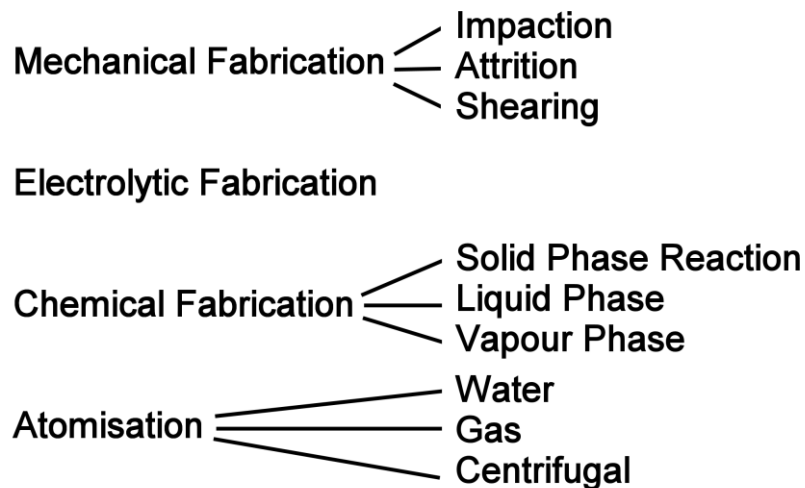


Figure 2.2. Methods of powder fabrication.

2.4 Powder Compaction

Compactibility and compressibility are terms which describe the ability of a powder body to be densified by the application of pressure alone⁽²⁾. Powder compaction is the first step in shaping and imparting specific properties to metal powder bodies⁽¹⁾. Due to a non-uniform response to applied pressure there are usually density gradients in the green part. This response is due primarily to the starting powder characteristics (section 2.2, 2.3) and additives such as lubricants and binders⁽²⁾. Lubrication is used to assist the ejection of the compact from the die. Two types of lubrication are commonly employed: the first method is to mix a dry lubricant with the loose powders, the second method is to lubricate the die walls⁽²⁾. Lubricants are discussed further in section 2.8.2.8. The pressure that is applied during compaction can be generated in either a continuous (powder extrusion) or discontinuous (die compaction) manner. Compaction methods are well reviewed in several texts⁽¹⁻⁵⁾, and only uniaxial compaction which is relevant to press and sinter operations is discussed further.

2.4.1 Uniaxial Compaction

Uniaxial compaction is generally employed in press and sinter operations^(1,3,5). When pressure is transmitted from only one punch, the process is known as single action pressing. Most compaction is performed using both an upper and lower punch with a floating die and is known as double action pressing. Double action pressing results in improved uniformity of density in a compact^(1,5) and results in improved uniformity of sintered bodies^(1,3). An increase in compaction pressure will generally result in an increase in green density. There is a logarithmic relationship^(2,3,6) between green density and compaction pressure, as shown in Figure 2.3.

The green density of a powder compact directly influences the sintered density and the dimensional change often decreases as green density increases⁽¹⁾. Optimum compaction pressures ideally should be as high as possible without being detrimental to the shape, dimensions and density of the processed part^(7,8,9).

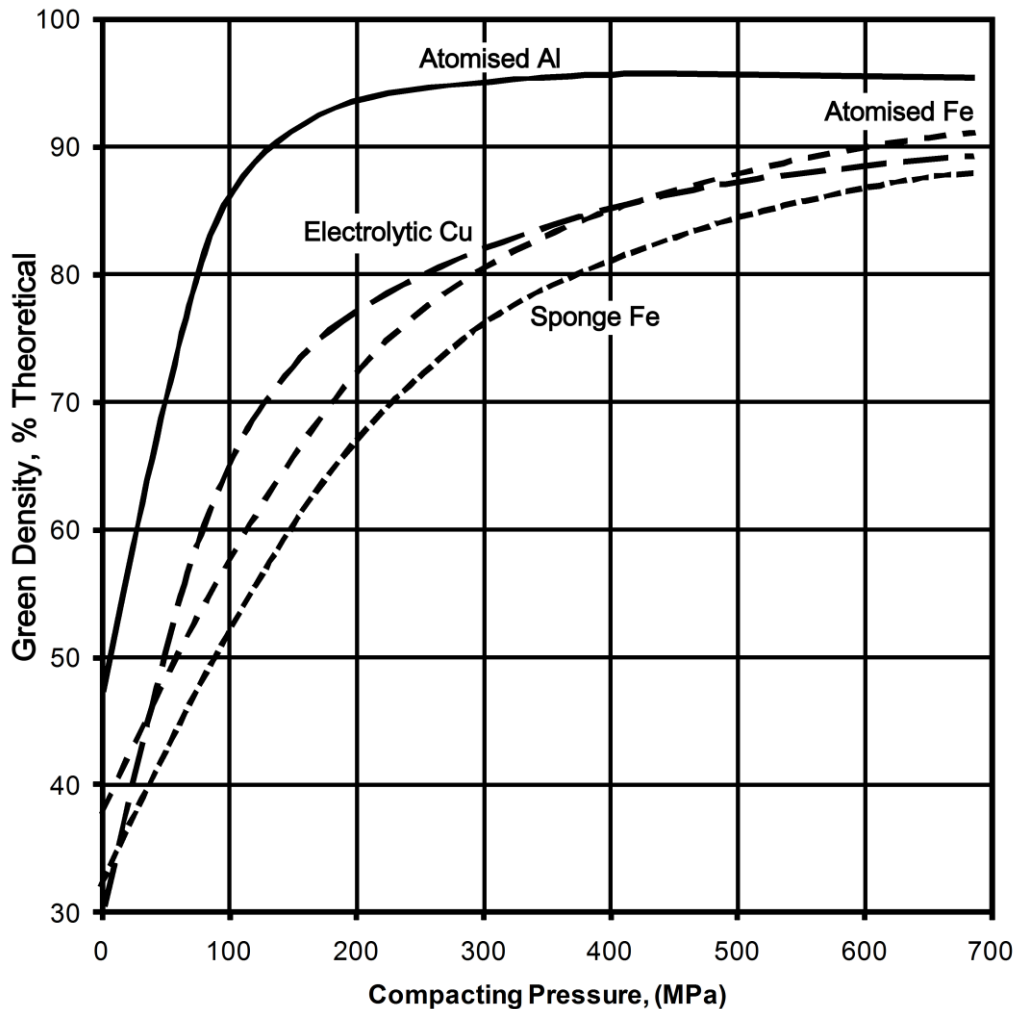


Figure 2.3 Typical plots of green density (as a percentage of theoretical) vs. compaction pressure for different metal powders (adapted from Metals Handbook, Vol.7⁽²⁾).

2.5 Sintering

Parts that are not thermally treated are termed green; once they have undergone thermal treatment they are considered sintered. Sintering processes are commonly divided into pressureless and high pressure sintering. High pressure sintering uses a combination of temperature, stress and strain to densify powder compacts, and parts fabricated in these ways often require secondary processing (ie. machining). Common methods are hot pressing, HIPing, hot forging and hot extrusion. Pressureless sintering involves three primary forms of mass transport, these being vapour phase, solid state and liquid phase sintering. Sintering can occur by one or more of these mass transport methods. The three primary methods can be divided further, (ie. Figure 2.4).

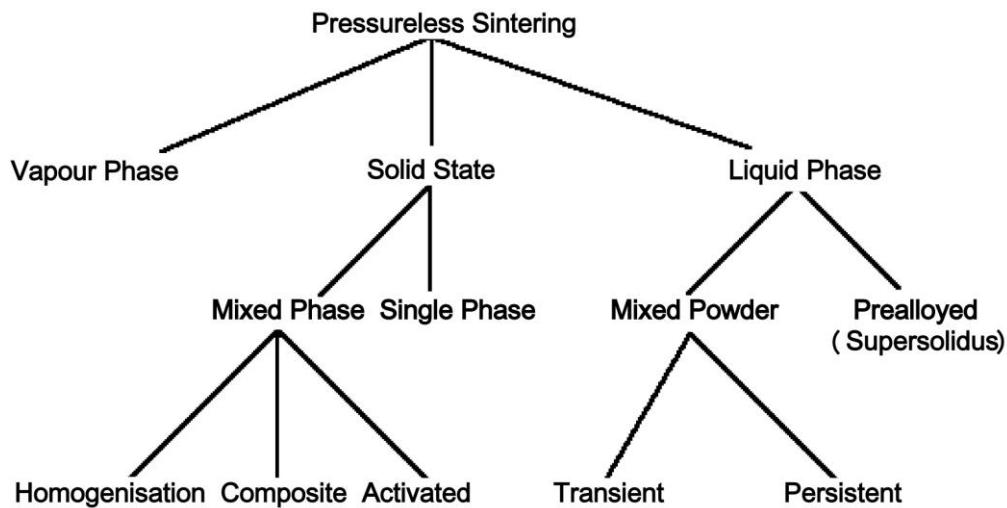


Figure 2.4 Types of pressureless sintering. (Adapted from German⁽⁹⁾).

Although solid state sintering is better documented and widely used, liquid phase sintering (l.p.s) has greater widescale practical use due to high final component densities and strengths⁽¹⁰⁾.

The aim of sintering particulate compacts is primarily to bond particles and secondly to increase compact density. The driving force for sintering is governed by surface energy or chemical potential^(10,11). The mechanisms of mass transport causing densification are all that differs between the various sintering processes.

2.5.1 Sintering in the Absence of a Liquid Phase

Sintering without a liquid phase is limited to mass transport by the vapour phase or by various types of solid state diffusion. These are summarised in Table 2.1 and Figure 2.5. Vapour phase transport alters the shape of pores present and achieves bonding between particles and thus increases material strength and decreases permeability due to open porosity. The material transport (sintering) mechanism is evaporation from the surface or source of matter (having a positive radius of curvature) followed by condensation of material in regions having a negative radius of curvature (necks)⁽¹²⁾ and reduced vapour pressure. Sintering using a vapour phase is important only when the vapour pressure of the condensing matter is sufficiently high, and has been confirmed as the material transport mechanism in the sintering of NaCl⁽¹³⁾. For micron range particles, the minimum vapour pressure required for sintering is of the order of 1 to 10 Pa.

Solid state sintering involves material transport by diffusional means where atoms or vacancies move through the material⁽¹⁴⁾. Material is transported by the most thermodynamically favourable route or routes⁽¹²⁾ in local regions. These diffusional events may result in shrinkage due to the centre to centre approach of adjacent particles,

which is driven by the differences in free energy or chemical potential between the surfaces of particles and points of contact. Densification via the solid state is described by the following relationship⁽¹⁴⁾,

$$\Delta L/L_0 = (K\gamma a^3 D^* t/kTd^n)^m \quad (2.1)$$

where ΔL is the change in length of the specimen, L_0 the initial length, K a geometric constant, γ is surface energy, a^3 the atomic volume of the diffusing vacancy, D^* the self diffusion coefficient, k the Boltzmann constant, T the temperature, t the time, d the average particle size, and m and n are empirically determined constants, being generally in the range of 0.3 to 0.5, and close to 3, respectively. Solid state sintering and shrinkage rates increase with increasing temperature and decreasing particle radius, and decrease with time. Also, finer powders can be sintered more rapidly at lower temperatures than coarse powders. Particle morphology and size distribution also play a vital role.

Table 2.1 Alternate paths for mass transport during the initial stages of sintering. (After Kingery *et. al.*⁽¹²⁾)

Mechanism Number	Transport Path	Source of Matter	Sink of Matter
1	Surface diffusion	Surface	Neck
2	Lattice diffusion	Surface	Neck
3	Vapour transport	Surface	Neck
4	Boundary diffusion	Grain Boundary	Neck
5	Lattice diffusion	Grain Boundary	Neck
6	Lattice diffusion	Dislocations	Neck

2.5.2 Sintering in the Presence of a Liquid Phase

Price *et al.*⁽¹⁵⁾ first reported liquid phase sintering of metals in 1938 for the W-Cu-Ni system. Since this time, extensive use has been made of the technology associated with liquid phase sintering in powder metallurgy. Liquid phase sintering occurs when a liquid component flows among original particles causing mass transfer. Additive components must have exceeded their melting or eutectic temperature, or have undergone an exothermic reaction raising internal temperature high enough to form a localised melt⁽¹⁶⁾.

Sintering in the presence of a liquid phase can be explained in terms of an idealised phase diagram (see Figure 2.6)⁽¹⁷⁾. When a powder mixture of components A and B (where A is the additive and B the base) is heated, diffusional events between particulate components occur. B dissolves readily in A, but (ideally) little or no A dissolves in B. When the local composition reaches or exceeds the solidus, a degree of melting occurs and the liquid rapidly dissolves more solid (B). The liquid eventually reaches the equilibrium composition c_L , and the excess solid phase (composition c_β) reprecipitates

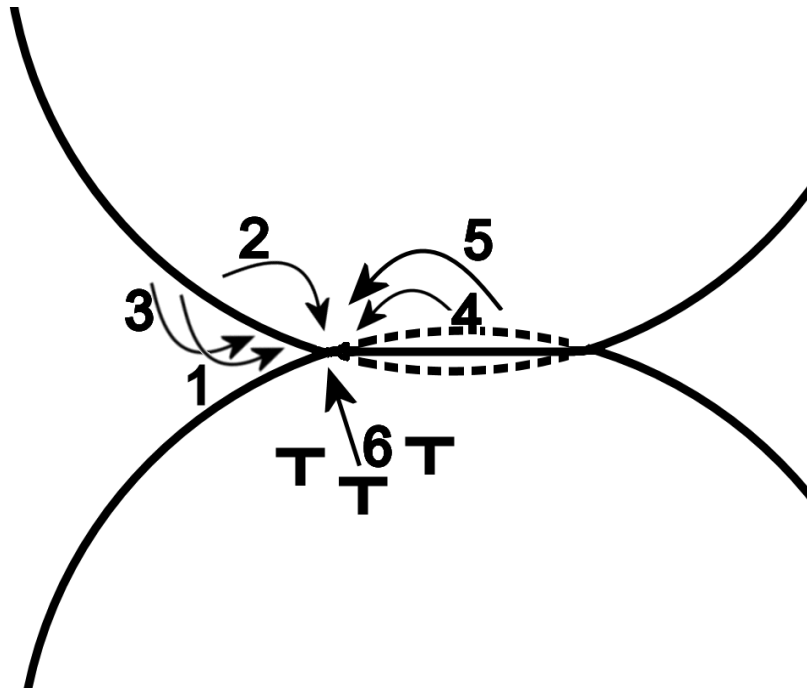


Figure 2.5 Alternate paths for matter transport during the initial stages of sintering⁽¹²⁾. See Table 2.1 for details.

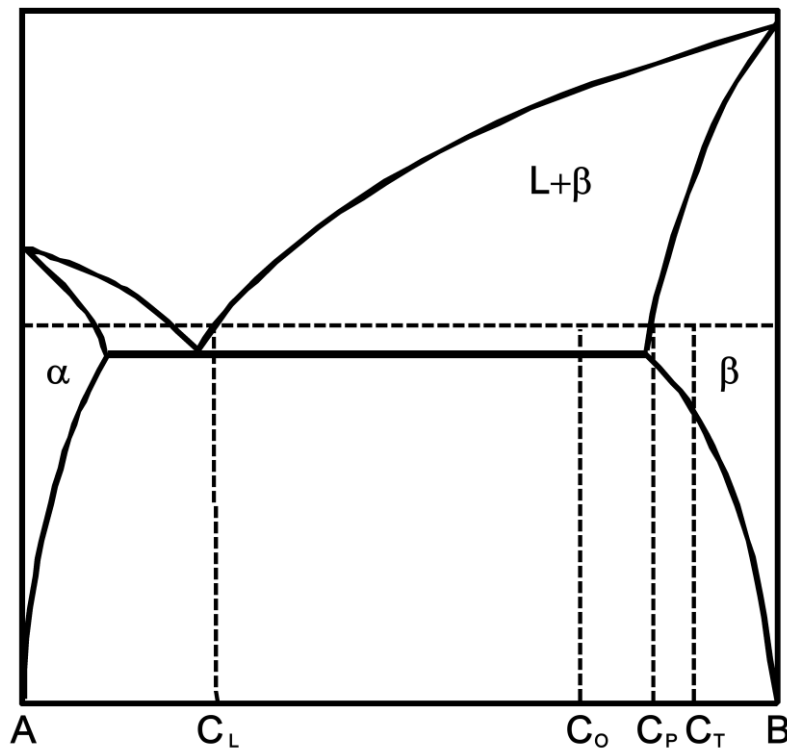


Figure 2.6 The phase diagram of a typical liquid phase sintering system. c_o =nominal composition of alloy, c_L =equilibrium composition of liquid phase. c_β =equilibrium composition of solid phase, c_T is the nominal composition of a transient system, and T_s is the sintering temperature. After Huppmann⁽¹⁷⁾.

forming solid solution β . In persistent liquid phase sintering this reprecipitation is maintained after the equilibrium condition is reached. In transient liquid phase sintering, the equilibrium composition is c_T and hence the liquid phase disappears as the bulk material approaches c_T .

When a liquid phase forms during sintering, there are at least three thermodynamic phases (with corresponding interfaces) present: liquid, solid and vapour. The wetting characteristics describe the equilibrium associated with the three phases⁽¹⁸⁾. A high wettability promotes good liquid phase sintering. Analysis of the equilibrium interfacial free energy ratios is described in several texts^(9,19) and the factors important for good liquid phase sintering correspond with those for a high degree of wetting. The degree of wetting is characterised by the contact angle shown in Figure 2.7, which is wholly dependent on the interfacial energies associated with the solid-liquid, solid-vapour and liquid-vapour interfacial regions. Hence if the contact angle, θ , is low, the flow of the liquid phase should be extensive. The horizontal components of the relative vectors must equal zero for the triple point of solid-liquid-vapour to be in thermodynamic equilibrium. The balance of interfacial free energies for three phases in equilibrium in the absence of interfacial torques (Figure 2.8) is given by the Dupre' equation, ie.

$$\gamma_{23}/\sin\Omega_1 = \gamma_{13}/\sin\Omega_2 = \gamma_{12}/\sin\Omega_3 \quad (2.2)$$

where γ_{xy} represents the phase boundary free energy between phases x and y, and $\Omega_1, \Omega_2, \Omega_3$ are the dihedral angles measured in phases 1, 2 and 3 respectively. Ω and θ are equivalent when phase 1 is vapour, phase 2 is liquid and phase 3 is solid. Equilibrium interfacial free energy ratios for interphase interface equilibria are then obtained as simple ratios of the dihedral angles. For a two phase system where one component is a liquid such as that present in liquid phase sintering systems, the interphase boundaries will generally form symmetrical configurations, ie.

$$\gamma_{11}/\gamma_{12} = 2\cos(\Omega_2/2) \quad (2.3)$$

and γ_{11} is any interface between two identical solids. If the interphase boundary free energy is greater than γ_{11} , the dihedral angle θ_2 will be positive. Since $\gamma_{12} < \gamma_{11}$, there is no value of θ_2 that can satisfy the equation, and the second phase (liquid) will wet the boundary and spread along the interface^(18,19). Also if $\gamma_{11} = \gamma_{12}$ then $\theta_2 = 120^\circ$, and if $\gamma_{12} > \gamma_{11}$, then $\theta_2 > 120^\circ$.

For all materials the contact angle is largely dependent upon surface characteristics. A pure metal surface with no impurities present (eg. oxide films) should be easily wet by another metal which is soluble in the first. However, due to the (oxidised) nature of most metal surfaces, the wetting is often poor. Altering surface characteristics, namely via the vapour phase, can greatly alter the dynamics of the situation. Examples of

materials sintered in oxidising and reducing atmospheres are shown in Figure 2.9⁽²⁰⁾. The differences are dramatic. It is considered good sintering practice to use reducing atmospheres and exclude oxidising atmospheres where possible.

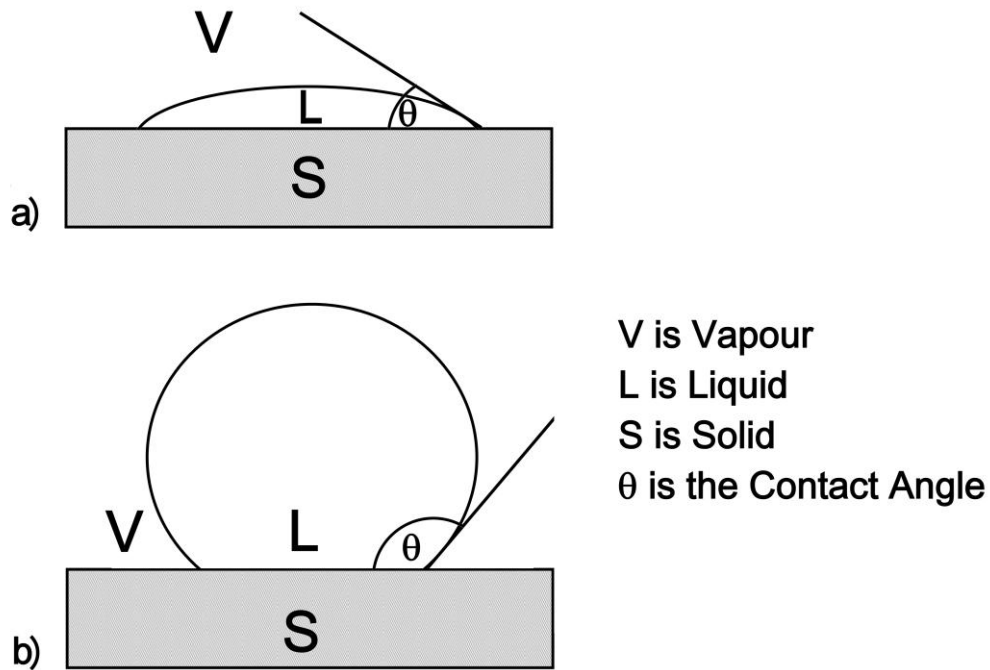


Figure 2.7 The solid-liquid-vapour equilibrium for (a) good wetting and (b) poor wetting. After German⁽⁹⁾.

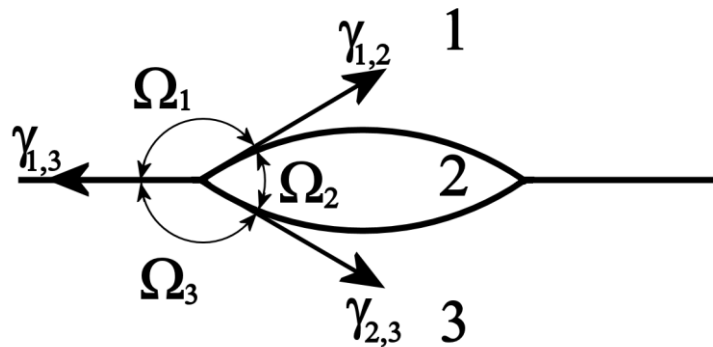


Figure 2.8 Interfacial free energy balance. Phases 1,2,3 may be any of solid, liquid or vapour. $\gamma_{x,y}$ represents the phase boundary free energy between phases x and y, and the Ω terms are the dihedral contact angles. After Murr⁽¹⁹⁾.

2.5.3 Primary Mechanisms of Liquid Phase Sintering- Rearrangement and Shape Change

The major mechanism of densification (shrinkage) during liquid phase sintering is based on the rearrangement and shape change of the solid particles⁽¹⁰⁾. Gravity induced viscous flow can also play a role in microstructural development⁽²¹⁾. The morphological

alterations in liquid phase sintering, while occurring due to essentially the same thermodynamic driving force as for solid state sintering, involve different mechanisms occurring on different time scales⁽¹⁰⁾. Rearrangement is divided into primary and secondary rearrangement and is extremely important to effective densification. The two types are generally distinguished on the basis of rate. Shrinkage due to the shape change of the solid always involves solution-precipitation processes and is therefore associated with secondary rearrangement⁽¹¹⁾.

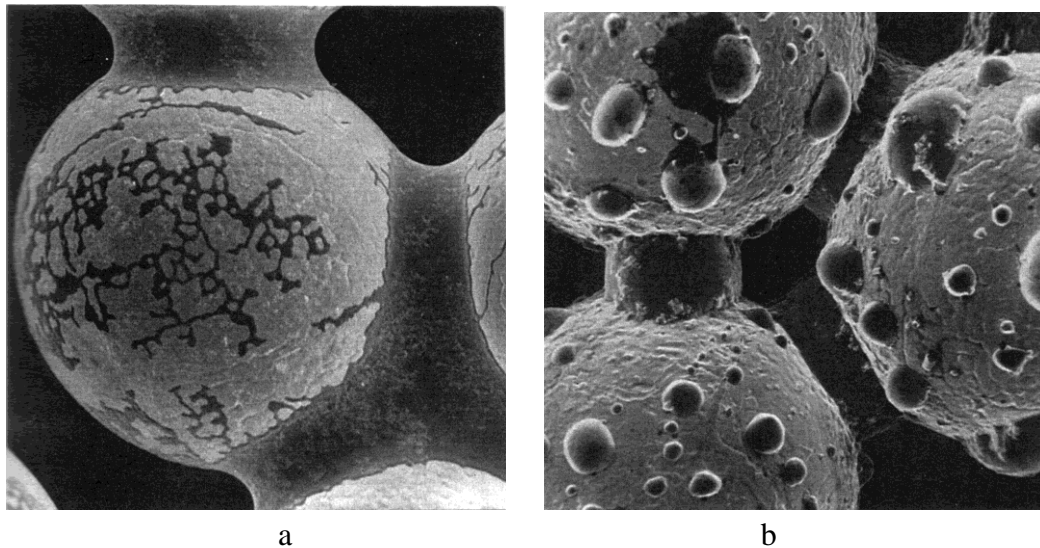


Figure 2.9 Structures of materials in different atmospheres. a) reducing, b) oxidising. From Petzow and Huppman⁽²⁰⁾. © Carl Hanser Verlag Munich.

2.5.3.1 Primary Rearrangement

The primary rearrangement rate is governed by mechanical movement induced by capillary forces⁽¹¹⁾. Where wetting of the solid by the liquid is good, the liquid phase is pulled into particle necks and small pores. Particles are rearranged as a reaction to the capillary forces if they have a degree of mobility. When the liquid phase volume is less than 10%, primary rearrangement leads to a local densification of some particles by their movement in directions of higher liquid bridge coordination. This localised densification results in some regions having a high density and others having low density (see Figure 2.10). This densification provides a degree of macroscopic shrinkage⁽¹¹⁾.

2.5.3.2 Secondary Rearrangement

The rate of secondary rearrangement is controlled by dissolution and reprecipitation processes⁽¹¹⁾. Dissolution of solid material in the liquid phase occurs in regions of high chemical potential and is subsequently reprecipitated at regions having lower chemical potential. Varying chemical potentials result from several factors, such as different activities or stresses due to curvature of interfaces and large concentration gradients⁽¹¹⁾. Several mechanisms have been suggested. These are discussed below.

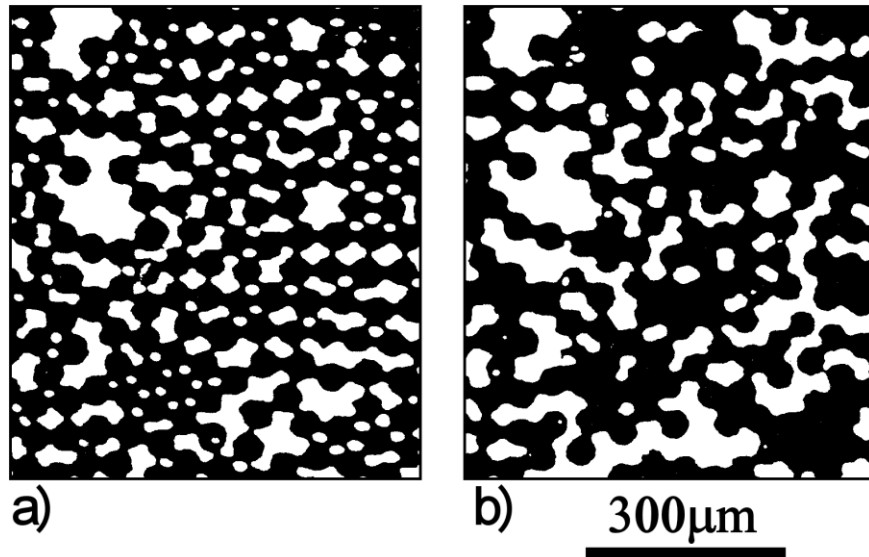


Figure 2.10 The formation of areas of varying density. a) initial state, b) sintered for a period. After Kaysser⁽¹¹⁾.

2.5.3.2(a) Contact Flattening

The contact flattening theory was the first mechanism proposed for liquid phase sintering. In simple terms it describes the process whereby neighbouring grains flatten in contact areas due to uniform centre-centre motion of particles, the material transport occurring via dissolution-reprecipitation⁽⁹⁾. The contact flattening theory provides simple time laws for densification. Kingery⁽²²⁾ found that the volume change is directly proportional to the cube root of the time, ie

$$\Delta V/V_0 \propto t^{1/3} \quad (2.4)$$

where V_0 is original volume, ΔV is the volume change and t is time. This general equation was found to describe systems where dissolution reprecipitation is controlled by diffusion through the liquid⁽¹¹⁾.

The initial stresses between two particles are elastic in nature⁽²²⁾. These stresses result from the wetting liquids' capillary forces exerted on both particles. The increased pressure results in an increased solubility of the solid phase in the liquid. The concentration gradient between solid areas and the liquid cause the liquid to move from particle contact areas towards other, less stressed areas⁽²³⁾. Densification results from uniform centre-centre motion.

In recent years criticism of the contact flattening theory has arisen because:

- 1) the microstructural evidence is ambiguous;
- 2) assumptions made in the contact flattening model are often not applicable in systems where "correct" time laws are measured;
- 3) particle growth, which is an important factor in liquid phase sintering, is neglected.

Kaysser⁽²³⁾ suggests that these factors infer that other mechanisms may determine morphological development and shrinkage phenomenon. German⁽⁹⁾ reports that the role of contact flattening is system dependent and that it is prominent in systems such as W-Ni. Raj⁽²⁴⁾ found that contact flattening is observable in ceramic systems containing an amorphous glassy phase between crystalline grains (eg. silicon nitride). Svoboda *et al.*⁽²⁵⁾ developed a constitutive model describing the shape accommodation process in silicon nitride by contact flattening, and this model showed a high correlation to experimental results. The effect of grain growth, as mentioned by Kaysser⁽²³⁾, was determined to be effective in the later stages of sintering, and was successfully incorporated in the model. The conclusions of Svoboda *et al.*⁽²⁵⁾ were that primary densification mechanisms in silicon nitride sintered with spinel were particle rearrangement and contact flattening, whereas grain growth played a key role in the later stages of sintering. It would appear that contact flattening is a valid mechanism in some systems but that the theory needs to be expanded and enhanced.

2.5.3.2(b) Ostwald Ripening

Particle growth in liquid phase sintering plays an important role in morphological development and sintered mechanical properties. In many systems, particle coarsening confirms diffusion controlled Ostwald ripening as the rate controlling step for sintering⁽¹¹⁾.

Associated with this coarsening is shape accommodation as a secondary rearrangement process. Morphological development observed by Yoon and Huppman⁽²⁶⁾ indicates that particle growth (in the W-Ni system) occurs by dissolution and reprecipitation, and is essentially nucleation of alloy crystals on particles, these crystals having a composition resembling the original particles. Their results suggest that centre attraction between particles is directly related to particle growth and shape accommodation. Figure 2.11 models the evolution of shape accommodation during particle growth and Figure 2.12 shows these effects in relation to other particles in close proximity. Figure 2.13 illustrates typical microstructures⁽¹⁵⁾. As part of the particle growth and shape accommodation events, small particles decrease in number as they dissolve preferentially and reprecipitate onto larger particles, aiding densification.

2.5.3.2(c) Pore Elimination

Increasing the density of a powder body is possible only by the elimination of pores. This can occur by liquid flow or by grain-liquid mixture flow and is a result of capillary pressures present in the compact. The difference between the two is that in grain-liquid mixture flow, particles or grains from around pores move with the liquid into the pore space resulting in a more homogeneous sintered material⁽²³⁾. Pore elimination may result from both primary and secondary rearrangement of particles and grains. If shape change of the primary particles occurs, less liquid is required to fill fine capillaries than was initially the case allowing excess liquid to move into the pore space. When this

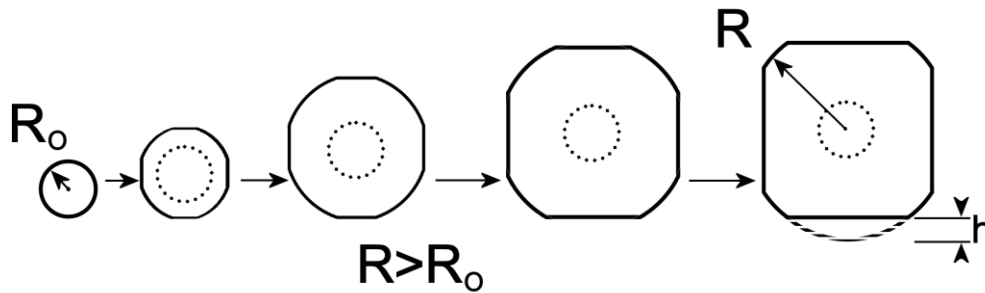


Figure 2.11 Shape change during liquid phase sintering by shape accommodation during particle growth. After Kaysser⁽¹¹⁾.

happens, material preferentially precipitates at the solid-liquid interfaces in the prior pore space.

Kang and Azou⁽²⁷⁾ studied grain growth mechanisms by observing the trapping of pores and liquid pockets during liquid phase sintering of Mo-Ni. Gas porosity was deduced to be essentially stable and spherical. Park *et al*⁽²⁸⁾ concluded that in Fe-Cu these stable pores contained a slowly diffusing gas, most likely nitrogen or water vapour. Liquid pocket entrapment depends largely on the growth rate of the edge region relative to the deposition rate of material in the liquid pocket. This was previously thought to be a coalescence phenomenon, but is now considered an effect of Ostwald ripening⁽²⁷⁾.

2.5.3.2(d) Coalescence

After the initial liquid flow, particles are in contact with the wetting liquid⁽⁹⁾. Coalescence is a possible intermediate densification and coarsening mechanism involving the bonding of particles in close proximity. For particles of differing sizes, the driving force for coalescence is boundary migration due to curvature. Other possible causes of coalescence are chemical, strain, or temperature gradients⁽⁹⁾. Three mass transport paths can cause coalescence. These are:

1. grain boundary migration via solid state diffusion,
2. grain boundary migration via moving liquid films (liquid film migration), and
3. solution-reprecipitation via the liquid phase⁽⁹⁾.

The first two of these have been experimentally proven⁽²⁹⁾, the third has not⁽⁹⁾. The three possible means of particle coalescence are shown by Figure 2.14.

Zukas *et al*⁽³⁰⁾ found that where dissolution is impossible, coalescence is a viable particle growth mechanism. The mechanism was proposed to operate by necks forming between contacting particles. Coalescence is completed by the migration of the newly formed grain boundary away from these neck areas⁽²³⁾. For the W-Fe-Ni⁽³⁰⁾ system, the particle size increased considerably where a large amount of interparticle contact occurred. Contact formation is a precursor to neck growth and subsequent coalescence⁽⁹⁾. New contacts form between particles due to gravity, thermal motion and settling. Once a contact has formed, the driving force for coalescence is a reduction in free energy due to

the removal of an interface. Areas in contact behave energetically like necks, having more extensive mass transport toward these regions, initiating sintering.

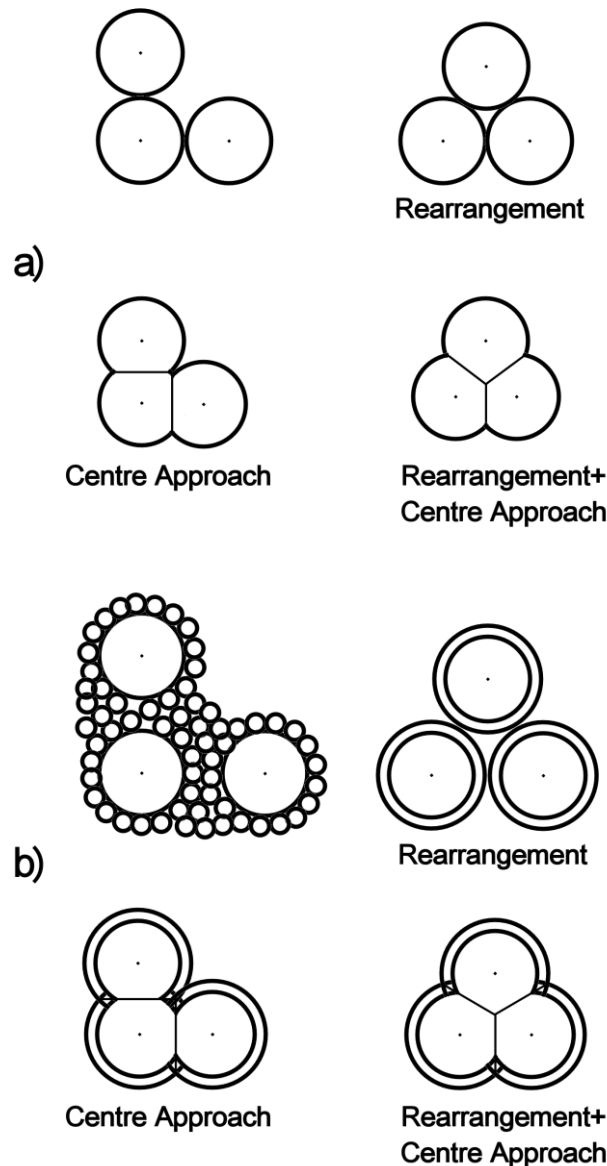


Figure 2.12 Shrinkage by centre arrangement and centre approach (shape change) during liquid phase sintering. (a) Monosized grains without coarsening. (b) Grains/particles with broad size distribution and coarsening. After Kaysser⁽¹¹⁾.

2.5.3.2(e) Directional Particle Growth

The phenomenon of directional particle growth is very similar to coalescence, and is often associated with it but has only been reported for heavy metal systems⁽³⁰⁻³²⁾. Zukas *et al*⁽³⁰⁾ found that there was some directional growth towards coalesced regions, possibly due to gravity induced^(21,33) slumping (see Figure 2.15). The major advantage of directional particle growth is largely associated with improved homogeneity, and occasionally better densification^(23,30). The contribution of directional particle growth to densification is usually small.

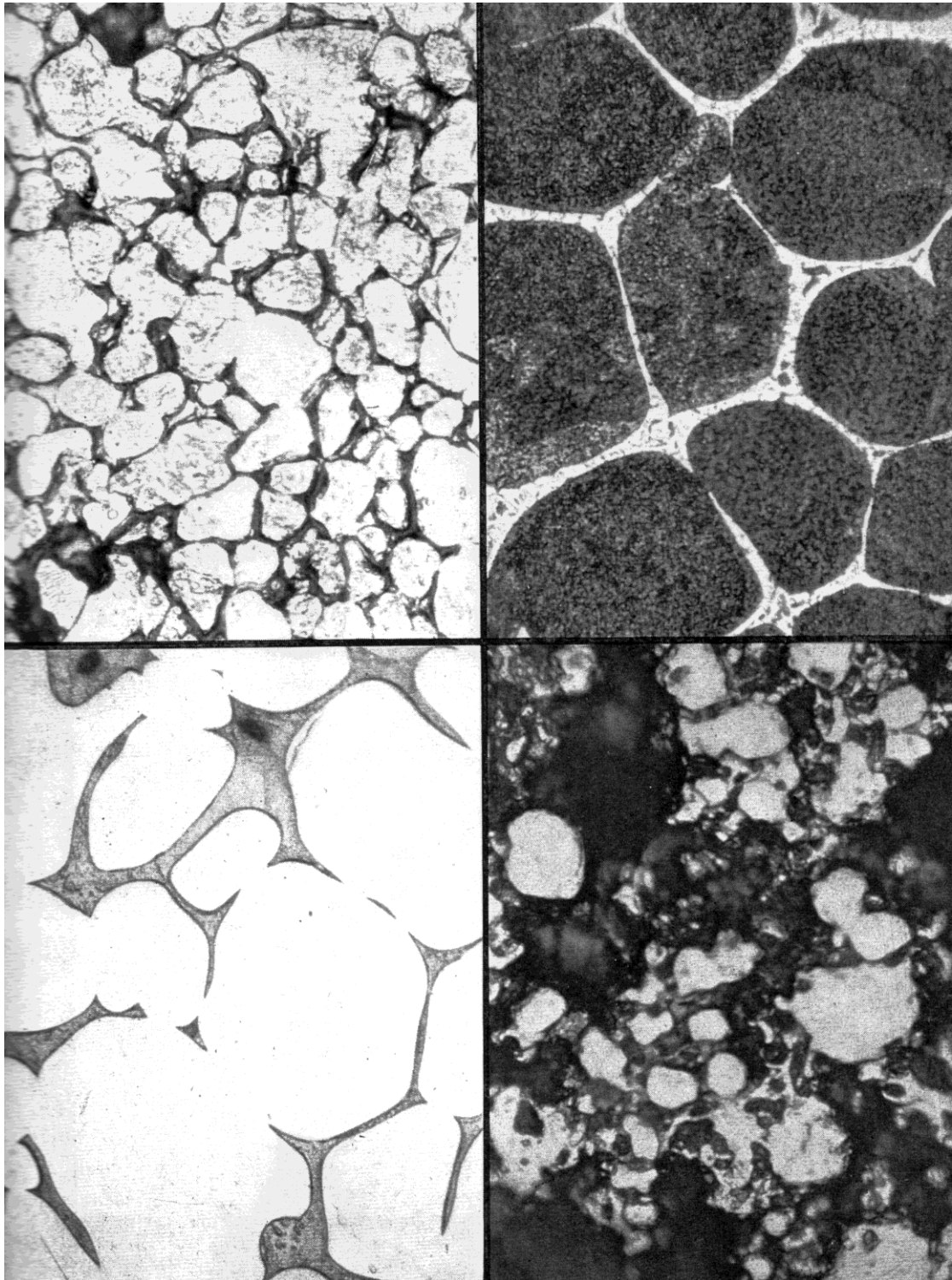


Figure 2.13 (a)(Top left) W-5Cu-2Ni, 675X, (b) (Bottom left) Cu-20Ag, 675X, (c) (Top right) Fe-20Cu, 675X, (d) (Bottom right) W-6Co-4Ag, 675X. From Price et. al.⁽¹⁵⁾
© Maney Publishing www.maney.co.uk

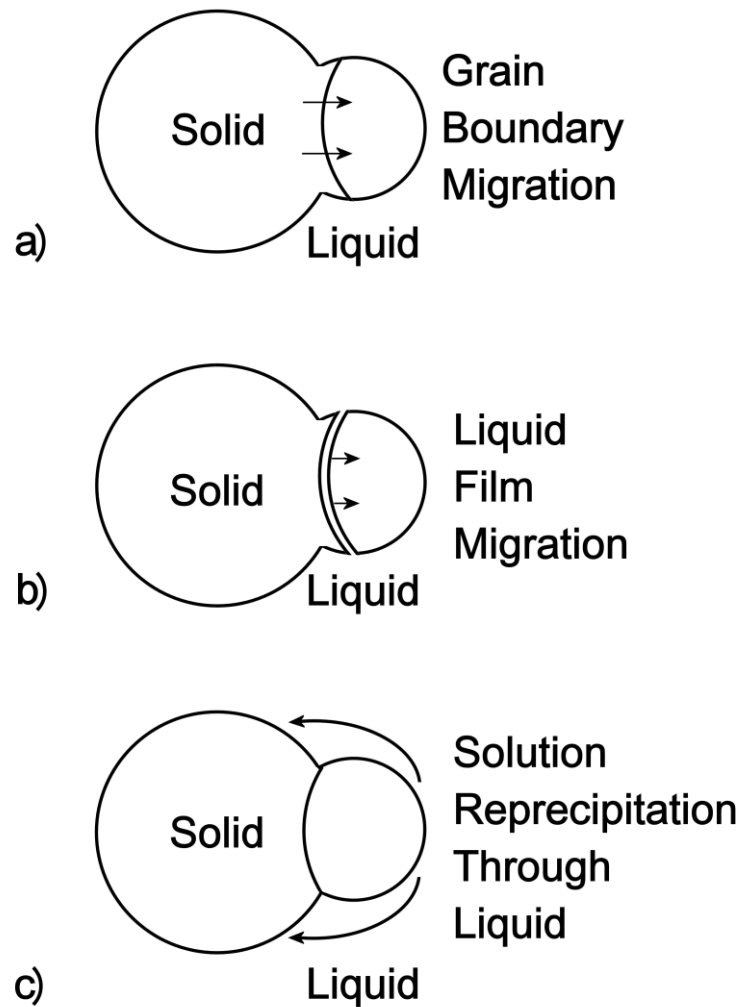


Figure 2.14 Three possible types of coalescence between contacting particles; (a) solid state grain boundary motion, (DIGM) (b) liquid film migration, and (c) solution reprecipitation through the liquid. (After German⁽⁹⁾).

It is possible, however, that the role of directional particle growth has been underestimated until recently. In a study of microstructural anomalies during liquid phase sintering of W-Ni under microgravity conditions⁽³⁴⁾ it was noted that preferential grain growth occurred in certain directions, this being noted by the entrapment of spherical pores within particles. These spherical pores resulted from entrapped gas vapour which could not exit the material in the absence of buoyancy forces. For the pores to be trapped, normal processes which allow the migration of pores to particle boundaries must have been reduced. Additionally, the growth of the solid phase in certain directions was such that it exceeded a critical velocity (overriding the processes for pore exclusion), resulting in entrapped porosity.

Hence it is possible that a re-evaluation of the role of directional particle growth is required to adequately elucidate this phenomenon, as it appears that it may be of greater importance than previously thought.

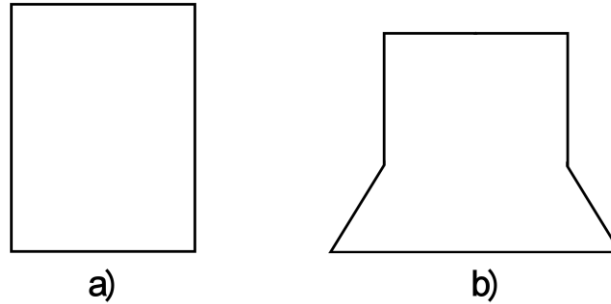


Figure 2.15. The effect of gravity induced slumping. (a) Before sintering, (b) after sintering in the presence of excess liquid phase or too high a temperature. After Kipphut et. al.⁽³³⁾

2.5.3.2(f) Particle Disintegration

Grain boundary attack by the melt and subsequent particle disintegration are observed in many systems, including Fe-Cu⁽²³⁾, Al-Zn⁽³⁵⁾, and Al-Cu⁽³⁶⁾. Steps reported for this particular phenomena are as follows: 1. the liquid phase leaves the initial sites due to capillary effects and penetrates prior particle boundaries, 2. grain boundary attack occurs, drastically reducing the effective particle size. Mass transfer occurs by solution-reprecipitation (Figure 2.16). Relatively pure α (where α is the base material) is taken into solution at the tip of the advancing melt, and is carried into the liquid phase and reprecipitated as solid solution β . Hence the liquid phase attacks grain boundaries⁽²³⁾. Kaysser *et al*⁽³⁷⁾ confirmed this metallographically with samples quenched at various points in the sintering cycle (Fe-Cu). This is summarised in Figure 2.17. Particle disintegration, however, generally appears only to occur in systems where the ideal solubility conditions are reversed⁽³⁵⁾. The exception to this is particle disintegration during supersolidus liquid phase sintering^(9,38-42). Supersolidus liquid phase sintering occurs when a prealloyed powder is heated to above the system solidus, and a liquid phase develops, fragmenting prior particles. This has the effect of decreasing the effective particle size, enhancing the sintering process⁽³⁹⁾. Supersolidus sintering is reviewed further in section 2.5.4.

2.5.3.2(g) Summary of Mechanisms Contributing to Secondary Rearrangement and Shape Change

The contribution of liquid phase sintering mechanisms to densification is summarised in Table 2.2.

2.5.3.3 Melt Penetration and Boundary Migration

Melt penetration along particle and grain boundaries can result in the preferential alloying of areas close to boundary regions⁽³⁷⁾. Unexpected phases may occur (especially if the compact has not been sintered to complete homogeneity) and these phases can determine the mechanical properties of the compact. An example is the formation of austenite at particle boundaries in Fe-Cu⁽¹¹⁾. Melt penetration along boundaries may also initiate boundary migration.

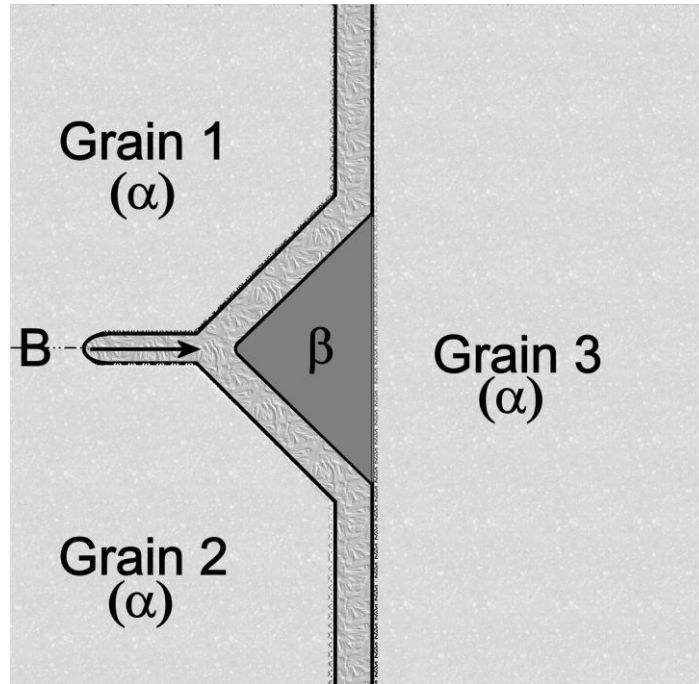


Figure 2.16 Model of grain boundary penetration of melt and bump formation in contact areas. B is the grain boundary, α the base material and β the precipitated material. After Kaysser⁽²³⁾.

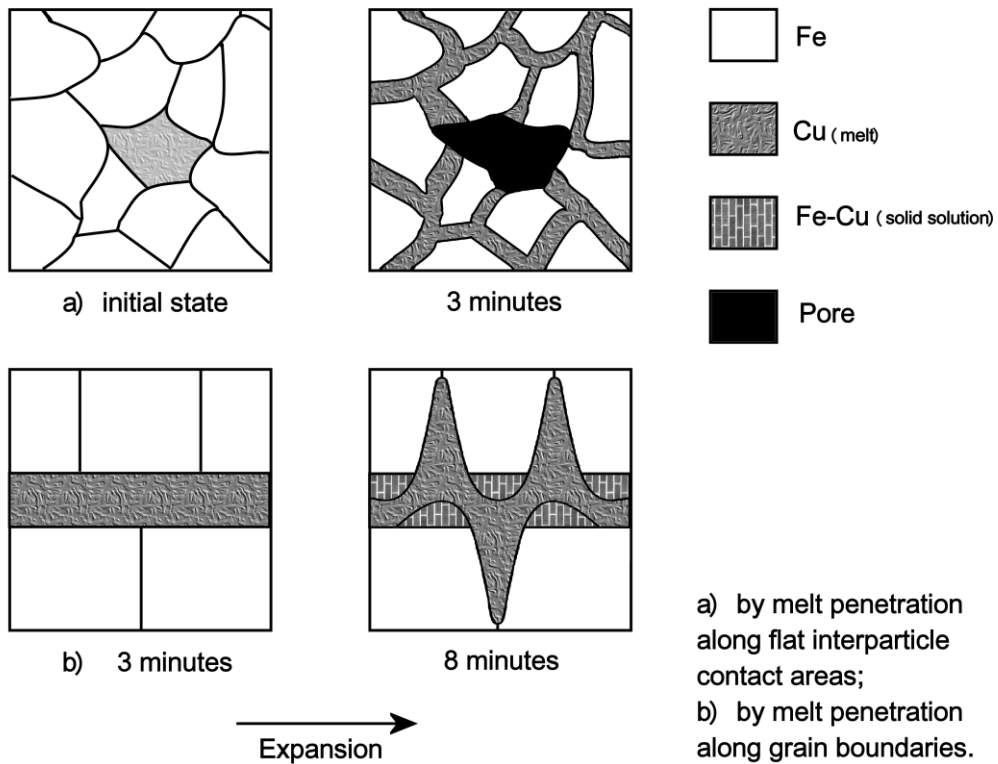


Figure 2.17 Models for penetration of Cu-rich melt along Fe interfaces and associated forms of swelling. After Kaysser et. al.⁽³⁷⁾.

Table 2.2 The contribution of liquid phase sintering mechanisms to densification. (After Kaysser⁽²³⁾).

Mechanism	Rearrangement	Shape change
Contact flattening	-	+
Ostwald ripening	O	-
Ostwald ripening with shape accommodation	O	+
Pore elimination by liquid flow	O	+
Pore elimination by grain-liquid mixture flow	+	O
Coalescence	O	-
Directional grain growth	O	O
Particle disintegration	+	-

+ = essential; O = modest; - = negligible.

Boundary migration is often associated with a noticeable concentration change in the wake of moving boundaries. This is known as chemically induced interface migration⁽⁴³⁾ (CIIM) and includes phenomena such as diffusion induced grain boundary migration (DIGM) and liquid film migration⁽¹¹⁾ (LFM).

2.5.3.3(a) Diffusion Induced Grain Boundary Migration

DIGM occurs when the diffusion of solute atoms along a grain boundary forces the boundary to migrate leaving a solute enriched zone in its wake⁽⁴⁴⁾. Kayssers⁽¹¹⁾ experiments on DIGM in the Mo-Ni system showed that a saturated solid solution was formed behind migrating boundaries, this being characterised by increases in (grain boundary) area. Bulges formed behind the mobile grain boundary were rich in second phase. This type of migration occurs when the solid solution left in the wake of the moving boundary has a lower free enthalpy than the material ahead of the boundary. The solute concentration in the wake of the moving boundary may be higher or lower than at the front of the boundary. Secondly, the boundary must provide a sink or source for the required solute changes. The solid in front of migrating boundaries is not in equilibrium with the solute concentration and solute either diffuses into or out of the solid. When the migration occurs at constant velocity, a steady state concentration profile develops. Coherency strains form if the lattice parameter of the material changes as part of this process. These coherency strains raise the free enthalpy of the solid in contact with the boundary. The solid in the wake of the moving boundary loses coherency with the initial grain due to the incorporation of misfit dislocations⁽¹¹⁾. A review paper by Yoon⁽⁴³⁾ examined the diffusional coherency strain theory and its

implications for chemically induced migration of liquid films and grain boundaries. It was noted that boundary migration occurs under the conditions where the solute diffusion ahead of migrating interfaces was expected to occur.

2.5.3.3(b) *Liquid Film Migration*

Liquid film migration (LFM) is defined as the migration of thin liquid films of one metal between grains of another from one grain into another leaving behind an alloyed region⁽⁴⁵⁾. Liquid film migration is analogous to DIGM^(11,45). The necessary conditions for the two processes to occur, the morphological development and the driving force are comparable⁽⁴⁵⁾. The major differences between the two processes appear to be the presence of the liquid phase. In their study of CIIM in an Al-2.07Cu alloy, Kuo and Fournelle⁽⁴⁵⁾ observed DIGM below the solidus temperature, and a combination of LFM and DIGM above the solidus temperature. Where LFM occurs, it is most likely that greater rates of mass transfer occur, due to the presence of the liquid phase.

Liquid film migration in sintering systems occurs simultaneously with the penetration of liquid along grain boundaries⁽¹¹⁾. In some systems (eg. Fe-Cu) rapid homogenisation may occur due to these migrations. Where carbon is present in Fe-Cu systems, liquid phase penetration is suppressed due to carbon increasing the dihedral angle of the liquid phase. This means that liquid does not penetrate the compact as completely as in a compact without carbon⁽⁴⁶⁾. Despite this problem, liquid film migration causes penetration of contact areas to occur by shifting the thin liquid layers⁽¹¹⁾. The properties of many systems are influenced by liquid film migration, as it can mechanically lock grains by producing bulged grain boundaries, improving properties considerably⁽¹¹⁾. Baik *et al*⁽⁴⁷⁾ described liquid film migration as a discontinuous precipitation of the liquid phases. Yoon⁽⁴³⁾ has characterised the effects of liquid film migration on morphological development in Mo-Ni alloys. During prolonged sintering, the particles/grains coarsened to large sizes by a diffusion controlled process. Most grains were separated by thin liquid films, with the remainder being separated by grain boundaries. When the matrix composition was altered either thermodynamically or chemically, both liquid films and grain boundaries migrated with a velocity which varied parabolically with the change in composition determined from the Mo-Ni phase diagram. This was in good agreement with predictions derived from coherency strain theory. It was noted that faceting of grain boundaries was common, as was corrugation of solid surfaces, particularly in systems that were sintered. Rhee and Yoon⁽⁴⁸⁾ were the first to report this phenomenon for the Mo-Ni system after noting that initially smooth particle boundaries became irregular and corrugated when Fe was added. The corrugation process was found to resemble liquid film migration, and the instability driven by the diffusional coherency strain energy. However the initiation process for corrugation was unclear.

The effect of chemically induced interface migration on liquid phase sintered materials is unclear, but may be of significant importance^(11,43,48). Savitskii⁽⁴⁹⁾ noted that unusually high rates of grain growth occurred during the sintering of Al-Cu. This was described as a type of activated recrystallisation, driven by boundary migrations. The diffusion coefficient was approximately 1000 times greater in the moving boundary than in a stationary one. Hence it is possible that enhanced sintering processes may occur during boundary migrations due to the increased rates of mass transfer associated with these boundaries.

2.5.4 *Supersolidus Sintering*

Supersolidus sintering is a type of sintering in which a prealloyed powder is sintered at a temperature just above the solidus. A small amount of liquid phase is formed within each powder particle allowing densification by rearrangement, liquid flow and diffusion⁽¹⁷⁾. Densification during supersolidus liquid phase sintering is analogous to viscous flow sintering, since the semisolid particles turn mushy and flow once liquid spreads along the grain boundaries^(42,50). Depending on the internal powder structure, the liquid phase can nucleate either in the interdendritic region, along the grain boundary or at interparticle contacts⁽⁴⁰⁾. After a threshold amount of liquid phase is developed, fragmentation of prior particles occurs^(39,40), reducing the effective particle size. The initial particles lose their rigidity during this process and almost complete densification via primary rearrangement^(39,50), solution reprecipitation, pore removal, contact flattening and grain shape accommodation may occur⁽⁴⁰⁾. The key process parameters in supersolidus liquid phase sintering are temperature and powder composition⁽⁹⁾ as these two parameters directly influence the volume of liquid phase developed. For high rates of densification during sintering, a volume fraction of ~20% is optimal. Despite being an attractive process, there are several problems associated with supersolidus sintering. If any sintering occurs before the solidus temperature is reached, densification may be retarded, due to solid bond formation. Additionally, as the volume fraction of liquid that develops directly controls the final density, slight changes in either composition or temperature can drastically effect the dimensional stability and strength of the sintered component⁽⁵⁰⁾.

2.5.5 *Transient Liquid Phase Sintering*

Transient or reactive liquid phase sintering occurs when the liquid phase exists for a finite period only, then disappears due to solubility effects or secondary reactions. Since remnants of the liquid phase are not present in the final sintered material, very good high temperature properties may result. The constitution point for a fully transient system always falls within a solid region of the phase diagram (eg. C_T in Figure 2.6). The materials morphological development is extremely process dependent^(9,51-53) because process variables control the amount of liquid which forms, and the duration for which it is present. Puckert *et al.*⁽⁵¹⁾ noted that for Cu coated Ni spheres the heating rate most effected the quantity of liquid phase that developed during sintering. No liquid formed

when a heating rate of 1°C/min. was used, while appreciable liquid phase developed when samples were heated at $\geq 15^\circ\text{C}/\text{min}$.

Three distinguishable variants of transient liquid phase sintering are possible⁽⁵⁴⁾. These are:

1. The powders go through a series of chemical reactions which are responsible for the liquid phase formation. This includes such processes as in-situ microfusion⁽¹⁶⁾ where an exothermic reaction occurs during the formation of an intermetallic. This raises the local temperature above the eutectic point, initiating liquid phase formation and causing bonding. Once the reaction is complete, the local temperature decreases back to the sintering temperature, which is below that of the eutectic.
2. Starting powders pass through a liquid stage but form a solid solution at equilibrium.
3. Cooling from liquid phase sintering temperatures forms a glassy phase in boundary regions, which is subsequently recrystallised. This is predominantly used in ceramic processing. A typical transient liquid phase sintered microstructure is shown by Figure 2.18⁽⁵⁵⁾.

A combination of transient liquid phase sintering and infiltration has been examined by Langford and Cunningham⁽⁵⁶⁾. Hot low carbon steel shot was infiltrated with a molten high carbon steel alloy. The liquid phase generated solidified by what was described as diffusional solidification as the material homogenised. It is of interest that almost no porosity was present in the final microstructures. This is in contrast to usual transient liquid phase sintering where secondary porosity remains in the material^(57,58).

2.5.5.1 Non Powder Metallurgy Utilisation of Transient Liquid Phases

Transient liquid phase bonding is a diffusion bonding process currently used for joining several types of heat resistant alloys⁽⁵⁹⁾. Generally, an interlayer material used as a bonding agent melts and re-solidifies as a result of interdiffusion with the base material, usually at a constant temperature. The possibility of forming brittle phases in the bond region is largely avoided because the final microstructure is homogeneous^(60,61). In principle, transient liquid phase bonding is applicable to eutectic or peritectic^(59,62,63) alloy systems, where a lowering of the liquidus temperature occurs during alloying. The transient liquid phase process can be analysed in four stages⁽⁶¹⁾:

1. dissolution of the additive interlayer;
2. homogenisation of the liquid;
3. isothermal solidification; and
4. homogenisation of the bond region.

The solid liquid interface is substantially altered between stage 1 and stage 3. Substrate material dissolves in the liquid during stage 1. The maximum liquid seam width is attained when the liquid is homogeneous (stage 2). The liquid seam then

decreases in width as the liquid changes composition and the additive phase passes into solution. The process is illustrated in Figure 2.19⁽⁶⁰⁾. An important factor influencing the efficiency of the process is the width of the filler metal thickness and the heating rate. Thinner metal thickness and slow heating rates result in a minimum of bonding via the liquid phase, because homogenisation occurs quickly (Figure 2.20⁽⁶⁴⁾).

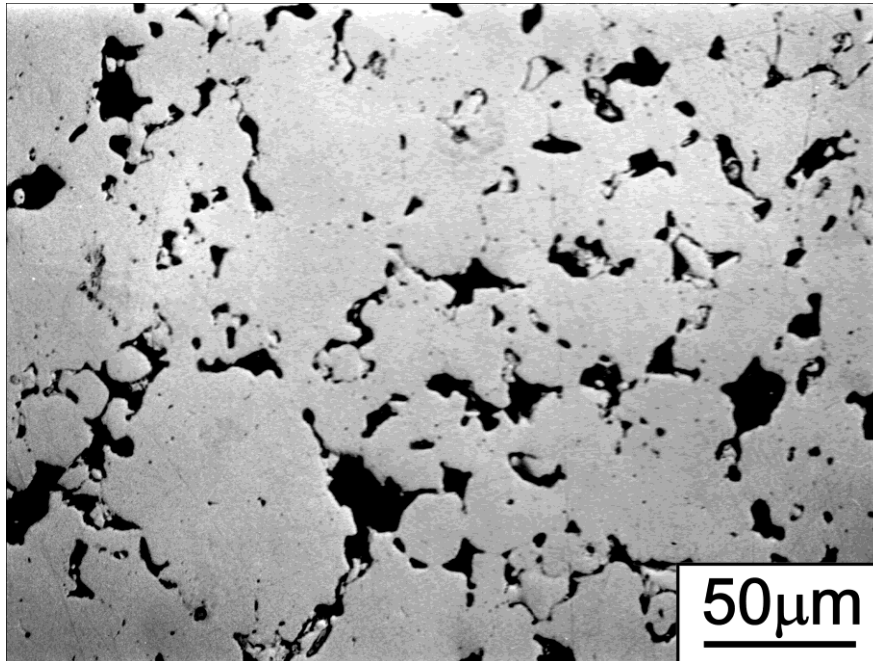


Figure 2.18¹ A typical transient liquid phase sintered microstructure. Alloy composition is Fe-7Cu. The sample was sintered at 1150°C. Complete homogenisation occurs during the sintering process, and the material is single phase. Ferrite (white) containing copper in solid solution, the pores are black. This microstructure should be compared with those for persistent liquid phase sintered microstructures shown in Figure 2.13.

2.6 The Microstructural Evolution of Liquid Phase Sintered Materials

The variety of materials fabricated by liquid phase sintering results in a spectrum of sintered microstructures^(9,55). Several factors change simultaneously during liquid phase sintering. Porosity decreases or increases, grain and particle sizes may increase, and the dihedral angle may vary widely. The goal of microstructural studies is to qualify the morphology and characteristics of the material. These various microstructural effects are usually interrelated and have a pronounced effect on properties. Manipulation of the various morphological characteristics results in an improved understanding of the behaviour of sintered materials during processing and in service⁽⁹⁾.

¹ The original image used for Figure 2.18 was of a Fe₃Cu alloy sintered at 1280°C⁽⁵⁵⁾. The image presented here is nearly identical, and from the authors' own collection of micrographs.

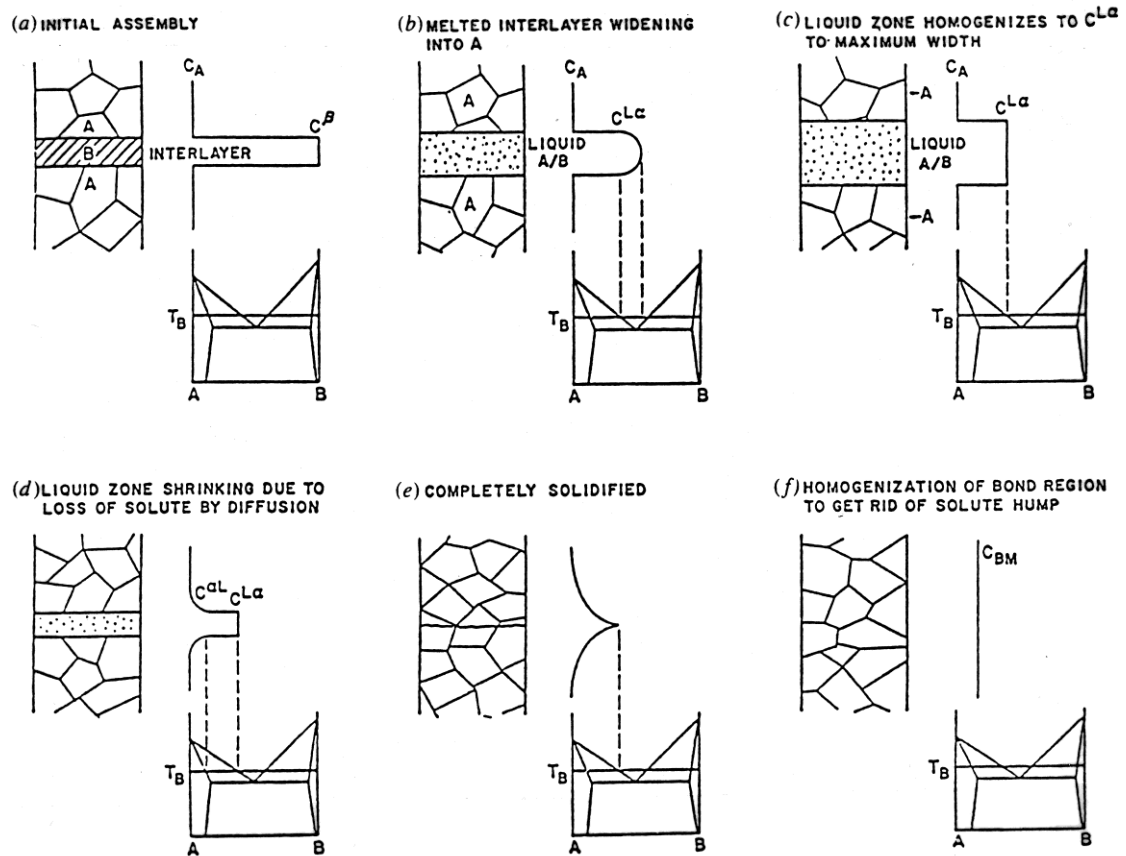


Figure 2.19 Schematic representation of the mechanism of the transient liquid phase bonding process. (From Tuah-Poku *et. al.* ⁽⁶⁰⁾) (© Reproduced with kind permission of Springer Science and Business Media.)

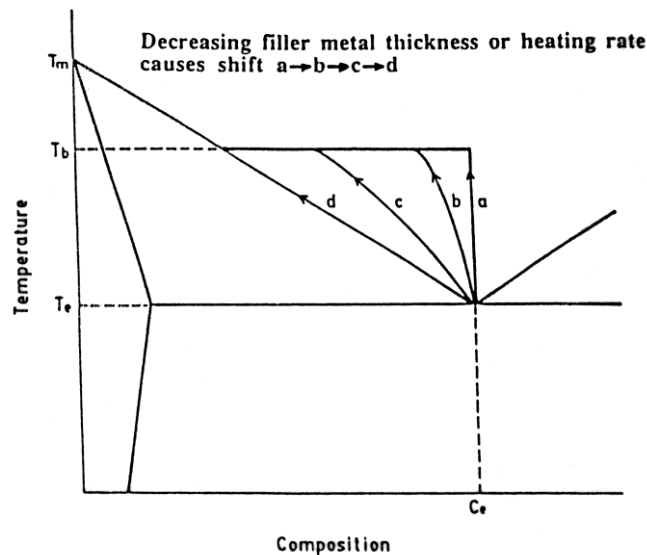


Figure 2.20 Effect of decreasing heating rate or filler metal thickness on the liquid composition during transient liquid phase brazing. (From Nakagawa *et. al.* ⁽⁶⁴⁾). (© Reproduced with kind permission of Springer Science and Business Media.)

Three basic microstructures develop during persistent liquid phase sintering. These are shown in Figure 2.21. Type (a) is referred to as an isolated structure, type (c) a skeletal structure and type (b) a mixed structure. Isolated structures are rarely observed and largely depend on thermal history (eg. W-Ni-Fe). Contacts between particles can form due to cold welding during compaction or by mass transport during sintering. Microstructural development relies on the probability, p_s , that two particles will join, and whether the time required to fuse the two particles, τ_f , is greater or less than the time required to produce further contacts by particle motion, τ_B/p_s , where τ_B is the time between subsequent contact formation developed by particle motion. It has been shown⁽⁶⁵⁾ that these parameters effect the microstructure in the following manner:

Condition	Microstructure
$\tau_B/p_s \ll \tau_f$	Highly connected / skeletal
$\tau_B/p_s \gg \tau_f$	Isolated or mixed
$\tau_B/p_s \rightarrow \infty$	Isolated

The surface area to volume ratio is decreased when particles come into contact and join. The rate of microstructural coarsening is limited by the time between particle contact formation, which for an isolated structure is long in comparison to the time required for fusion to occur. Skeletal structures exhibit similar mechanisms of formation, but coarsening, which is a result of particle fusion, is limited by the rate at which the particle necks grow, since this takes more time than does the establishment of the contacts⁽⁶⁵⁾.

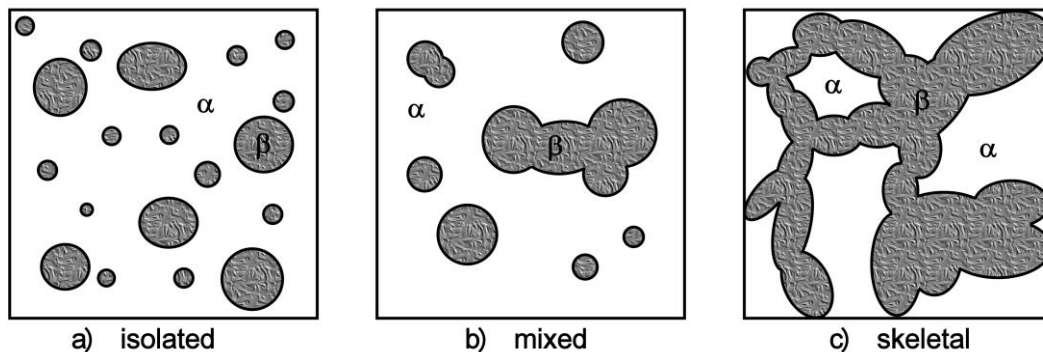


Figure 2.21 The types of microstructures observed in liquid phase sintered products. (a) isolated, (b) mixed, (c) skeletal. After Courtney⁽⁶⁵⁾.

2.7 The Sintering of Fe-Cu Compacts

Kayser⁽³⁷⁾ characterised the microstructural development of the Fe-Cu system, which is used for more liquid phase sintered powder metallurgy components than any other. Iron and copper powders of approximately 100 μm in size were compacted at 785 MPa and sintered for varying periods at 1165°C. After 8 minutes, the liquid which was a saturated solution of Fe in Cu, had penetrated prior particle boundaries and grain boundaries within particles. Due to the high compaction pressure and hence high

relative green density (>90% of theoretical), little particle rearrangement occurred. Spaces originally occupied by Cu particles became pores as the liquid spread away from the prior particle sites. With limited particle rearrangement, shrinkage did not occur, which would have been necessary to counteract the effect of swelling. There was a net volume increase of 6%, 65% of which was attributed to copper penetration along grain boundaries. The remainder was due to diffusion of Cu into Fe⁽³⁷⁾. Assumptions were made to the effect that the width of the copper seams stays constant and the iron dissolved at grain boundaries is reprecipitated (see Figure 2.16). The dihedral angle was close to zero at the sintering temperature. At sintering times greater than 8 minutes particle rearrangement was evident. This was a consequence of the liquid phase penetration into grain boundaries. Individual grains became separated from the original particles facilitating rearrangement due to their fine size. This rearrangement causes shrinkage, counteracting the diffusion of Cu into Fe. After long sintering periods the particles form necks and a solid skeleton forms.

Widely differing views have been expressed about the origins of the dimensional change in Fe-Cu compacts. Magee and Lund⁽⁶⁶⁾ conducted dilatometer studies on Fe-Cu and suggested that there were three stages to densification. The first stage corresponds to normal linear thermal expansion. The second corresponds to expansion due to grain and particle boundary penetration by the liquid, and the third stage is interpreted as solid state shrinkage. These results are not universally observed, when compared to other Fe-Cu dilatometric analyses⁽³⁾.

Lee and German⁽⁶⁷⁾ report that binary systems exhibiting swelling have some notably similar characteristics. These systems have relatively low melting point additives and a higher solubility of the additive in the base than vice versa. This results in a net diffusional flow from the additive into the base. Slow heating rates in these systems (which are often transient or partially transient) results in diffusional homogenisation and liquid formation is suppressed (eg. Fe-Ti⁽⁵³⁾, Ni-Cu⁽⁵¹⁾). Systems with non-ideal solubilities will be process sensitive, whether they are transient or persistent.

Wanibe *et al.*⁽⁶⁸⁾ assessed quantitatively the extent of swelling on the basis of the bulk density of green compacts, reflecting powder characteristics and compaction conditions. It was noted⁽⁶⁸⁾ that expansion in a Fe-15Cu alloy compressed at 300 MPa was greater in the axial than in the radial direction. The most pronounced shrinkage noted followed excessive expansion at above 10%Cu. It was concluded from this work that the sintered density of Fe-Cu compacts was directly related to the copper content for all compaction pressures.

When carbon is added to Fe-Cu sintered alloys, the liquid phase formation along grain boundaries is suppressed^(9,11) and the dihedral angle is increased^(46,69). This results in a reduction in swelling, while acting to increase the final properties of the iron⁽⁷⁰⁾. By

control of sintering parameters and powder characteristics, zero dimensional change can be attained in Fe-Cu-C alloys⁽⁷¹⁾.

2.8 Aluminium Powder Metallurgy

Much work has been performed on improving the properties of aluminium powder alloys⁽⁷²⁾. Early work⁽³⁾ showed that exceptional tensile properties could be generated in heat treated extrusions of 7xxx series wrought alloys (784 MPa UTS, 781 MPa yield stress, 4% elongation). Common consolidation processes often employed include press and sinter, extrusion, and powder forging operations⁽²⁾.

Research has been performed on the processing routes of rapid solidification and mechanical alloying techniques. Rapidly solidified Al alloys can be divided into five groups^(72,73). These are: 1) high strength / corrosion resistant alloys, 2) low density / high stiffness Al-Li alloys, 3) high temperature alloys, 4) intermetallic compound alloys (aluminides), 5) metal matrix composites.

Mechanically alloyed aluminium development has been built around combining ambient temperature strength from solid solution strengthening and precipitation hardening, with elevated temperature strength from dispersoid content and composition. Developments have generally been in low density aluminium alloys, high temperature alloys and metal matrix composites. Mechanically alloyed aluminium alloys generally exhibit exceptional resistance to corrosion and to stress corrosion cracking⁽⁷³⁾.

Exceptional properties can be attained from rapidly solidified and mechanically alloyed aluminium⁽⁷²⁾. However, due to the increased number and difficulty of processing steps involved in these processes, the widescale utilisation of these materials is limited by their cost.

2.8.1 Utilisation of Aluminium Powder Metallurgy Components

P/M aluminium combines the advantageous aspects of net shape powder processing with the desirable physical and mechanical properties of aluminium⁽⁷⁴⁾. Aluminium P/M parts are used in an increasing number of applications, having replaced materials previously made by traditional means⁽⁷⁵⁾. Use in business machine parts has been one of the major applications of aluminium P/M technology. Lighter weight components reduce vibration and inertia on startup and stopping, reducing power requirements⁽⁷⁶⁾. Moving parts such as drive belt pulleys, hubs, end caps and connecting collars are some of the business machine applications^(2,76). Aluminium P/M offers a cost effective alternative to stainless steel in applications where the manufacturer cannot risk corrosion, or anti-rust oil contamination^(75,76). Examples of these components are in pumps, outdoor equipment, meters, gauges and fluid control devices⁽⁷⁵⁾. The high precision of powder metallurgy components can be combined with the thermal and conductive properties of aluminium for use in electronic devices⁽⁷⁵⁾, especially where non-magnetic components are required.

Other markets include automotive components (a large potential growth area), aerospace components, power tools, and whitegoods. Their current commercial use in these areas is, however, small. Aluminium has not gained widespread acceptance as a commercial material for P/M part fabrication^(74,77). Potential military applications exist, and include such items as rifle parts, projectile fuses, cartridge cases, artillery shells and rocket warheads⁽²⁾. The machinability of aluminium P/M parts makes it an attractive processing route for parts requiring further processing. Aluminium powder metallurgy materials provide flexibility in materials selection and design, combined with the economic advantages of these processing methods.

2.8.2 The Sintering of Aluminium Liquid Phase Sintered Materials

The aluminium systems which have undergone study are those based on additions of Si, Cu, Sn, Zn and Mg^(8,35,36,75,78-94). Compared with the well known production of sintered Fe parts, the production of aluminium based P/M materials is an area requiring more research as part manufacturers move towards using more light metals and improved processing methods.

A major problem with aluminium powder materials is the stable oxide film covering each particle^(74,81,84,86,89,92,94-103). This oxide layer forms during the production of the powders, and shows a strong tendency for hydration reactions when exposed to humid environments⁽¹⁰⁴⁾. The presence of a surface oxide shifts the sintering process from one dominated by a bulk transport mechanism to one controlled by surface transport, with the associated lack of densification⁽¹⁰⁵⁾. Calculations and analysis by Munir⁽¹⁰⁵⁾ predict that Al powders will not sinter if coated with an oxide layer. The basis of these calculations was the ratio of the rate of neck growth in unretarded sintering to the rate of neck growth controlled by diffusion through the oxide layer. Ideal sintering conditions are observed when this ratio equals 1. This ratio decreases with increased temperature, but for Al is $\sim 3 \times 10^{17}$ at 660°C which clearly indicates no sintering occurs. Conventional reducing atmospheres are unable to remove the oxide layers, and only a limited amount of cold welding occurs on compaction. Success in applying reducing atmospheres to aluminium has recently been gained where Mg_3N_2 is formed under reduced pressure⁽¹⁰³⁾. This Mg_3N_2 vapour was found to be able to reduce the oxide layer, facilitating sintering. Other methods have been employed to break up the oxide. The method which has achieved most attention is by using a low temperature eutectic or melting point material as an additive. The liquid phase that forms is able to disrupt the oxide layer sufficiently to allow sintering⁽⁷⁹⁾.

2.8.2.1 Sintering of Aluminium Based on Tin Additions

Sunderesan and Ramakrishnan⁽⁸¹⁾ examined tin based aluminium alloys with the aim of producing anti-friction materials. Specific alloys tested were Al-4Sn, Al-7Sn, and Al-7Sn-2Cu-1Ni. Tin has a limited solubility in aluminium and the eutectic temperature is very close to the melting point of tin. There were three distinct regions of the

dilatometry curves: thermal expansion, pronounced dilation and then shrinkage at 600°C (for the binary alloys). The extent of dilation was found to depend on tin content. For Al-7Sn-2Cu-1Ni, the transition to shrinkage from expansion occurred at 550°C, presumably due to lower temperature eutectic transformations. The extent of dilation was affected by the initial porosity and is greater for specimens with lower initial porosity, although no reason was provided. It was suggested that sintering in the initial stages occurs by rearrangement, followed by solution reprecipitation in the latter stages, which is consistent with Kingerys⁽²²⁾ findings (section 2.5.3.2(a)).

2.8.2.2 Sintering of Aluminium Based on Silicon Additions

Based on the wrought 6xxx series alloys, these materials exhibit moderate properties and have had some industry utilisation^(2,75,80). The existence of a low temperature binary eutectic at 577°C provides the basis for liquid phase sintering of Al-Si alloys. Despite these alloys' use, there is a limited amount of information on the sintering and microstructural development of these materials^(102,106). Alloy 601AB has a nominal composition of Al-1Mg-0.6Si-0.25Cu and the tensile properties (T4) of this alloy show a UTS of 141 MPa with 5% elongation⁽²⁾. As-sintered microstructures exhibit poor sintering⁽¹⁰⁶⁾. Shibli and Davies⁽¹⁰²⁾ note that the mechanical properties of alloys tested (Al-0.9Si) were degraded with silicon additions for both air and nitrogen atmospheres. In their analysis it was found that the oxidation rate of alloys containing silicon was greater than that of pure aluminium, which impeded sintering. However, Daver *et. al.*⁽⁷⁵⁾ reports that in the range of aluminium filters available from Alcan, those based on an Al-2Si alloy sintered in nitrogen exhibited approximately double the shrinkage of those based on Al alone with a correspondingly improved strength. The basis of these contrasting analyses is unknown.

High silicon alloys have undergone more alloy development^(78,103). High silicon alloys⁽⁷⁸⁾ tensile strengths (T4) are generally in the range of 220-270 MPa, and have elongations of between 0.7%-8%. The best combination of properties for these alloys was gained from a Al-12.4Si-0.98Cu-0.5Mg alloy which developed a tensile strength (T4) of 270 MPa and 8% elongation. Alloys containing greater amounts of Si (up to 35%) generally have poorer mechanical properties, but improved (reduced) coefficients of thermal expansion. In their development of reducing atmospheres for Al alloys, Nakao *et al.*⁽¹⁰³⁾ noted an increase of 43% in the tensile properties of an Al-10Si-4Cu alloy when Mg₃N₂ was used as a sintering aid. Maximum tensile strengths (T6) were a UTS of 315 MPa and an elongation of 4%.

The Al-Si system is one in which a limited amount of information exists regarding the science of the sintering processes. It is apparent that the majority of the alloy development in this area has centred on high Si alloys^(78,103). It is possible that Al-Si alloys could be developed further, specifically if Si additions between 1 and 12% were investigated more thoroughly.

2.8.2.3 Sintering of Aluminium based on Magnesium Additions

Magnesium is usually used in aluminium P/M alloys as an additive for improved work hardening and most importantly, for enhancing the precipitation hardening of alloys containing Cu, Si or Zn. Studies devoted to the binary Al-Mg system have been limited⁽⁷⁹⁾. The major finding of this work on Al-Mg was that magnesium causes compact growth, and porosities of 40-43% were recorded for specimens of composition 15% Mg sintered at 460°C. The green compact of this material was approximately 85% dense. Specimens sintered in the single phase (α) region showed growth only; those sintered in the α +L region showed growth followed by shrinkage, presumably due to the partially persistent nature of the liquid phase. It is notable that there is a correlation between the increase in lattice parameter and the dimensional growth of the powder bodies. This suggests that the main cause of growth in Al-Mg alloys was a diffusion controlled process, unlike that for Fe-Cu⁽³⁷⁾, where 65% of the compact growth was attributed to boundary penetration by the liquid phase.

2.8.2.4 Sintering of Aluminium Based on Copper Additions

Kehl and Fischmeister⁽⁸⁶⁾ report that during the sintering of Al-Cu compacts, sudden specimen growth occurs upon reaching and passing the eutectic temperature. The extent of the dimensional change in these alloys is largely dependent on process variables. The swelling has been described as being due to liquid phase penetration of grain boundaries, and is followed by a rapid contraction. Savitskii⁽⁴⁹⁾ also noted these dimensional changes, and as in the Al-Mg system, was able to attribute the majority of the expansion present to the diffusion of Cu into Al, based on the changes in lattice parameter. A characteristic of the Al-Cu system is that many intermetallic phases are stable in this system, mainly when reaction between the Al and Cu is incomplete^(86,49). Kehl and Fischmeister⁽⁸⁶⁾ observed that the volume increase in this system acts to move the whole block of intermetallic phases (corresponding to phase regions at the copper end of the phase diagram) which form away from prior copper particle sites. At the aluminium end, copper is continually taken from the liquid and diffuses through the solid. If the system is transient, no Al₂Cu-Al eutectic remains. If the system is persistent, a small amount of liquid remains. At 600°C, the liquid phase penetrates most of the aluminium, whereas at lower temperatures (eg. 560°C) the liquid phase shows limited spreading. Farzin-Nia and Davies⁽⁸⁷⁾ found that at just above the eutectic (ie. 550°C) the liquid phase existed for only a limited time, and some primary copper remained in the compact. This presumably would also pass into solution at longer sintering times. Additions of silicon to Al-Cu alloys have not proved advantageous, rather Si decreases strengthening during ageing. Esper and Leuze⁽⁸⁸⁾ conducted experiments in Al-Cu with and without additions of magnesium and silicon, the emphasis of their research being on the additive powder particle size. Their results indicated that a finer additive particle size results in higher tensile strengths. It was also noted that the Al-Cu system is non-ideal and the liquid phase is transient. When using fine powders, shrinkage occurred at lower temperatures and dilation decreased in comparison to large powders.

Watanabe and Yamada⁽⁸⁹⁾ examined different methods of adding copper to aluminium powder alloys. Mixed powders (primary Al and Cu), prealloyed powders and composite powders (Al with Cu coatings) were tested. The mixed powders showed superior sintering to the other forms because larger volume fractions of liquid were present. The prealloyed powders had only a small amount of liquid in contact regions between particles, and composite powders showed much faster diffusion and hence less liquid formation. This may have been due to an improved distribution of the Cu where Al powders were coated, and the lack of an oxide barrier due to the coating.

2.8.2.5 Sintering of Aluminium Based on Zinc Additions

Savitskii *et al.*^(49,90) studied the volumetric changes experienced by Al-Zn compacts during liquid phase sintering and the effect of aluminium particle size. Dilatometric analyses showed an initial expansion, followed by a region of no volume change, then further expansion to the sintering temperature at which point little or no dimensional changes occurred. This region of no volume change was assumed to be liquid induced shrinkage although no direct proof was provided. Increasing the aluminium particle size increased the compact dilation. From this work⁽⁹⁰⁾ an equation for the growth of compacts was determined:

$$\eta = K C_s + \eta_0 (1 - C_s) \quad (2.5)$$

where η_0 is the porosity of the green compact, η the porosity of the sintered compact, K a proportionality coefficient and C_s the concentration parameter associated with the concentration of Zn in Al (where $C_s = \text{Vol. additive} / \text{Vol. additive} + \text{base}$). The validity of this equation was verified by German *et al.*^(53,67) on the Fe-Ti and Fe-Al systems. The proportionality constant K was assigned physical meaning by German who hypothesised that the coefficient was related to differences in mutual solubility⁽⁶⁷⁾ or shrinkage due to solid state sintering⁽⁵³⁾.

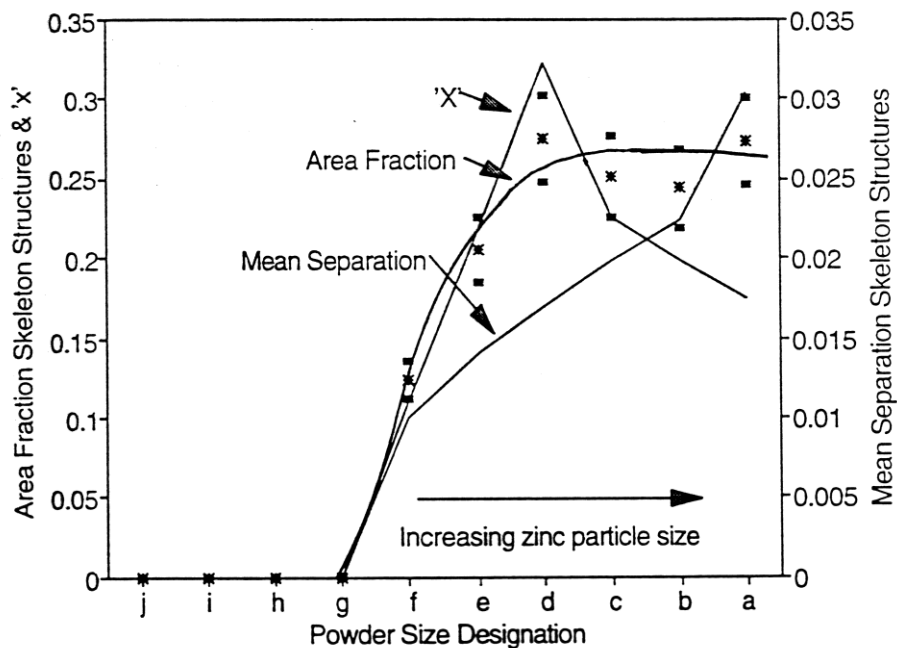
The effect of sintering temperature for an Al-24Zn alloy was examined⁽⁴⁹⁾ and at between 550°C and 610°C this system changes from exhibiting only expansion at 550°C (fully transient condition) to expansion plus shrinkage at 610°C (partially transient condition). The effect of temperature on the dilation was similar to that which occurred in the Al-Mg system⁽⁷⁹⁾.

Another study⁽³⁵⁾ of the binary Al-Zn system showed findings consistent with those of Savitskii^(49,90). However, in this case the sample was sintered under fully transient conditions. Shrinkage at higher temperatures was largely due to solid state sintering, as no evidence of the liquid phase was present. There was also a relationship between the additive particle size and the amount of liquid phase which formed. This relationship had three main stages and is illustrated in Figure 2.22. The microstructural evolution was vastly different where fine zinc additions were used compared to coarse zinc. This phenomenon was termed the particle size effect. Fine zinc powders diffused very quickly into the aluminium and homogenisation was rapid. In this case the liquid phase

existed for a very short period. Where large zinc powders were used, a substantial quantity of liquid phase formed. This was present for approximately 20 minutes (420°C to 620°C at 10°/minute). Observations of the effect of additive particle sizes in Fe-Ti⁽⁵³⁾ and Cu-Sn⁽⁵²⁾ indicate that finer particles can be beneficial, despite reduced liquid formation. Coarse zinc particles generated extensive liquid phase formation which spread among particle and grain boundaries. A substantial degree of vapour phase sintering occurred, as zinc vaporised during the sintering period. When coarse particles were used the microstructure evolved in the following manner:

1. liquid pools formed and increased in size and limited flow occurred along grain and particle boundaries,
2. grains near edge regions of liquid pools were dislodged from Al particles and travelled into the liquid,
3. liquid phase penetrated along particle and grain boundaries, initiating extensive liquid networks.

In contrast, limited sintering occurred where fine particles were used. Mechanisms of sintering present in Al-Zn were found to be consistent with those found in other systems having opposite to ideal solubilities, eg. Fe-Cu.



X is volume fraction distribution.

Figure 2.22 The effect of particle size on compact morphology. Samples were quenched from 610°C into water. Note the area fraction liquid shows three main stages. At small powder sizes there is essentially no liquid present; at larger sizes there is substantially more liquid present. (j is <38µm, i is 38-45µm, h is 45-53µm, g is 53-75µm, f is 75-106µm, e is 106-125µm, d is 125-150µm, c is 150-180µm, b is 180-212µm, and a is 212-250µm)⁽³⁵⁾

Ternary and quaternary alloys based on Al-Zn with additions of magnesium (ternary) and copper (quaternary) have attracted much attention for possible high strength P/M alloys⁽⁹¹⁾, but due to the processing problems associated with these alloys, high strengths have not been attained from elemental blends until recently⁽⁸³⁾. This is attributed to low liquid volumes due to non-ideal solubility ratios and the poor wetting of the aluminium by the liquid phases.

The actual phases which form from elemental powders⁽⁹¹⁾ are:

1. Mg+MgZn₃ eutectic liquid forms in very limited amounts at 343°C where Zn and Mg are in intimate contact. This phase does not wet the aluminium particles.
2. ZnAl+Zn forms a larger amount of liquid, but the high diffusivity and solubility of Zn in solid Al means the liquid disappears quickly and it also does not wet well.
3. Al+Mg₅Al₈ and Al+MgZn₂ do wet the aluminium but volume fraction is low.
4. Al+Al₂Mg₃Zn₃ forms at 489°C and wets the aluminium well but volume fraction is still relatively low
5. No zinc melting is observed because the zinc has already diffused into the aluminium.

A pre-alloyed additive was superior to additions of elemental powders. The composition of the prealloyed powder was 14Al-20.5Mg-53Zn-12Cu, which when added to aluminium powders brought about an alloy of composition Al-7.4Zn-2.8Mg-1.7Cu. Prealloyed additive powders were mostly <5µm in size. These compacts reportedly densified up to >99% of theoretical density when sintered. The prealloyed additive was found by this study to give a sintered product that when peak aged had a maximum tensile strength of 480MPa⁽⁹¹⁾.

2.8.2.6 Metal Matrix Composites Based on Aluminium Powder Metallurgy Alloys

There have been several studies on aluminium metal matrix composites formed via press and sinter operations^(75,96,107-110), based primarily on 2xxx and 6xxx series alloys. These alloys combine the advantages of powder metallurgy processing with properties and characteristics which are tailored to particular requirements⁽¹⁰⁷⁾. For aluminium components, either a lubricating phase^(107,109,110) or a hard phase^(75,96,107,108) can be added to improve wear resistance. The particulate additives that have been studied include mica⁽¹⁰⁹⁾, talc⁽¹⁰⁷⁾ and graphite^(107,110) as a solid lubricant for bearing applications, or TiC^(96,107), alumina^(96,107), WC⁽¹⁰⁸⁾, superalloys⁽⁷⁵⁾, stainless steels, Fe-Si alloys, glass, SiC and ZrSiO₄⁽⁹⁶⁾ for wear resistant alloys. Almost universally the tensile strength of these materials is reduced^(75,96,107-110) by dispersoid additions, although the hardness and/or wear resistance can be dramatically improved. In these materials, dimensional stability can be a problem, as most of the composites studied to this time exhibit additional swelling during the sintering cycle^(75,96,107-110). The exception to this was noted by Danninger⁽⁹⁶⁾ who found that densification could actually be improved by additions of ZrSiO₄, when compared to sintered (2000 series, Alumix123) alloys containing no dispersoids. The reasons for this are unclear, but note was made to the

effect that the adhesion of $ZrSiO_4$ particles to the base material was superior to the other additives tested.

2.8.2.7 *The Effect and Use of Atmospheres in Liquid Phase Sintered Aluminium*

Amongst the atmospheres often used in sintering (nitrogen, vacuum, dissociated ammonia, hydrogen and argon⁽²⁾) nitrogen is the popular choice for use with aluminium based parts. A dew point of at least -40°C is generally considered critical⁽⁷⁵⁾. Due to the high affinity of aluminium for oxygen, the atmosphere must be very pure⁽⁸⁴⁾. Microstructural development of Al-Cu under air and nitrogen was studied by Amato *et al*⁽⁹²⁾. Specimens sintered in air showed a large amount of eutectic segregation at grain boundaries and a heterogeneous structure, due to the poor wetting in the presence of oxygen. Those sintered in nitrogen were homogeneous and good bonding had occurred, presumably due to the inert nature of the atmosphere. The use of nitrogen improved the tensile properties of the alloy by 10% when compared to air.

2.8.2.8 *The Effect and Use of Lubricants in Aluminium Powder Metallurgy*

Appropriate lubricant selection and its subsequent removal from a powder body is crucial for obtaining the desired sintered properties in a powder metallurgy part⁽¹¹¹⁾. The lubricant can serve many different purposes, depending on what is required. The presence of the lubricant ensures even compaction, therefore providing a uniform green density of the part. Also, the friction between metal powders and the die wall is substantially reduced, allowing easy compact ejection and reduced die wear. For powders with low ductility a lubricant that has the effect of binding the powders is essential for attaining stability and reducing damage of the green compact⁽¹¹¹⁾. In addition, lubricants containing lithium are sometimes used to remove water and oxygen from the compact, due to lithiums' affinity for water and oxygen⁽¹¹²⁾. Either internal or die wall lubrication is usually employed in press and sinter operations⁽¹¹³⁾. Die wall lubrication is preferable in terms of sinterability, but internal lubrication is simpler and more consistent. Typical concentrations of (internal) lubricants are between 0.5 and 1.5 wt%. Those used in practice are often organic waxes or stearate compounds based on Al, Zn, Li, Mg or Ca^(1,78). Common commercial lubricants used for aluminium components are Microwax C⁽⁹⁶⁾, Acrawax C⁽⁷⁵⁾, Nopcowax 22, Sterotex⁽⁷⁴⁾, or zinc stearate⁽¹¹⁴⁾.

The important steps involved in lubricant removal are as follows⁽¹¹¹⁾:

1. Heat up until the temperature of vaporisation of the lubricant is reached,
2. transfer the vapour (and often liquid) lubricant from the inside to the surface,
3. remove vapour from the compact, preferably without burning,
4. remove the vapour from the furnace and burn off if required.

Typically, lubricant removal is studied using thermogravimetric analysis^(111,115). This allows thorough characterisation of the dewaxing process.

2.8 Summary

Liquid phase sintering theory is of major importance to gaining a comprehensive understanding of sintering science. A degree of ambiguity has existed, at least until recently, regarding the contribution of various mechanisms to liquid phase sintering. Mechanisms of liquid phase sintering have been debated for over 40 years. Each powder system should be analysed independently, with the understanding that dominant mechanisms may vary between different systems.

Aluminium powder metallurgy has enormous scope for alloy development. Present alloys are generally based on wrought compositions, which may not be the most suitable for P/M processing. Research on aluminium powder metallurgy has been limited. Despite the progress that has been made in the knowledge of sintered aluminium, much of the work conducted has been from a technological view. The production of aluminium based P/M materials is an area requiring further research as component producers move towards using more light metals and improved processing methods. By investigating the science of sintering Al, a thorough understanding of the processes involved can be gained, facilitating alloy development.

This thesis is therefore aimed at analysing the sintering of Al based materials, with additions of Zn, Mg and Cu, singularly and in combination. This includes the effect of select process variables.

Chapter 3 Experimental Methods

3.1 Specimen Preparation

All binary Al alloys contained 1wt% stearic acid except Al-4Cu alloys which contained 0.5% stearic acid. Higher order alloys also contained 0.5wt% stearic acid. Iron-copper alloys contained 1wt% lithium stearate. These powder blends were mixed for ~20 minutes in a Turbula powder mixer. Aluminium specimens for metallography, densification and hardness measurements initially weighed 3 grams and were pressed at 250 MPa to a theoretical density of 88-94%. Iron specimens weighed 4 grams and were pressed at 400 MPa to a theoretical density of ~86%. A bar shaped die (~40mm x ~9mm) or a cylindrical die (D=14.34mm) was used. Tensile specimens weighed 4-4.5 grams and were pressed at 250MPa with the bar shaped die. After sintering and heat treatment these were machined to give a dumbbell shape. Dimensions of these bars were ~40mm x ~9mm x ~2.5mm with a gauge length and width of 20mm and ~4.5mm respectively. Samples for examining the effect of gravity weighed ~5 grams and were pressed at 125MPa in the cylindrical die. All slow cooling experiments were conducted using the cylindrical die and samples had a compaction pressure of 125MPa.

3.2 Particle Size Effect

Starting powder characteristics are given in Table 3.1. The compositions of the systems examined (wt%) are listed in Table 3.2. Figure 3.1 shows SEM micrographs of all powders used. All powders had a purity >99.5%. The copper, tin and zinc size fractions were cropped from a wide as-received distribution. The size distributions for zinc 3, 4 and 5 were determined using a Malvern Instruments Mastersizer (Figure 3.2).

3.3 Effect of Composition

The effect of additive concentration on the sintering of aluminium was examined in binary systems using alloys containing up to 14wt% Mg or Zn, and up to 5%Cu. Zinc 4 and copper 2 were used. Samples containing Mg were reactive with water and were quenched into liquid nitrogen after sintering.

The effect of composition was investigated using ternary and quaternary aluminium alloys. Compositions examined are given in Table 3.3. Zinc 4 and copper 2 were used. The compaction pressure was 250 MPa. Samples were sintered for 1 hour at 600°C.

3.4 Sintering

The sintering cycles used are presented in Table 3.4. Samples were quenched at various stages during the sintering cycle and the microstructures examined using optical and scanning electron microscopy.

Table 3.1. Powder Characteristics

Powder	Fabrication Method	Powder Shape	Powder Sizes	Source
Aluminium	Atomised	Rounded	<150µm	Comalco
Magnesium	Atomised	Flake	<45µm	Cerac
Iron	Electrolytic	Sponge	<150µm	Hogaenas
Copper 1 (coarse)	Gas atomised	Spherical	125-150µm	Alcan
Copper 2 (fine)	Electrolytic	Irregular	<45µm	Cerac
Copper 3	Air atomised	Rounded	<100µm	ACL
Copper 4+	Air atomised	Rounded	<150µm	ACL
Copper 5	Gas atomised	Spherical	75-106µm	Alcan
Tin 1 (coarse)	Atomised	Rounded	125-150µm	ACL
Tin 2 (fine)	Atomised	Rounded	<45µm	ACL
Zinc 1 (coarse)	Atomised	Rounded	125-150µm	Pometon
Zinc 2 (fine)	Atomised	Spherical or Rounded	<45µm	Cerac
Zinc 3	Atomised	Rounded	d50=37µm*	Pometon
Zinc 4	Atomised	Rounded	d50=121µm*	Pometon
Zinc 5#	Atomised	Rounded	d50=71µm*	Pometon

*Particle size distributions are shown in Figure 3.2. #Zinc 5 made by blending equal amounts of zinc 3 and zinc 4. +Copper 4 made by blending equal amounts of copper 3 and a cropped selection (106-150µm) also from ACL.

Table 3.2. Alloy Systems Composition-Particle Size Effect

Binary Alloy Systems and Powders Used		Ternary Alloy Systems and Powders Used		Quaternary Alloy Systems and Powders Used	
Al-10Zn	Zn 1&2	Al-8Zn-2Mg	Zn 1&2	Al-8Zn-2.5Mg-1Cu♦	Zn 1&2
Al-4Cu+	Cu 1-5	Al-8Zn-1Cu#	Zn 1&2		
Al-5.5Cu	Cu 1&2	Al-8Zn-3Cu*	Zn 4, Cu 1&2		
Al-5Sn	Sn 1&2	Al-4.5Cu-1.6Mg	Cu 1&2		
Fe-7Cu	Cu 1&2				

+For examining effect of particle size on mechanical properties.

#For examining zinc particle size effect.

*For examining copper particle size effect.

♦ Zn 3,4&5 used for effect of Zn particle size ranges.

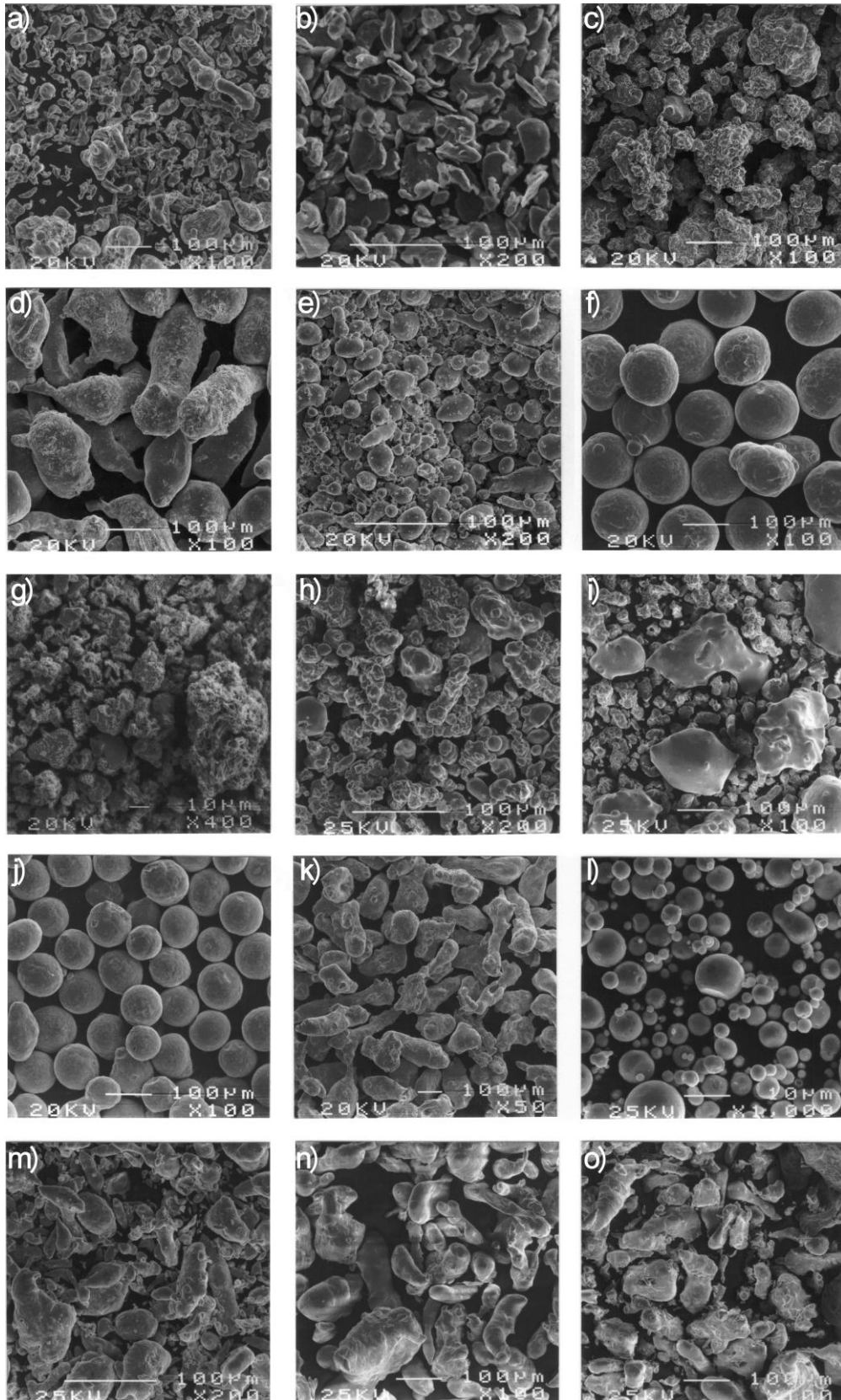


Figure 3.1 SEM micrographs of the starting powders used in experiments. (a) aluminium, (b) magnesium, (c) iron, (d) tin 1, (e) tin 2, (over), (f) copper 1, (g) copper 2, (h) copper 3, (i) copper 4, (j) copper 5, (k) zinc 1, (l) zinc 2, (m) zinc 3, (n) zinc 4, (o) zinc 5.

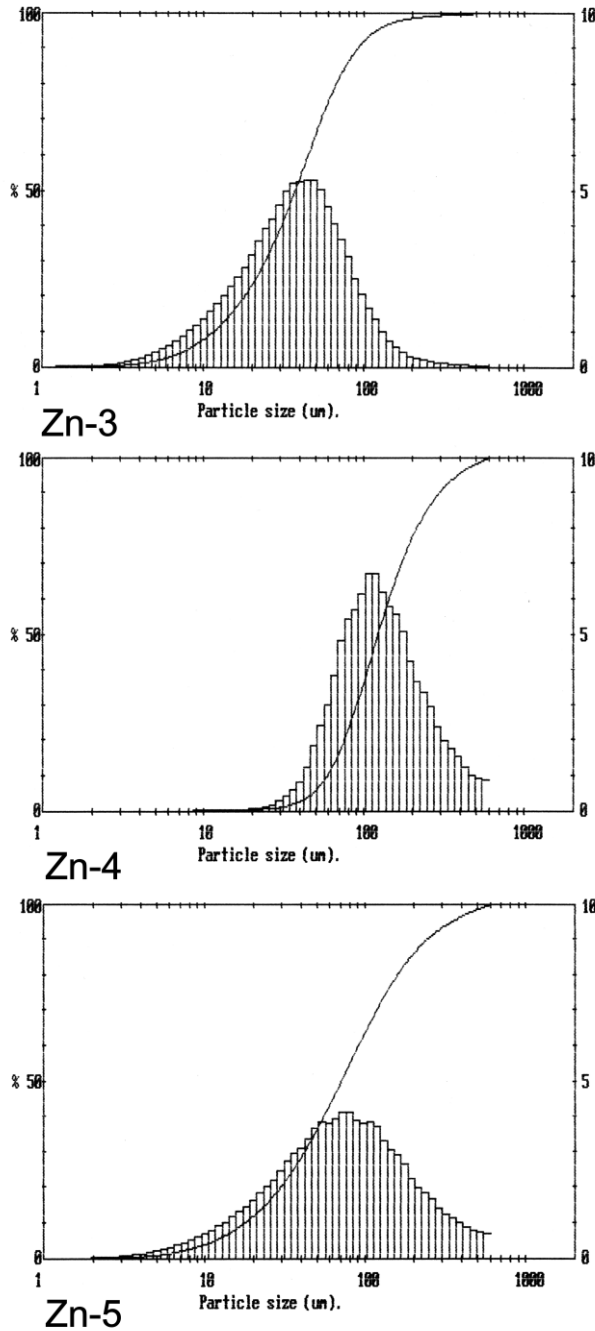


Figure 3.2 Particle size distributions of zinc 3, 4 and 5

3.5 Atmospheres

For the sintering of aluminium a high purity nitrogen atmosphere was used. This atmosphere was dried to better than 0.0005mg/litre of gas (theoretical) residual water content⁽¹¹⁶⁾ using a two step process. The gas passed through a tube containing silica gel and magnesium perchlorate and then through steel wool heated to 400°C. Measurement of residual water content was conducted using a Meeco Inc. Model W Moisture Analyser. This showed a dew point of $\leq -40^{\circ}\text{C}$. For the sintering of iron, a high purity nitrogen atmosphere with no further drying was used.

Table 3.3. Compositions Examined to Determine the Effect of Additive Elements.

Al-8Zn	Al-8Zn-0.5Cu	Al-8Zn-1.0Cu	Al-8Zn-1.5Cu	Al-8Zn-2Cu	Al-8Zn-3Cu
Al-8Zn-0.2Mg	Al-8Zn-0.2Mg-0.5Cu	Al-8Zn-0.2Mg-1Cu		Al-8Zn-0.2Mg-2Cu	Al-8Zn-0.2Mg-3Cu
Al-8Zn-0.5Mg	Al-8Zn-0.5Mg-0.5Cu	Al-8Zn-0.5Mg-1Cu		Al-8Zn-0.5Mg-2Cu	Al-8Zn-0.5Mg-3Cu
Al-8Zn-1Mg	Al-8Zn-1Mg-0.5Cu	Al-8Zn-1Mg-1Cu		Al-8Zn-1Mg-2Cu	Al-8Zn-1Mg-3Cu
Al-8Zn-1.5Mg	Al-8Zn-1.5Mg-0.5Cu	Al-8Zn-1.5Mg-1Cu		Al-8Zn-1.5Mg-2Cu	Al-8Zn-1.5Mg-3Cu
Al-8Zn-2.5Mg	Al-8Zn-2.5Mg-0.5Cu	Al-8Zn-2.5Mg-1Cu		Al-8Zn-2.5Mg-2Cu	Al-8Zn-2.5Mg-3Cu

3.6 Characterisation Techniques

All materials were prepared for microstructural analysis using standard polishing methods. Aluminium alloys were finished on silica. Fe-Cu samples (SEM) were finished on 1 μ m diamond. Aluminium alloys for optical metallography were etched in 0.5% HF for 30 seconds (Al alloys). Compacts for SEM were unetched. Water had to be excluded when polishing Al-Mg and Al-Sn. Ethanol, instead of water, was used as the lubricant in these cases.

DSC was carried out on Al-Zn based alloys using a Perkin Elmer DSC7 under a high purity nitrogen atmosphere. For calibration of temperature and enthalpy pure zinc and one of either indium or tin were used for lower temperature cycles (25°C-500°C), while pure zinc and aluminium were used for calibration of cycles between 300°C and 650°C. Thermogravimetry (TGA) was performed using a Perkin Elmer Thermogravimetric analyser (TGA7).

Al-Mg samples for TEM were air cooled. Thinning was accomplished by employing the window technique with a solution of 10% perchloric acid in methanol at ~0°C using a Struers Polipower unit. TEM analysis was performed with a Jeol 4000FX microscope with LINK EDS facilities operating at 400keV. A Jeol 6400F scanning electron microscope was used for all SEM metallography and quantitative analysis. Quantitative image analysis was performed on Al-Sn, Al-Zn (particle size effect) and Al-Zn-Mg-Cu alloys (effect of gravity) using a Cambridge Instruments Quantimet 570 in conjunction with a JVC KY-F30 colour camera. Backscattered electron images taken at various magnifications covering the entire specimen were used for quantitative analysis to ensure accuracy. This gave a 95% confidence interval with confidence limits of $\pm 10\%$. XRD was conducted using a Phillips X-ray diffractometer with CuK α radiation. Measurement of dihedral angles was conducted by tracing at least 20 angles per condition onto paper and measuring the angles with a protractor.

Table 3.4 Sintering Cycles

Alloy System	Sintering Cycle	Purpose
Al-Zn, Al-Cu, Al-Zn-Mg, Al-Zn-Cu, Al-Zn-Mg-Cu	Heated at 10°C/min. to a dewaxing temperature of 300°C for 20 min., then heated at 10°C/min. to 600°C and sintered for 1 hour.	Effect of increasing additions of Zn, Mg and Cu in aluminium alloys
Al-Sn	Heated at 10°C/min. to a dewaxing temperature of 200°C for 30 min., then heated at 10°C/min. to 600°C and sintered for times up to 1 hour.	Particle size analysis
Al-Zn	Heated at 1,10 and 40°C/min. to a dewaxing temperature of 350°C for 20 min., then heated at 1,10 and 40°C/min. to 620°C and sintered for times up to 10 min.	Particle size analysis
Al-Cu	Heated at 10°C/min. to a dewaxing temperature of 350°C for 20 min., then heated at 10°C/min. to 600°C and sintered for times up to 40 min.	Particle size analysis
Al-Cu	Heated at 10°C/min. to a dewaxing temperature of 300°C for 20 min., then heated at 10°C/min. to 600°C and sintered for times up to 40 min.	The effect of particle size on mechanical properties
Al-Zn-Mg	Heated at 10°C/min. to a dewaxing temperature of 300°C for 20 mins., then heated at 10°C/min. to 600°C.	Particle size analysis
Al-Cu-Mg	Heated at 10°C/min. to a dewaxing temperature of 300°C for 20 min., then heated at 10°C/min. to 600°C and sintered for times up to 1 hour.	Particle size analysis
Al-Zn-Cu	Heated at 10°C/min. to a dewaxing temperature of 300°C for 20 min., then heated at 10°C/min. to 600°C and sintered for times up to 1 hour.	Particle size analysis
Al-Zn-Mg-Cu	Heated at 10°C/min. to a dewaxing temperature of 300°C for 20 min., then heated at 10°C/min. to 620°C and sintered for times up to 2 hours.	Particle size analysis
Al-Mg	Heated at 10°C/min. to a dewaxing temperature of 250°C for 20 min., then heated at 10°C/min. to 550°C and sintered for times up to 1 hour.	Effect of increasing Mg additions, also TEM analysis of oxides
Fe-Cu	Samples inserted at 600°C and held at this temperature for 20 min. for dewaxing, then heated at 10°C/min. to 1150°C and sintered for times up to 12 hours.	Particle size analysis

Sintered density measurements were obtained by following the MPIF standard 42 except that alcohol was used instead of water wherever magnesium was present in samples. Densification was determined using equation 3.1⁽³⁾

$$\psi = \frac{\rho_s - \rho_g}{\rho_t - \rho_g} \quad (3.1)$$

Where ψ is the densification parameter, ρ_s the sintered density, ρ_g the green density and ρ_t the theoretical density. Theoretical densities were determined using equation 3.2.

$$\rho_t = \sum_{i=1}^t \rho_i n_i / n \quad (3.2)$$

where ρ_i is the density of element i , n_i is the weight% of element i divided by the atomic weight of element i , ie. $n_i = \text{wt}\%i / (\text{atwt})i$, t is the number of elements in the alloy and n is the total number of moles given by equation 3.3:

$$n = \sum_{i=1}^t n_i \quad (3.3)$$

3.7 Heat Treatment

For Al-4Cu alloys which were to be tensile tested, the T4 condition was used. Samples were solution treated at 540°C for 1 hour and water quenched, then left to attain the T4 condition in 10-11 days. For quaternary Al-Zn-Mg-Cu alloys, solution treatment was conducted at 490°C, then artificial ageing at 180°C for 16 hours.

3.8 Mechanical Properties

Hardness measurements (Rockwell H and E) were conducted following standard Rockwell testing procedures⁽¹¹⁷⁾ and at least 5 hardness measurements were taken for each condition tested. For tensile testing an Instron (screw drive) tensile machine with a 10 KN load cell was used. Strain rate was 0.6mm/min. and strain was measured by an Instron model 2620/603 dynamic extensometer with a full scale range of 1mm.

3.9 The Effect of Gravity

The effect of gravity was examined in the quaternary Al-8Zn-2.5Mg-1Cu system. Zinc 4 and Copper 2 were used. Quantitative analysis of area fraction liquid phase for the alloy sintered 2 hours at 620°C was conducted on four positions of the sample, being at 1,5,9 and 13mm from the top or bottom centre of the sample. Eleven backscattered SEM micrographs were taken for each position (1 centrally and 5 either side over the whole width of the sample).

3.10 The Effect of Cooling Rate

The effect of cooling rate was examined in the quaternary Al-8Zn-2.5Mg-1Cu alloy sintered 2 hours at 620°C then cooled at 2°C/min. to 200°C. Zinc 4 and copper 2 were used in these experiments. Again, for these experiments, samples for further analysis were quenched from various temperatures in the cooling cycle.

Chapter 4 Results

4.1 The Effect of Zinc on Sintering Aluminium

Compositions up to 14wt% Zn were examined. There is a linear relationship between sintered density and Zn concentration for Zn additions between 0 and 14 % (Figure 4.1). Hardness measurements indicate that the properties gradually increase with Zn concentration, but appear to reach a limit at approximately 10% Zn.

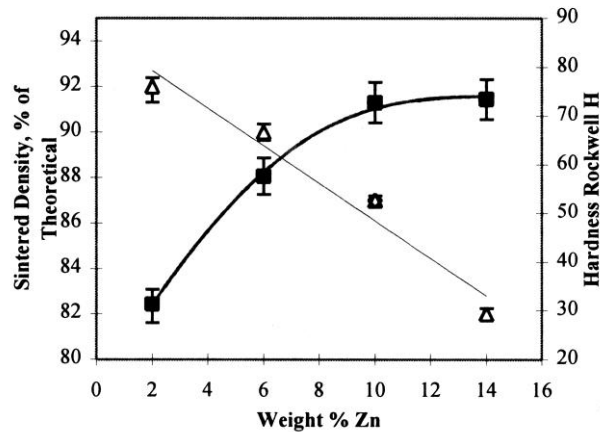


Figure 4.1 The effect of increasing zinc concentration on sintered density (open triangles) and on sintered hardness (closed squares).

The effect of compaction pressure on the green and sintered density for Al-10Zn is presented in Figure 4.2 and 4.3. The green density of compacts follows a logarithmic relationship with compaction pressure (Figure 4.2). The maximum sintered density and hardness both occur at 500 MPa although the values do not change appreciably above 250 MPa. The sintered density as a function of green density is shown in Figure 4.3. The microstructural evolution of Al-Zn alloys is presented in section 4.4.1.

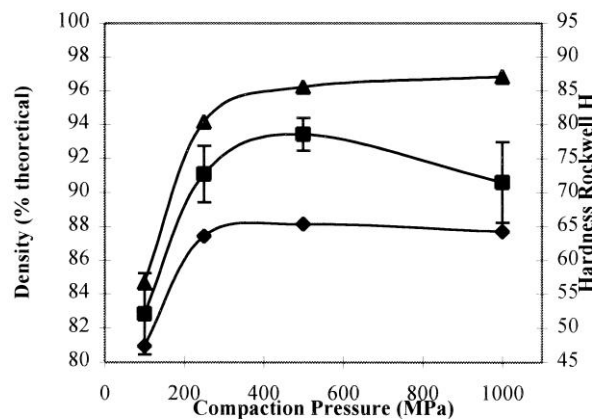


Figure 4.2 The effect of compaction pressure on green density (triangles), sintered density (diamonds) and sintered mechanical properties (squares) for Al-10Zn. Error on all density measurements was <0.7% (1 standard deviation).

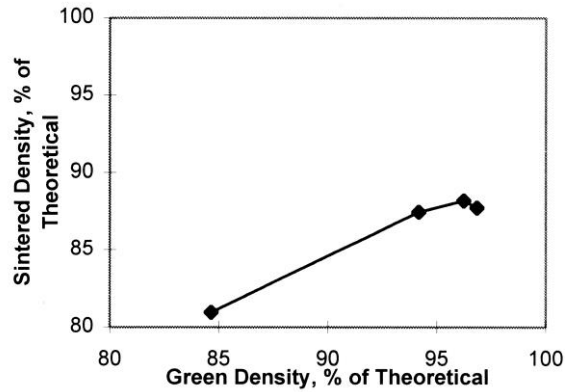


Figure 4.3 The sintered density as a function of the green density for the 4 pressures tested. Compaction pressure is increasing to the right of the plot. There is a departure from linearity at very high compaction pressures, due to the sintered density passing through a peak at ~500 MPa.

4.2 The Effect of Copper on Sintering Aluminium

Copper additions between 1 and 5 wt% were tested. Green densities were approximately 93% of theoretical. The relationship between sintered density, hardness and wt% copper additions is shown by Figure 4.4. The sintered density decreases linearly with Cu additions up to 3wt%. Above 3% Cu, the sintered density increases rapidly and appears to increase no further above 4% Cu. The hardness rises almost linearly with increasing wt% Cu additions up to 4% Cu, after which there is no further increase. The microstructural evolution of Al-Cu alloys is presented in section 4.4.2.

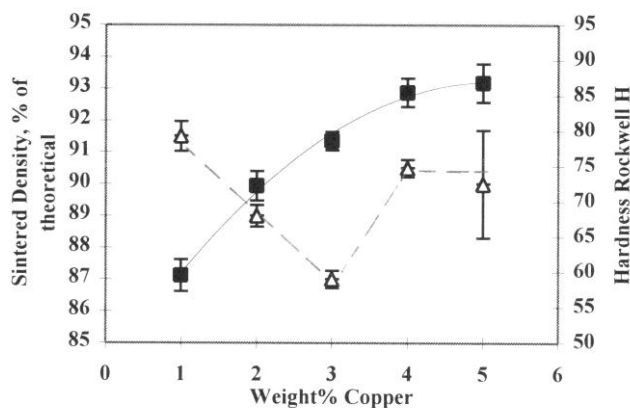


Figure 4.4 The effect of copper additions on sintered density (open triangles) and sintered mechanical properties (closed squares).

4.3 The Effect of Magnesium on Sintering Aluminium

Compositions up to 14 wt% Mg were examined. There is a linear relationship between sintered density and Mg concentrations between 0 and 14% (Figure 4.5) for samples sintered at 550°C for 1 hour. Although the sintered density decreases linearly with increasing Mg content, hardness values are independent of density. There were two

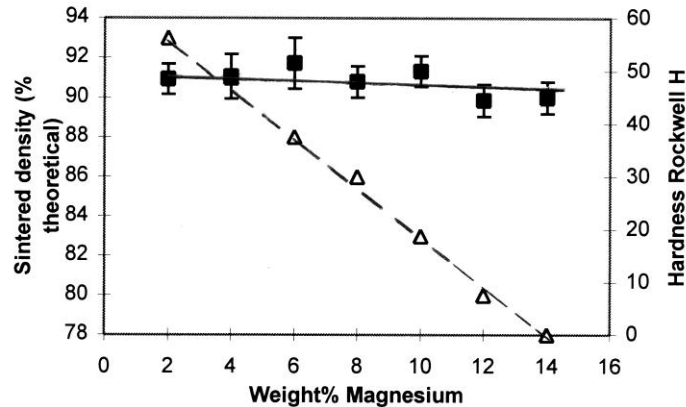


Figure 4.5 The relationship between wt% Mg additions, sintered density and hardness. Square points are hardness values. Error on density is negligible.

major melting endotherms in the DSC spectra at 437°C and 450°C (Figure 4.6), corresponding to the two eutectic temperatures for this system. Microstructures of high Mg samples (>6%) showed that at 445°C there is evidence of eutectic formation at Mg particle sites (Figure 4.7). At 455°C, all the Mg had reacted (Figure 4.8). At 465°C, the material appeared to be approaching equilibrium, and no liquid remained (Figure 4.9). However, for lower Mg concentration samples (2.5% Mg), the reaction sequence was slower and although only limited liquid formed, there was evidence of its presence up to 525°C (Figure 4.10). For the persistent system (Al-14Mg), some supersolidus liquid returns later in the sintering cycle. This was determined by rerunning the same sample in the DSC and observing the difference in the area under the eutectic melting endotherms. This was calculated at 15% of the original liquid (Figure 4.6) (assuming that the endotherm of melting is directly proportional to the amount of liquid present). Al-0.2Mg samples were tested using DSC to examine if Mg diffuses into the Al during the dewaxing cycle. The dewaxing cycle was simulated by holding at selected temperatures. These results are shown in Figure 4.11 and indicate that the amount of melt formed decreases rapidly above a dewaxing temperature of 300°C. TGA of Al-6Mg showed 3 major effects during the sintering cycle (Figure 4.12). There are two weight loss events at ~13 minutes (128°C) and at 46 minutes (310°C). At 65 minutes (500°C) a weight gain is noted which continues through to the end of sintering.

4.3.1 The role of magnesium in oxide disruption

TEM was conducted on an Al-2.5 Mg alloy heated to 550°C and air cooled. The measured lattice spacings on the diffraction pattern taken from a region exhibiting a structure of fine crystals (Figure 4.13) are presented in Table 4.1. These showed a high correlation with the accepted values⁽¹¹⁸⁾ for cubic spinel, MgAl₂O₄. EDS of this region showed aluminium, magnesium and oxygen to be the predominant elements in this area (Figure 4.14a). EDS of a nearby aluminium region is presented in Figure 4.14b. This scan exhibits a larger Al peak and reduced Mg and O peaks than those in Figure 4.14a.

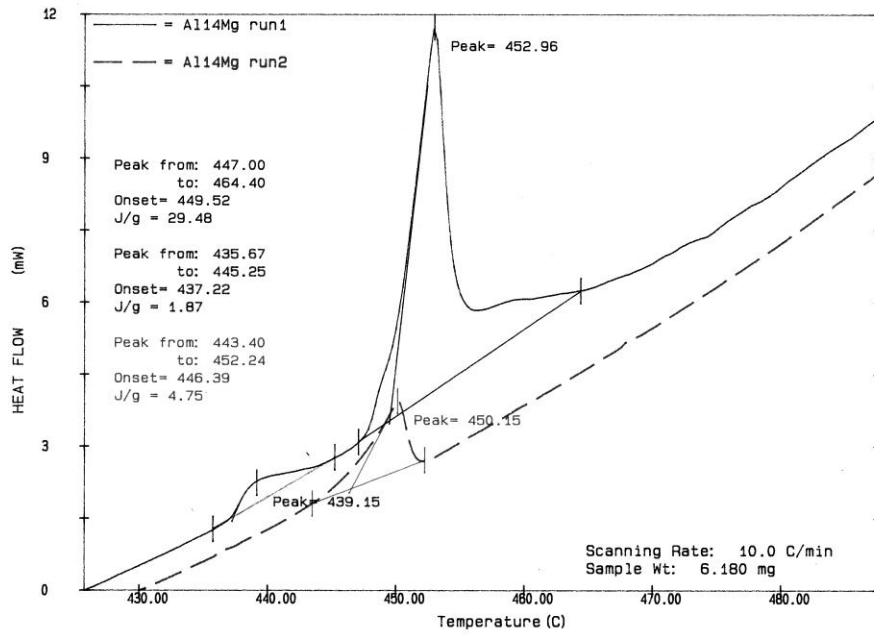
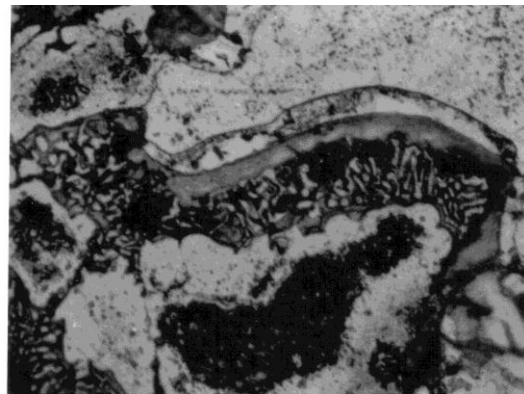
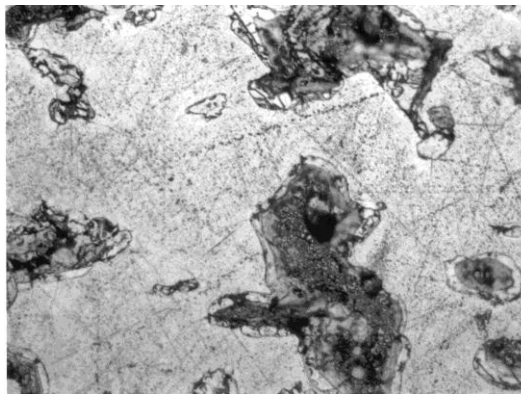


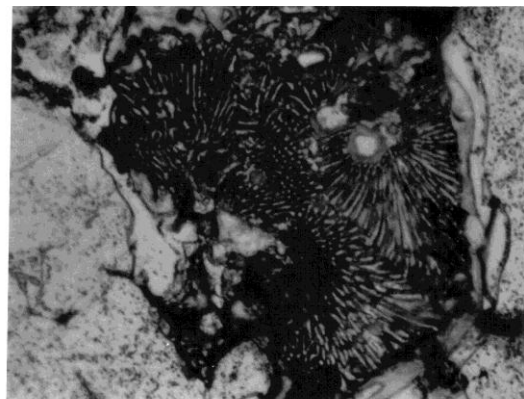
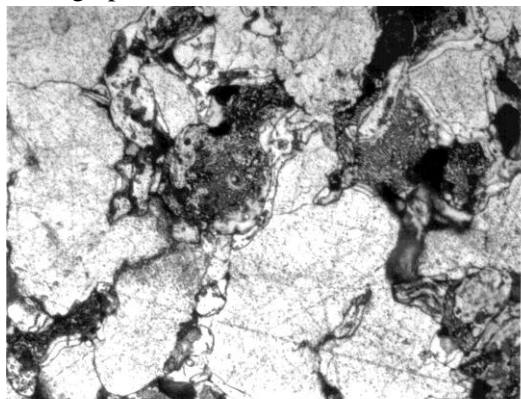
Figure 4.6 DSC of Al-14Mg showing two eutectic melting peaks for run 1 (solid top line) and reduced melting peak for run 2 (dashed line).



50µm

15µm

Figure 4.7 Initial liquid formation in an Al-14 Mg alloy quenched from 445°C. Optical micrographs.



50µm

15µm

Figure 4.8 The liquid phase present in an Al-14Mg alloy quenched from 455°C. Optical micrographs.

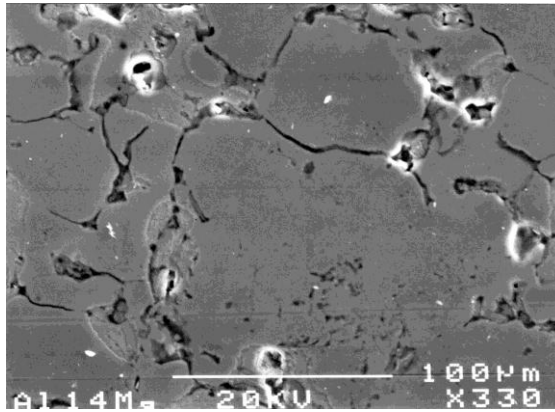
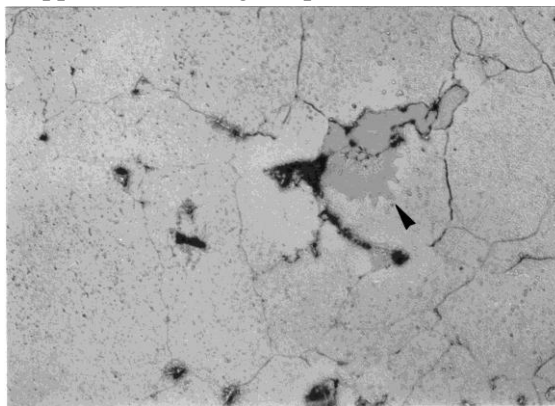


Figure 4.9 Backscattered SEM micrograph showing that no liquid remains in an Al-14Mg alloy quenched from 465°C. It appears that all Mg has passed into solution.



50 μm

Figure 4.10 Evidence of remaining liquid in a low Mg (2.5 wt%) alloy quenched from 525°C. The liquid phase is arrowed. Optical micrograph.

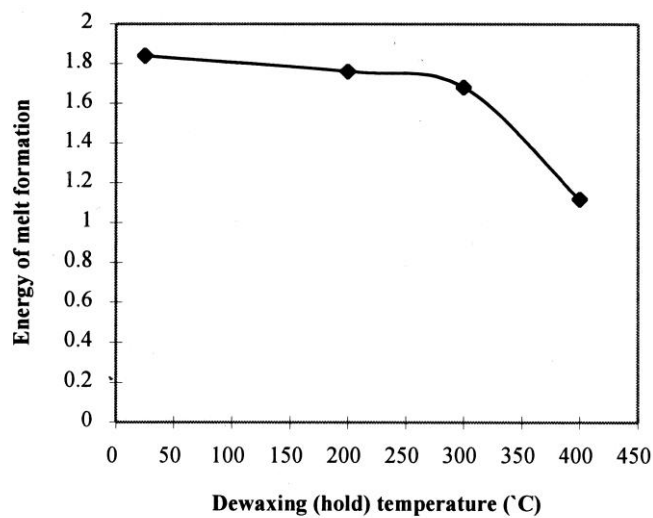


Figure 4.11 Energy of melt endotherms (area under the peaks) as a function of dewaxing temperature for Al-0.2Mg materials held in the DSC at varying temperatures to simulate the dewaxing cycle.

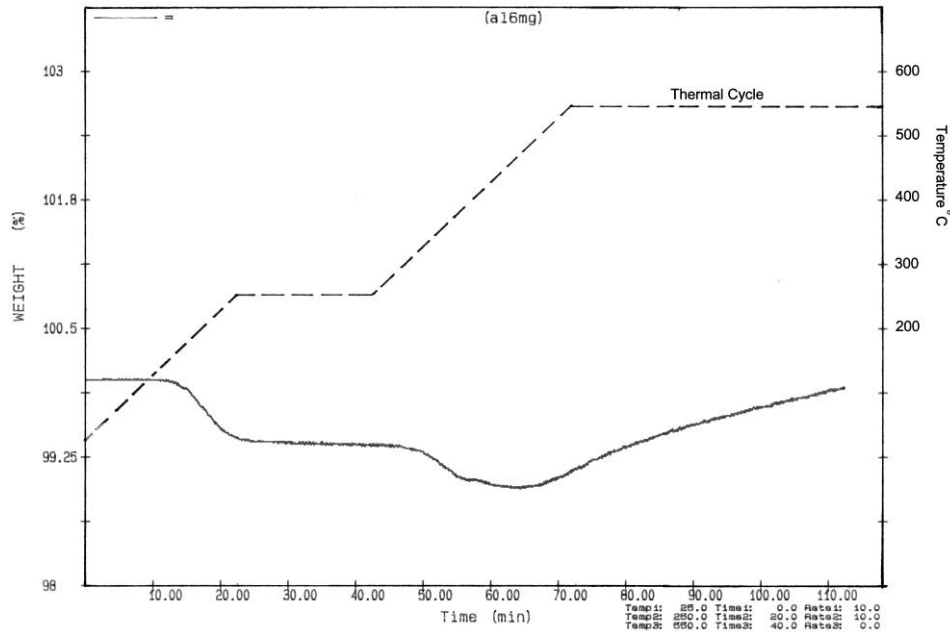


Figure 4.12 Thermogravimetric analysis of an Al-6Mg alloy exhibiting 2 weight loss events and a weight gain at the sintering temperature.

4.4 The Particle Size Effect in Binary Systems

4.4.1 Al-Zn

The microstructural evolution of aluminium sintered with coarse and fine zinc powders at 10°C/minute (up to 620°C and held 10 minutes) is illustrated in Figures 4.15a-d for coarse zinc powders and in Figures 4.15e-h for fine zinc powders. Where fine zinc particles were used, there was limited reaction with the aluminium up to 525°C (Figure 4.15e). The zinc was completely absorbed by the aluminium by the time the compact had reached 580°C (Figure 4.15f) and the alloy was homogeneous by 620°C (Figures 4.15g&h). The structure that forms is virtually unsintered; that is, there is very limited connectivity. However, substantially different structures result where coarse zinc particles are used. There is limited reaction between Zn and Al by 525°C, but this is not widespread. Most Zn particles are unreacted (Figure 4.15a). Note that the reaction does not begin until ~140°C above the eutectic temperature (381°C) and ~100°C above the melting point of zinc. Also, the reaction occurs not at a particular temperature, but over a temperature range. Once the compact (coarse Zn) reaches 580°C, all primary zinc particles have reacted, forming large liquid pools and initiating liquid phase sintering (Figure 4.15b.). At 620°C, an extensive liquid skeleton network is observed, as in Figure 4.15c. This spreads quickly to its maximum extent. Over the following 10 minutes the zinc diffuses into the matrix, and the alloy becomes homogeneous (Figure 4.15d).

DSC of Al-10Zn indicated that the endotherm of melting for fine zinc powders (~6J/g) was always less than that for coarse zinc powders (~10J/g) (Figure 4.16). No eutectic melting peak was observed. The effect of zinc particle size on liquid formation was

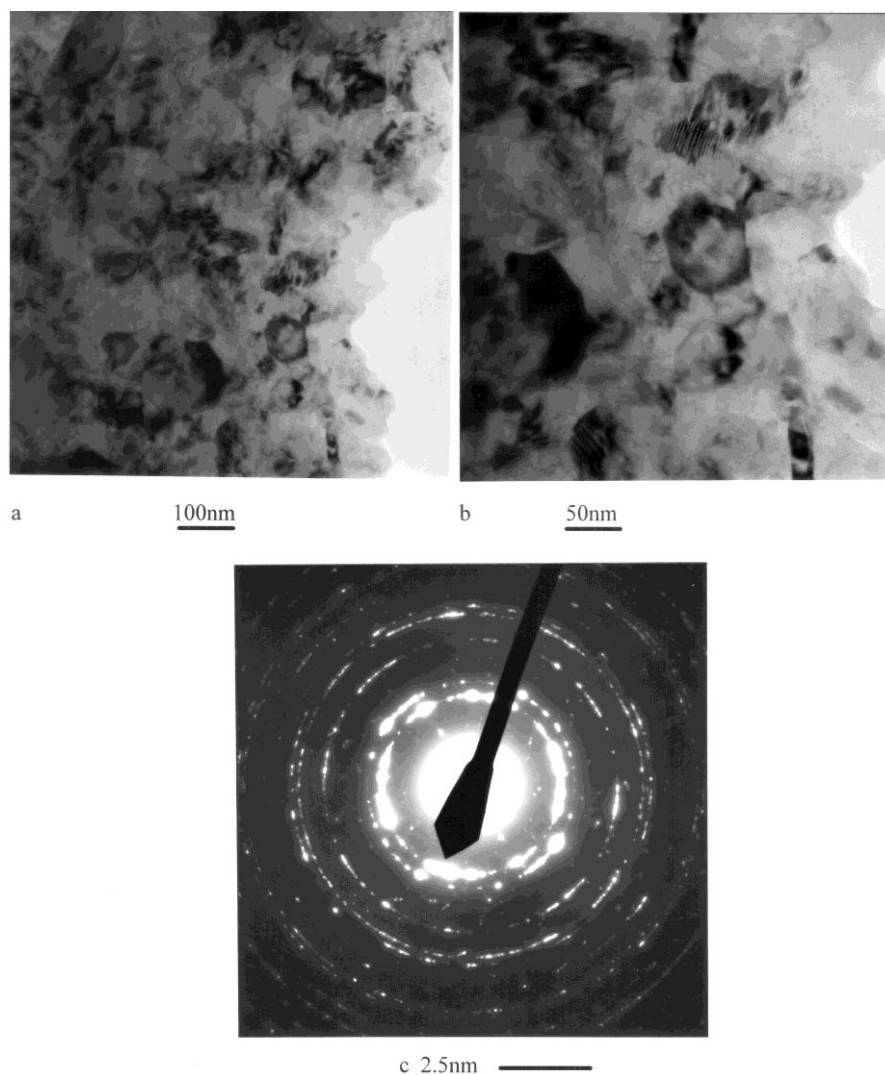


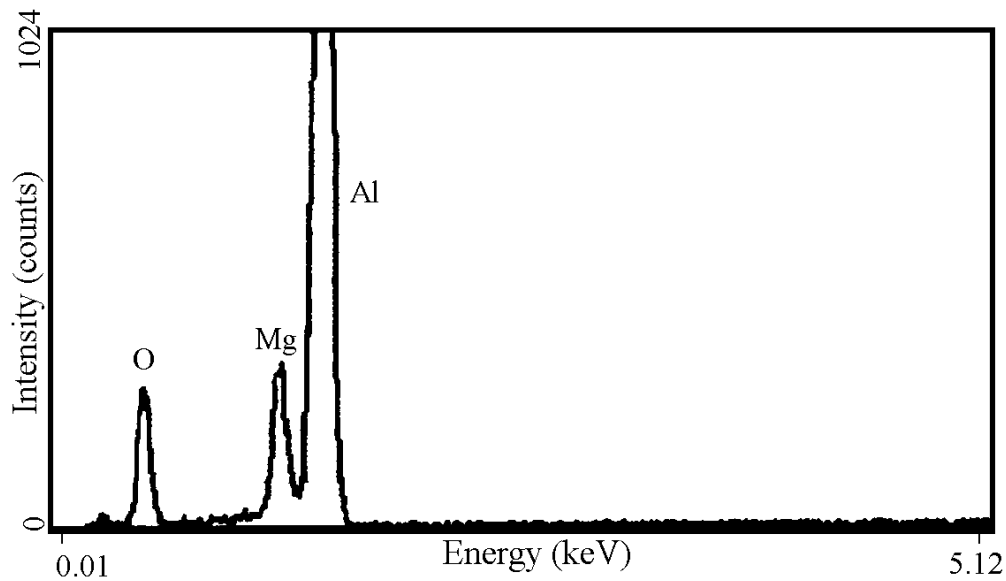
Figure 4.13 TEM micrographs of a region of sintered Al-2.5Mg. Figures (a) and (b) show the crystalline structure of the area examined. Figure (c) is the diffraction pattern taken from the region in (b). Interplanar -spacings taken from the diffraction pattern are given in Table 4.1 and show a high correlation to the accepted values for spinel, $MgAl_2O_4$. EDS of this region and a nearby aluminium region are shown in Figure 4.14.

Table 4.1. Interplanar Spacings For Spinel

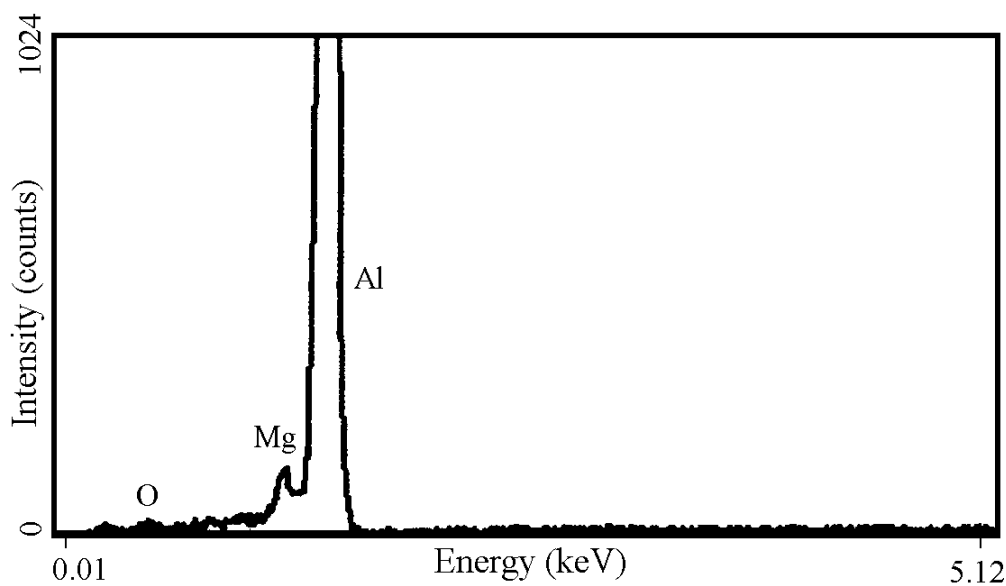
Experimental interplanar spacings of the oxide phase.	Interplanar spacings for spinel ⁽¹¹⁸⁾	h k l	Difference(%)
--	4.66	1 1 1	
2.778	2.858	2 2 0	3
2.439	2.437	3 1 1	0
2.272	2.335	2 2 2	3
2.041	2.02	4 0 0	1
1.72	1.65	4 2 2	4
1.538	1.555	5 1 1	1
1.389	1.4289	4 4 0	3

examined using quantitative SEM by measuring the volume fraction liquid phase that developed over time. These results are shown in Figure 4.17. Not only is the liquid phase present for three times longer when coarse zinc particles are used instead of fine zinc particles, the maximum amount of liquid formed is more than doubled.

The effect of heating rate on the Al-Zn system was also examined. At high heating rates (40°C/min.) the quantity of liquid phase is increased for fine powders (Figure 4.18a&b), but the particle size effect is still apparent. At very low heating rates (1°C/min.) liquid phase sintering is negligible for both coarse and fine powders (Figure 4.18c). The zinc diffuses away from prior zinc particle sites by 450°C, whether coarse or fine, without



a



b

Figure 4.14. EDS scans taken from (a) the region of fine crystals shown in Figure 4.13, and (b) a nearby aluminium region.

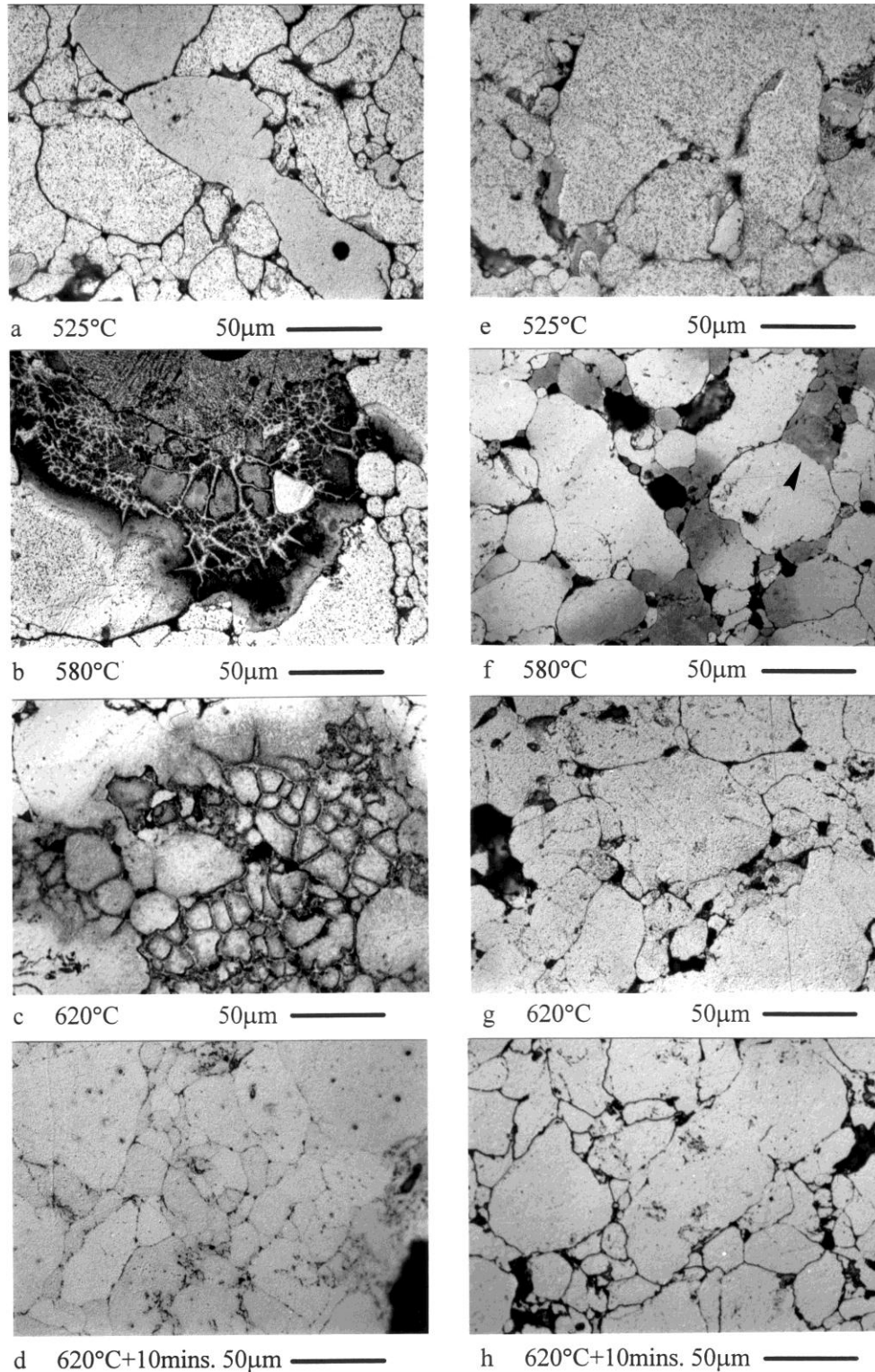


Figure 4.15. The microstructural evolution of aluminium sintered with zinc. Typical optical micrographs of structures formed at various stages of sintering; a-d are for coarse zinc powders, e-h are for fine zinc powders. Note the extensive liquid fraction that forms with coarse zinc powders (b), which flows around particles and grains (c) leaving a well sintered structure(d). Comparative microstructures for fine zinc powders show only solid state diffusion. Dark areas (arrowed) in (f) are zinc diffusion zones around prior zinc particles, now pores. Little liquid forms, and the resultant microstructure is poorly sintered (h).

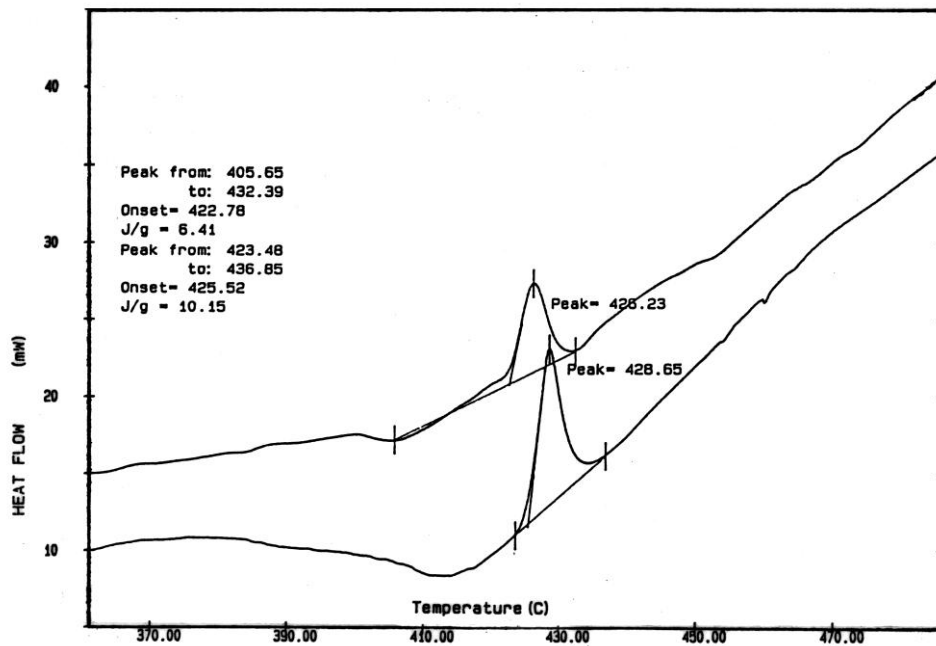


Figure 4.16 DSC spectra of Al-10Zn alloys exhibiting reduced energy of melt formation when fine Zn powders were used as the additive. The spectra for the coarse Zn (bottom line) has an area under the curve of 10.15 J/g, and the spectra for the fine Zn (top line) has an area under the curve of 6.41 J/g.

instigating liquid phase sintering. The microstructures remain unchanged through to the end of sintering. Additionally, at high heating rates (40°C/min.) where coarse zinc powders were used, the manner in which the liquid interacts with the matrix when the liquid flow is maximised is different to a moderate heating rate (10°C/min.) (compare Figure 4.18a with 4.15c). It is noteworthy that more interparticle liquid flow and less grain boundary attack has occurred where heating rates were high.

4.4.2 Al-Cu

The microstructural evolution of Al-5.5Cu for coarse and fine copper powders is shown by Figure 4.19. The sintering liquid is a eutectic (Al-CuAl₂) which forms above 548°C. There was little or no reaction between the Al and Cu for both fine and coarse powders at 550°C. At 575°C, melt pools have formed around coarse Cu particles (Figure 4.19b), whereas limited liquid forms with fine Cu powders (Figure 4.19g). At 600°C, the fine powders had all reacted and the volume of liquid phase had reached a maximum (Figure 4.19i). The remaining Cu diffuses rapidly into the Al matrix over the following five minutes and the system approaches equilibrium (Figure 4.19j). There is no significant change over the next 35 minutes (Figure 4.19k and 4.19l). For coarse Cu powders, however, the case is very different. At 600°C, liquid seams have penetrated grain and particle boundaries and many of these grains move into the melt pools (Figure 4.19c). This continues for the remainder of the sintering time and extensive liquid networks form (Figure 4.19d). The sintering at 600°+40 minutes is thorough, especially in

comparison to that for fine powders (compare Figures 4.19e and 4.19k). The density increase for samples containing fine copper powder was ~3%, giving a sintered density of ~92% of theoretical; the density increase for coarse sizes was ~7%, giving densities of ~94% of theoretical.

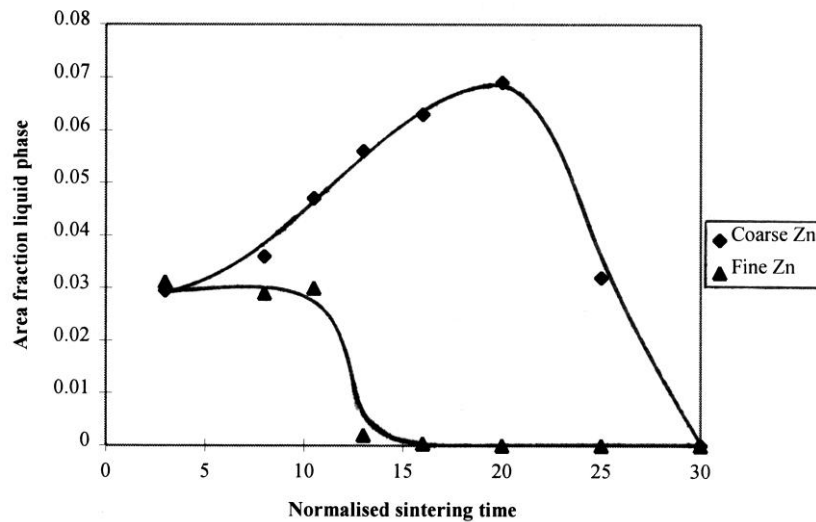


Figure 4.17 A quantitative analysis of area fraction liquid phase for coarse and fine zinc powder additions. The normalised sintering time is the time for which the sample was above the melting point of the liquid forming phase. It is notable that the Zn powder size greatly effects the quantity of liquid phase developed.

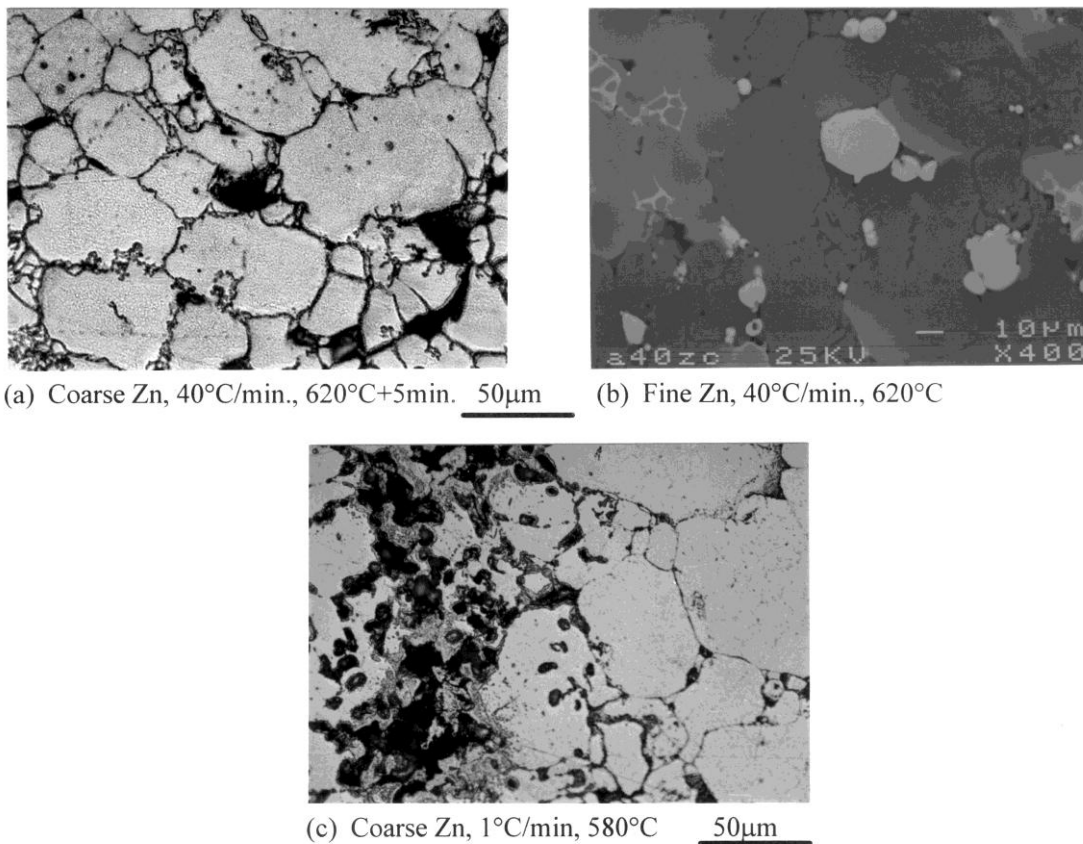


Figure 4.18. The effect of heating rate on the particle size effect in Al-10Zn alloys. ((a)&(c) are optical micrographs, (b) is backscattered SEM.)

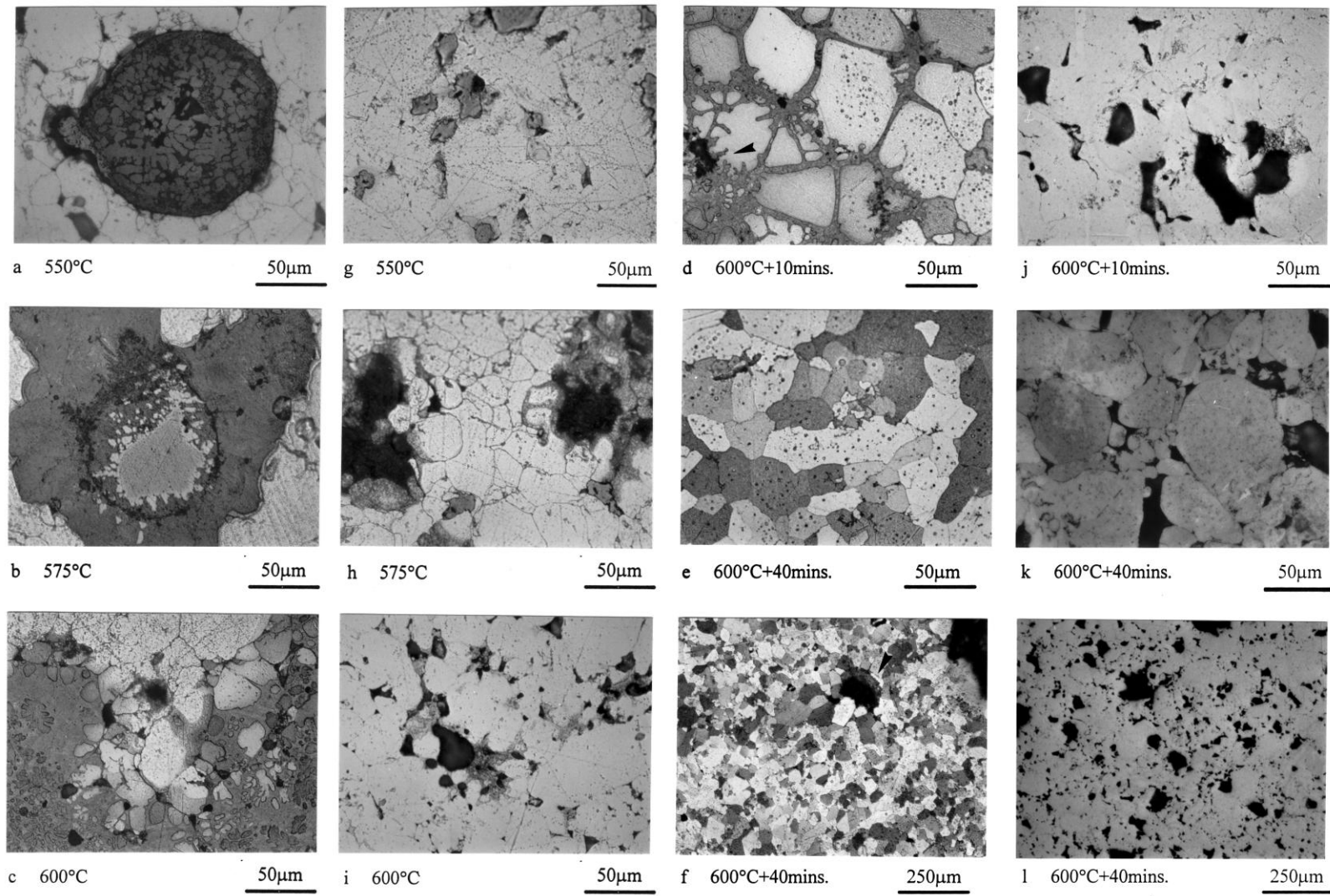


Figure 4.19 Typical optical micrographs of Al-5.5Cu comparing the effect of copper particle size on the sintering of aluminium (a-f coarse particles, g-l fine particles). More liquid develops and the structures are better sintered where coarse rather than fine powders were used. The remaining equilibrium liquid phase is arrowed in (f).

The tensile properties of Al-4Cu in the T4 condition for the 5 copper sizes examined are shown in Table 4.2 and Figure 4.20. Corresponding densification values for these samples (as sintered) are shown in Figure 4.21. Optical micrographs of the sintered and aged material are shown in Figure 4.22(a-e). SEM fractography was conducted on representative samples from each condition tested (Figure 4.23(a-e)). Where fine additive particles were used (Figure 4.23a), the fracture surface is relatively planar. Where coarse particles were present a large pore size was evident on the fracture surface (eg. Figure 4.23e) and the fracture is of a more angular nature. It should be noted also that for the coarsest particle size examined, that crack initiation did not start from secondary pores. Rather the fracture started from regions which had a fine pore size but poor bonding (Figure 4.24). However, as seen in Figure 4.20, the mechanical properties pass through a maximum before decreasing at coarser additive sizes despite the increase in pore size. Figure 4.25 displays typical load-displacement curves for samples having the three cropped particle sizes. It is noteworthy that the 0.2% proof stress is essentially equivalent for all three conditions tested, with the major difference being the plastic strain and hence tensile strength. Tensile tests were also performed on Al-4Cu with the smallest particle size (<45 μ m) sintered with the maximum attainable heating rate. This was achieved by placing samples in a furnace preheated to 600°C and eliminating the dewaxing cycle. The samples reached the sintering temperature in under 10 minutes and were sintered for 40 minutes. Tensile properties for this condition are given in Table 4.2. The optical micrograph and SEM fractograph for this condition are shown in Figure 4.22f and 4.23f respectively.

TABLE 4.2 Tensile Properties of Al-4Cu (T4 condition)

Additive particle size	Proof stress (MPa) (0.2% strain)	UTS (MPa)	Strain at failure %	Sintered Density (% theoretical)	Densification parameter
<150 μ m	120	187	4.89	87	-0.892
<100 μ m	124	203	6.22	87	-0.796
<45 μ m	118	187	4.75	89	-0.485
75-106 μ m	127	217	7.26	90	-0.457
125-150 μ m	120	176	3.82	90.5	-0.505
<45 μ m, *	139	231	6.73	91	-0.32

* Samples were placed directly into the furnace at 600°C with no dewaxing cycle. Samples reached the sintering temperature in approximately 10 minutes. Other samples were heated at 10°C/min.

4.4.3 Al-Sn

A quantitative analysis for the Al-Sn system of the amount of liquid phase developed with time (and temperature) is shown in Figure 4.26. It is noteworthy that the amount of liquid phase is independent of particle size. The microstructures developed from coarse and fine Sn powders are shown in Figures 4.27a-c and 4.27d-f, respectively. Despite tin's low melting point (232°C) there did not appear to be liquid flow until 550-575°C (Figure 4.27b). The compacts containing coarse tin powders developed similar

microstructures to those with fine powders, but only after longer times (compare Figures 4.27c&e).

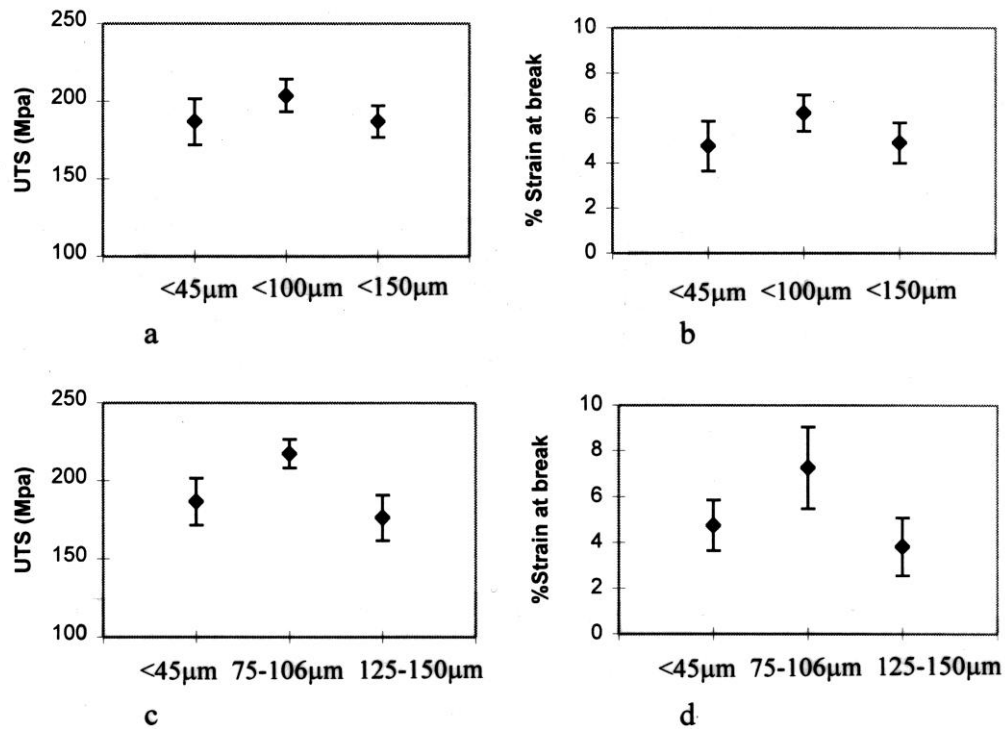


Figure 4.20. Mechanical properties (T4) as a function of copper additive particle sizes. Tensile strength (MPa) and strain (%) at failure is shown on each plot. (a&b) are for the three size ranges examined, and (c&d) for the three cropped sizes. (Error is for a 95% confidence interval).

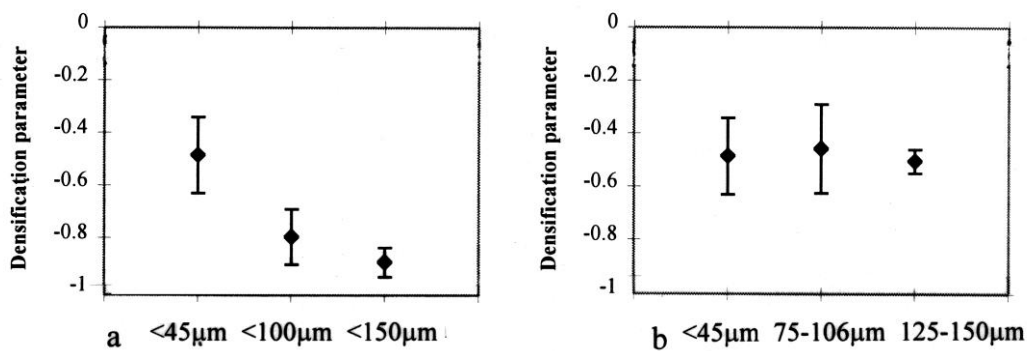


Figure 4.21. Densification as a function of copper additive particle sizes. (a) is for the three size ranges examined, and (b) for the three cropped sizes. (Error 1 standard deviation).

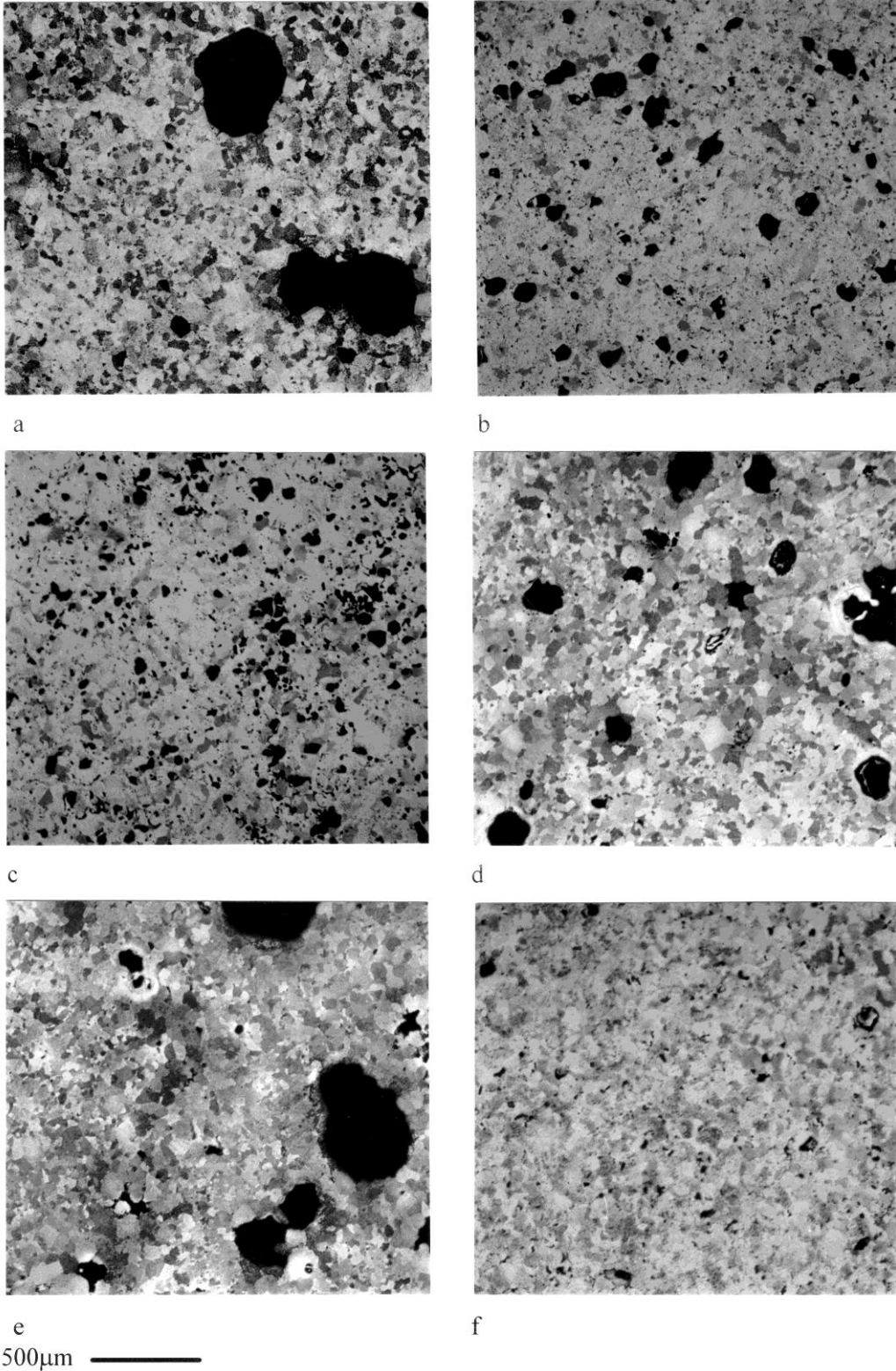


Figure 4.22 Optical sections for Al-4Cu of the 5 conditions tested exhibiting secondary pore sizes. (a) is <math><150\mu\text{m}</math> Cu, (b) is <math><100\mu\text{m}</math> Cu, (c) is <math><45\mu\text{m}</math>, (d) is $75\text{-}106\mu\text{m}$, (e) is $125\text{-}150\mu\text{m}$ and (f) is <math><45\mu\text{m}</math> at a high heating rate.

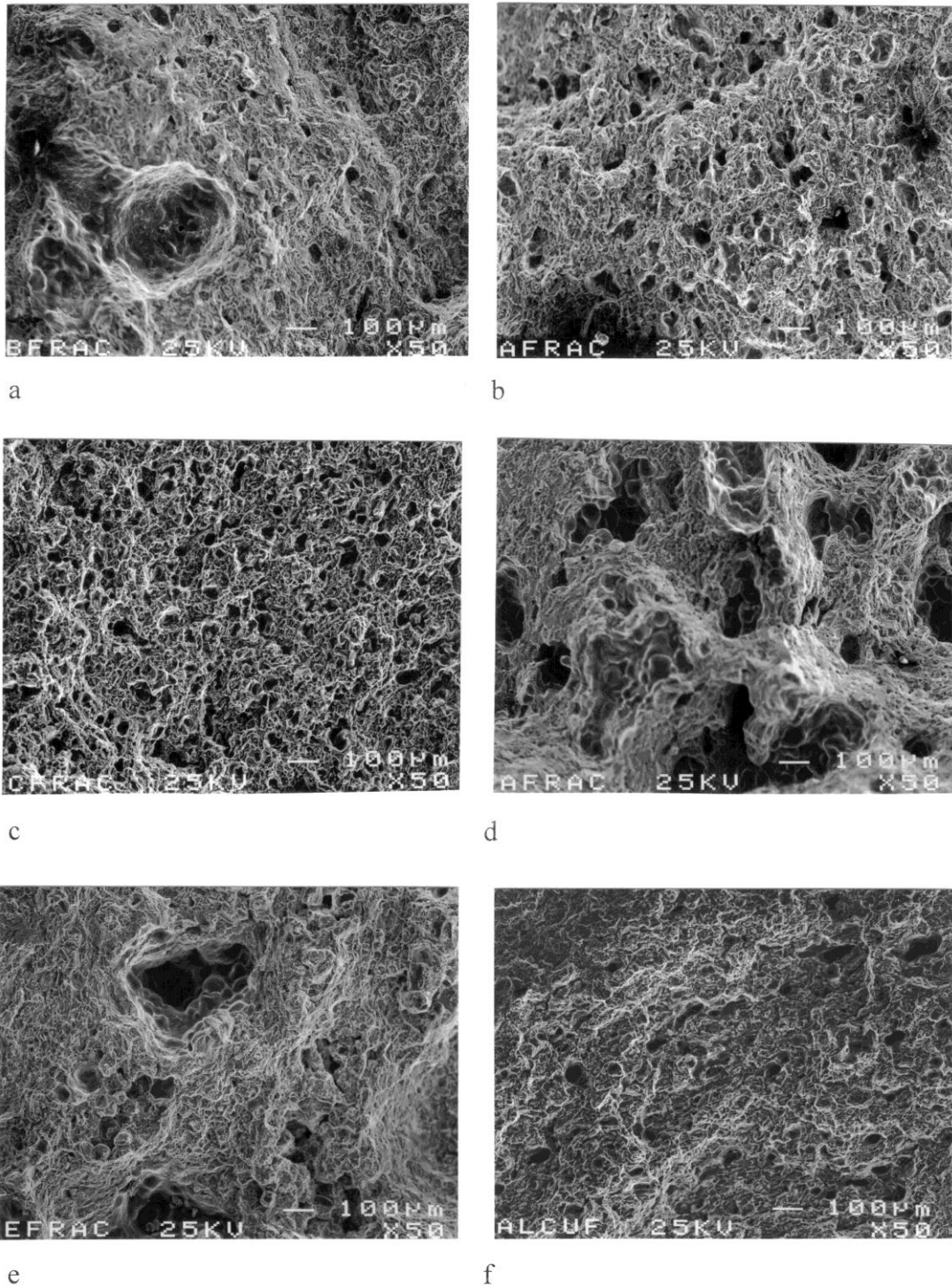
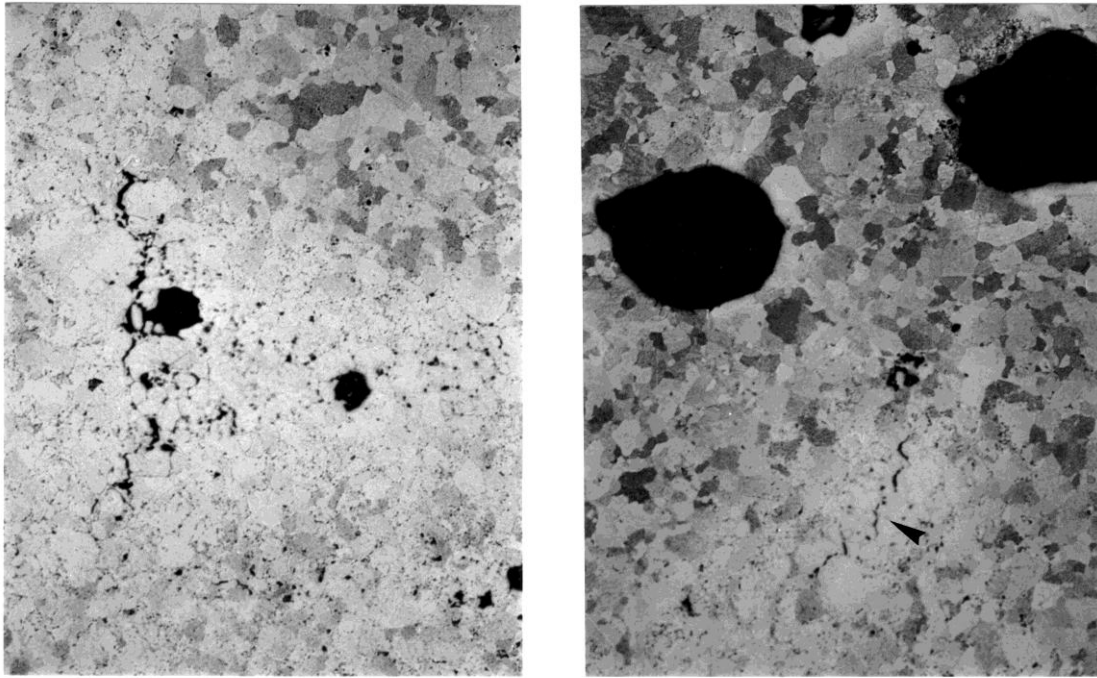


Figure 4.23 SEM fractographs of typical tensile samples for the 5 conditions tested. Note pore sizes and pore area fraction of the fracture surface. (a) $<150\mu\text{m}$, (b) $<100\mu\text{m}$, (c) $<45\mu\text{m}$, (d) $75\text{-}106\mu\text{m}$, (e) $125\text{-}150\mu\text{m}$, (f) $<45\mu\text{m}$ at a high heating rate.



230µm ————— ← tensile direction →

Figure 4.24 Regions of the gauge length of Al-4Cu (T4), copper particle size 125-150µm, after tensile testing. It is of note that fracture did not initiate from the coarse secondary porosity. Instead, regions with apparent concentrations of fine porosity were crack initiation sites (arrowed at right).

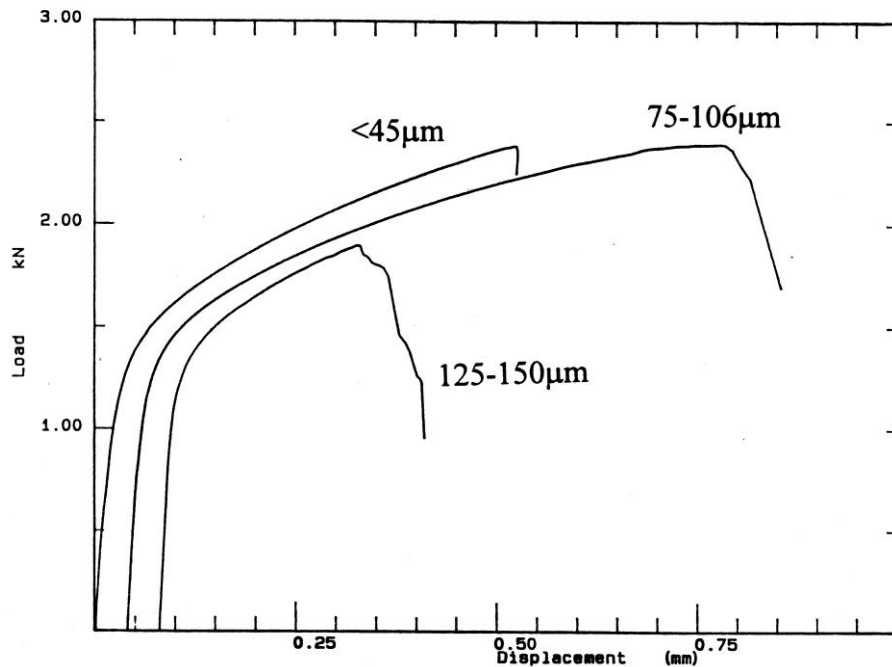


Figure 4.25. Typical behaviour of the tensile curves for the three cropped sizes tested in Al-4Cu (T4). The elongation to failure is reduced where both the minimum and maximum copper particle sizes tested were used. Note the proof stress is essentially the same for all three conditions.

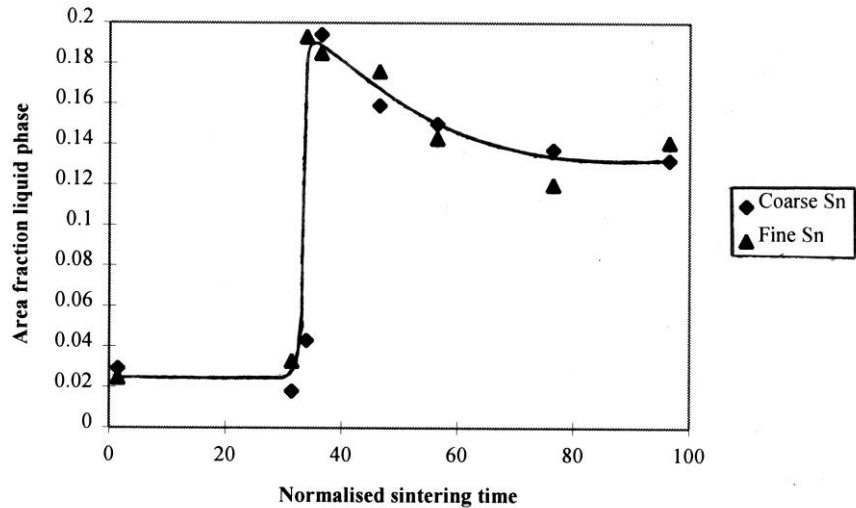


Figure 4.26 A quantitative analysis of area fraction liquid phase for coarse and fine tin powder additions. The normalised sintering time is the time for which the sample was above the melting point of the liquid forming phase. There is no difference in the volume of liquid phase that develops whether coarse or fine additives are used. This figure should be compared to Figure 4.17, which is the equivalent analysis for the Al-10Zn system. The powder size effects the liquid phase development in the Al-Zn system, but not in the Al-Sn system.

4.4.4 Fe-Cu

The microstructural evolution during sintering of Fe-Cu for the two copper sizes examined is compared in Figure 4.28. It is again apparent that the coarser additive particle sizes produced a larger quantity of liquid phase. At 1050°C, both the fine and coarse copper powders had started to bond with the iron powders by solid state diffusion (Figure 4.28a&e). At 1100°C (16°C above the melting point of Cu), much of the fine copper had already diffused into the iron (Figure 4.28f, arrowed). However, where coarse copper powders were used a greater volume of liquid was present (Figure 4.28b) and there was a corresponding decrease in the amount of porosity (Figure 4.28c&g). During the next 15 minutes of sintering with fine particles, the copper is effectively absorbed by the iron. (Figure 4.28h). When coarse particles are used, a substantial amount of liquid remained, although much of the copper had passed into solution after 15 minutes at 1150°C (Figure 4.28d). The iron is well sintered where coarse particles are used (Figure 4.28d) and most of the remaining porosity is present in prior copper particle sites. This is substantially different to fine copper particles (Figure 4.28h). Although the system is entirely transient, the samples were inhomogeneous, even after 12 hours at 1150°C for both coarse and fine powders.

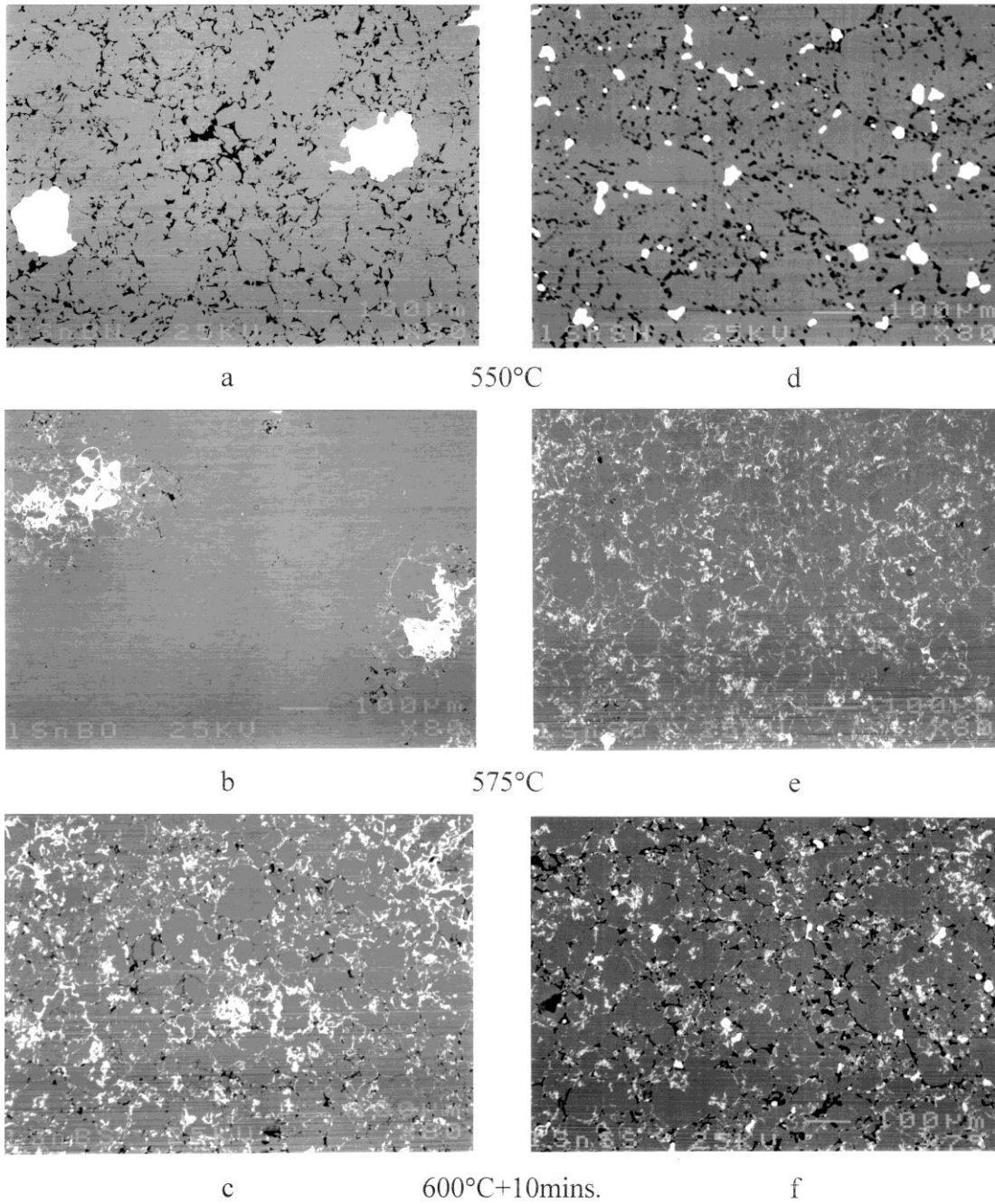


Figure 4.27 A comparison of the sintering of aluminium with coarse and fine tin powders. Typical backscatter SEM micrographs; (a-c are for coarse tin powders, d-f are for fine tin powders). There is no significant difference in microstructural development between compacts containing coarse and fine tin powders, except for the rate at which the structure develops.

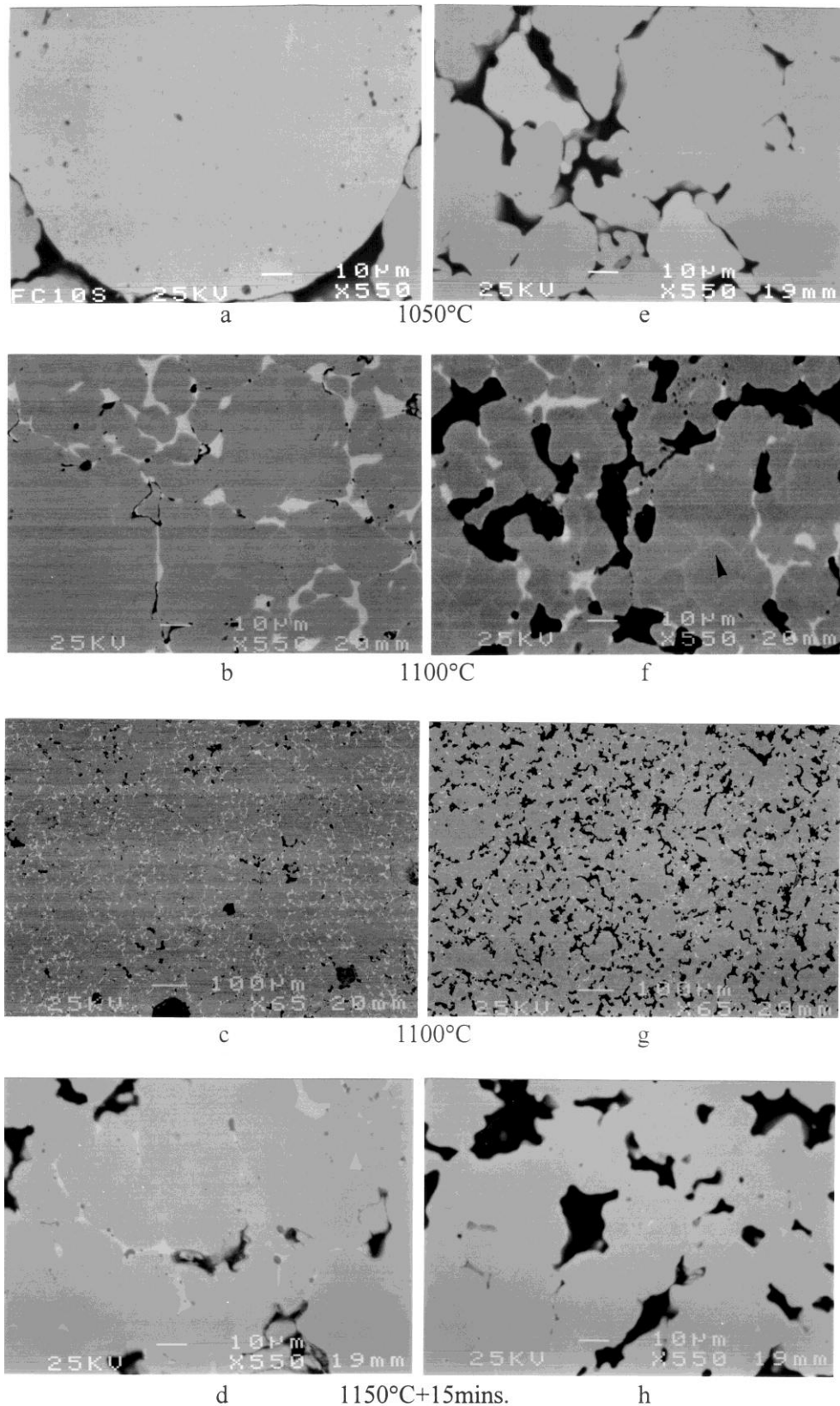


Figure 4.28 Typical backscattered SEM micrographs showing the effect of copper particle size on the sintering of iron powder; (a-d coarse Cu and e-h fine Cu). The difference in the amount of liquid formed and the resulting porosity is evident. Diffusion of copper along grain boundaries is visible in (f) (arrowed).

4.5 The Particle Size Effect in Ternary and Quaternary Systems

For all ternary and quaternary systems where coarse and fine additive powders were compared (Al-Cu-Mg, Al-Zn-Mg, Al-Zn-Cu and Al-Zn-Mg-Cu), more liquid phase was formed by the coarse particles and it persisted for a longer period than that produced from fine particles. Fine particles consistently formed only minimal quantities of liquid phase. The ternary and quaternary alloying elements caused some variation to the sintering liquids that formed, but the particle size effect was still apparent. Where fine additive particles are used (zinc 2 and copper 2) there is a tendency to form additional eutectics at lower temperatures, but the elements have to be in contact for this to occur (Figure 4.29). There is a lesser tendency for these mixed liquids to form where coarse particles are used (zinc 1 and copper 1). This is confirmed by DSC (Figure 4.30) which shows spectra for the quaternary system for both the coarse and fine zinc additive particle sizes. For the fine powder, there is a small endotherm at $\sim 340^{\circ}\text{C}$, which may correspond to the formation of a ternary or quaternary eutectic, whereas the first melting peak for the coarse powder sample corresponds to the melting point of pure Zn. In these spectra, the total energy absorbed where fine zinc powders were used was less than that for samples containing coarse powders (13.7 J/g compared to 27.7 J/g, respectively).

When Mg is added to Al-Cu, there is no significant change in the particle size effect compared to the binary system. However, when Mg is added to Al-Zn or Al-Zn-Cu (where Zn is the major alloying element) the particle size effect is enhanced. Minimal liquid phase is formed where fine zinc particles are used, whereas substantial liquid phase forms where coarse zinc is used. For coarse zinc particles in the binary Al-Zn system, a substantial quantity of liquid phase is formed at 580°C , (Figure 4.31a) but at least as much liquid phase occurs at 525°C in the ternary (Figure 4.31b) and is completely absorbed by 580°C (Figure 4.31c). For fine zinc in the binary Al-Zn and ternary Al-Zn- Mg systems, a negligible quantity of liquid forms and homogenisation is faster in the ternary system.

When low concentrations of copper are added to the Al-Zn system, the zinc particle size effect is still apparent (Figure 4.32a&b) while the influence of the copper particle size is insignificant. For a high concentration of copper, the copper particle size is important (Figure 4.33). There is also some ternary eutectic formation during sintering for both high and low copper alloys. When copper is added to Al-Zn-Mg, a series of ternary and/or quaternary eutectics form; also, unreacted copper forms liquid phases with the Al above 550°C . Additionally, the quaternary system exhibits supersolidus characteristics at $\sim 580^{\circ}\text{C}$. The particle size effect for this system is illustrated in Figure 4.34 which shows not only the effect of additive particle size but also the absorption and reappearance of the liquid phase.

The manner in which additive particle size ranges effect microstructures is illustrated in

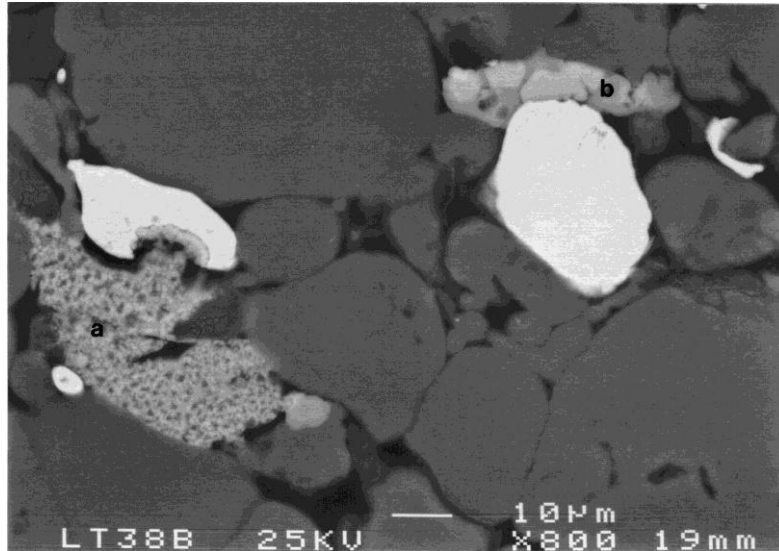


Figure 4.29 Typical backscattered SEM micrograph for the quaternary alloy containing fine additive particles only (zinc 2 and copper 2) quenched from 375°C. EDS showed the liquid at (a) to be a quaternary phase and the liquid at (b) to be a ternary Al-Zn-Mg phase.

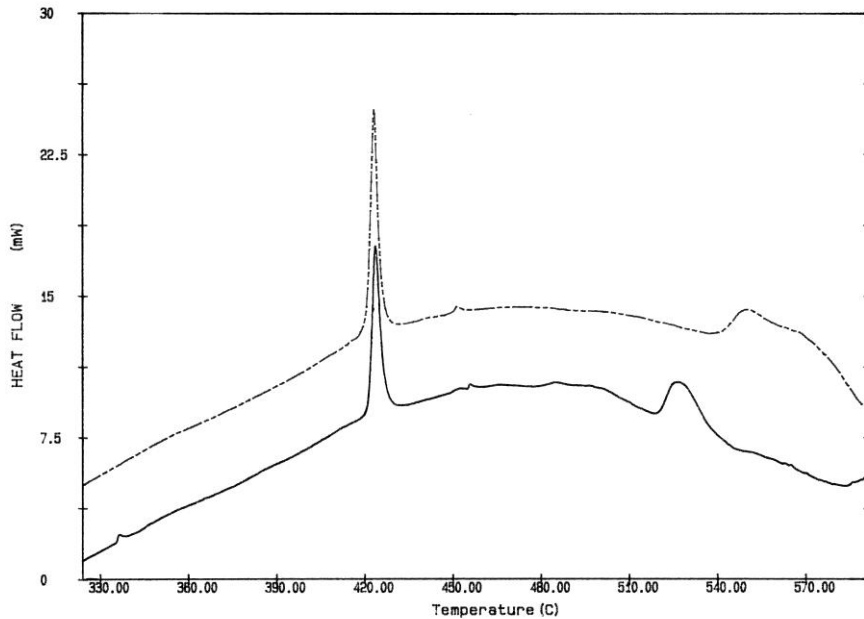
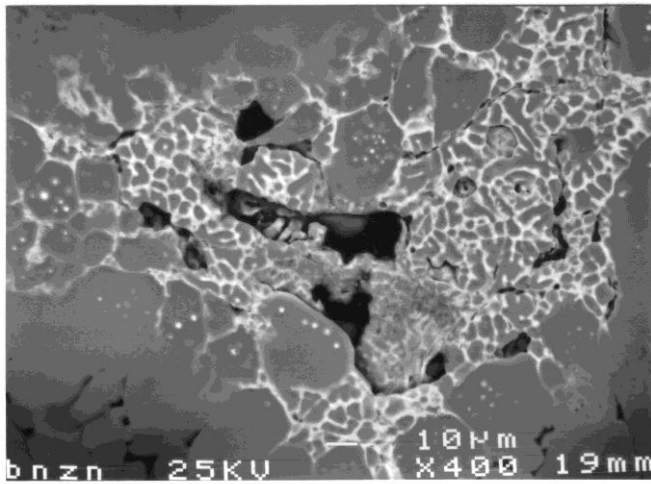
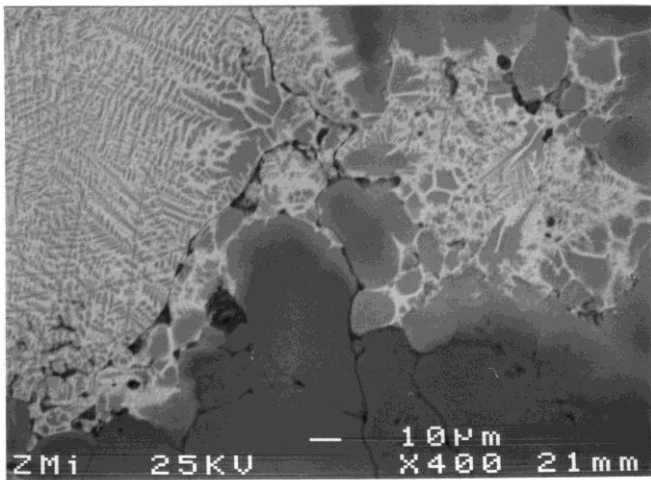


Figure 4.30 DSC curves for an Al-8Zn-2.5Mg-1Cu alloy, comparing the effect of zinc particle sizes on melt formation. The broken line is for coarse powders (zinc 1), the solid line is for fine powders (zinc 2). Fine copper powders were used for both.

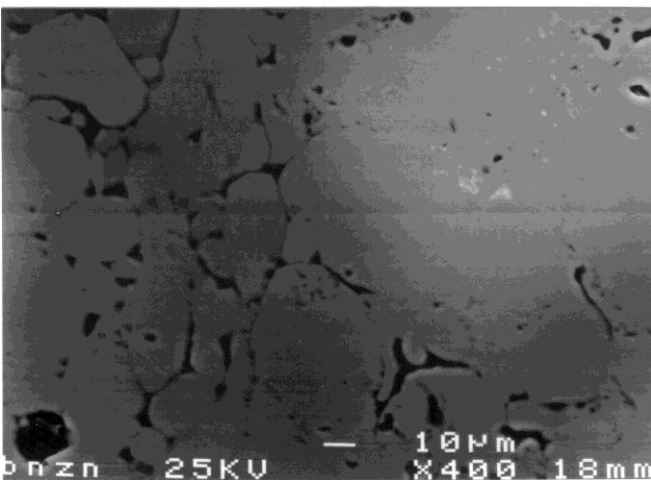
Figure 4.35 and summarised in Table.4.3. Binary and higher order eutectics were differentiated using E.D.S. When a narrow range of fine zinc particles is used (Figure 4.35a), many higher order eutectics form but there is little total liquid. When a narrow range of coarse zinc particles is used (Figure 4.35b) a large volume of binary and near binary Al-Zn eutectic liquid forms. When a wide size range of zinc particles is employed, large quantities of higher order eutectic liquid forms (Figure 4.35c). There is significant rearrangement and good interparticle bonding leaving a minimal number of large pores in the final product.



a

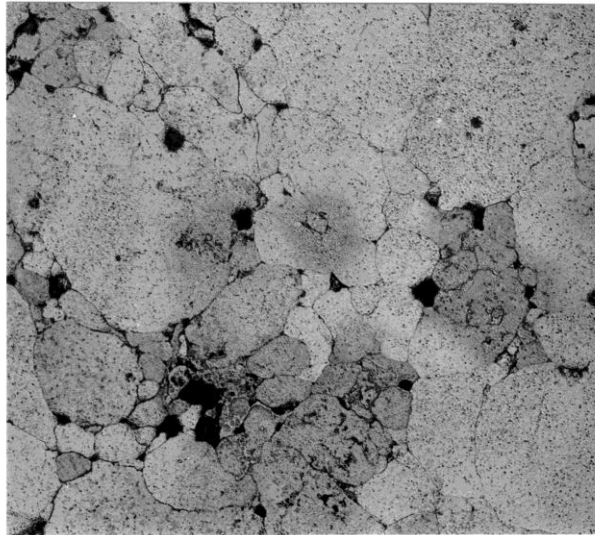


b

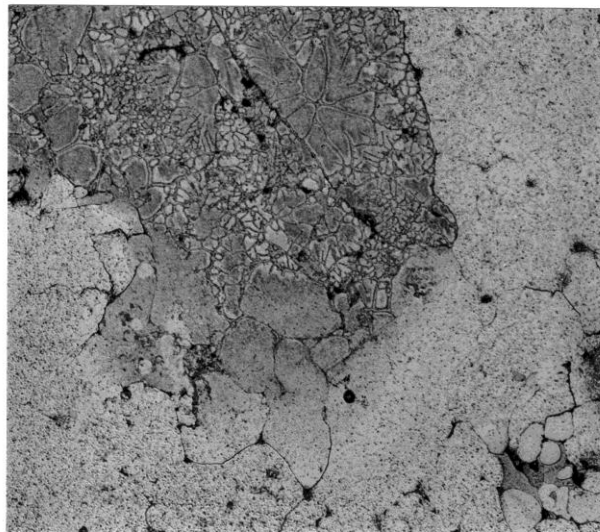


c

Figure 4.31 The effect of Mg on an Al-8Zn alloy with coarse zinc particles (zinc 1); (a) is a binary Al-8Zn alloy quenched from 580°C, (b) a ternary Al-8Zn-2Mg alloy quenched from 525°C and (c) a ternary alloy quenched from 580°C. For the binary Al-Zn system, a large quantity of liquid still exists at 580°C; for the ternary system, the compact contains a large quantity of liquid at 525°C, but by 580°C is approaching homogeneity, and exhibits little or no remaining liquid phase. (Backscattered SEM).



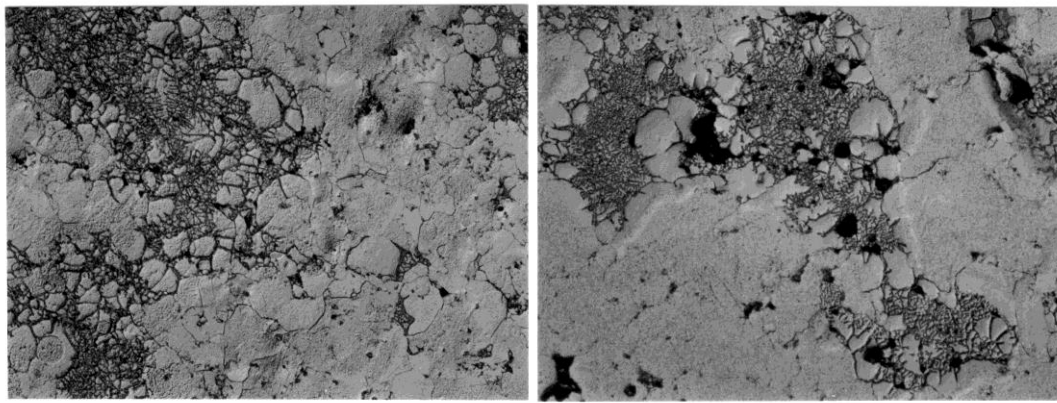
a



50μm

b

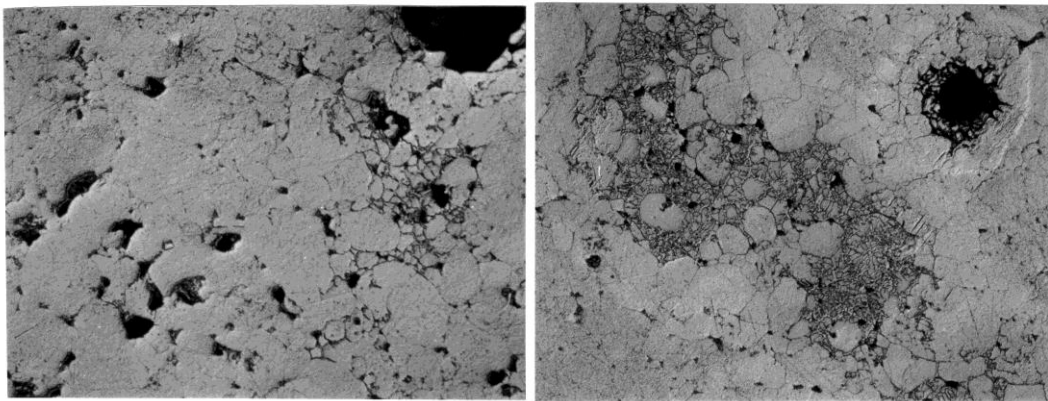
Figure 4.32 The effect of additive particle size in a ternary Al-8Zn-1Cu alloy. Copper 2 was used in both instances. (a) is for fine zinc powders (zinc 2); little liquid remains as diffusion predominates. (b) is for coarse zinc powders (zinc 1) and a large volume of sintering liquid is present. Samples were water quenched from 575°C. (Optical micrographs).



(a) Fine Cu

600°C

(c) Coarse Cu



(b) Fine Cu

600°C+2mins.

(d) Coarse Cu

100μm 

Figure 4.33 The effect of copper particle size in Al-8Zn-3Cu. Zinc 4 was used as the Zn addition, while copper 1 was used as the coarse additive and copper 2 used as the fine copper additive. Where fine Cu was used the liquid is diminishing rapidly at 600°C (a&b). Where coarse Cu was used a large quantity of liquid remains. (Optical micrographs).

4.6 The Effect of Composition in Ternary and Quaternary Alloys

The effect of altering composition on the ternary Al-Zn-Mg system was investigated. Zinc 4 (d₅₀=121μm) was used throughout all of these experiments. Increasing magnesium levels from 0 to 2.5% decreased the amount of liquid which formed and the duration for which it persisted (Figure 4.36). The low concentration magnesium samples (a&b) develop and maintain large quantities of liquid phase whereas at higher levels (e&f) the liquid has disappeared. Corresponding densification and hardness values are given in Figure 4.37.

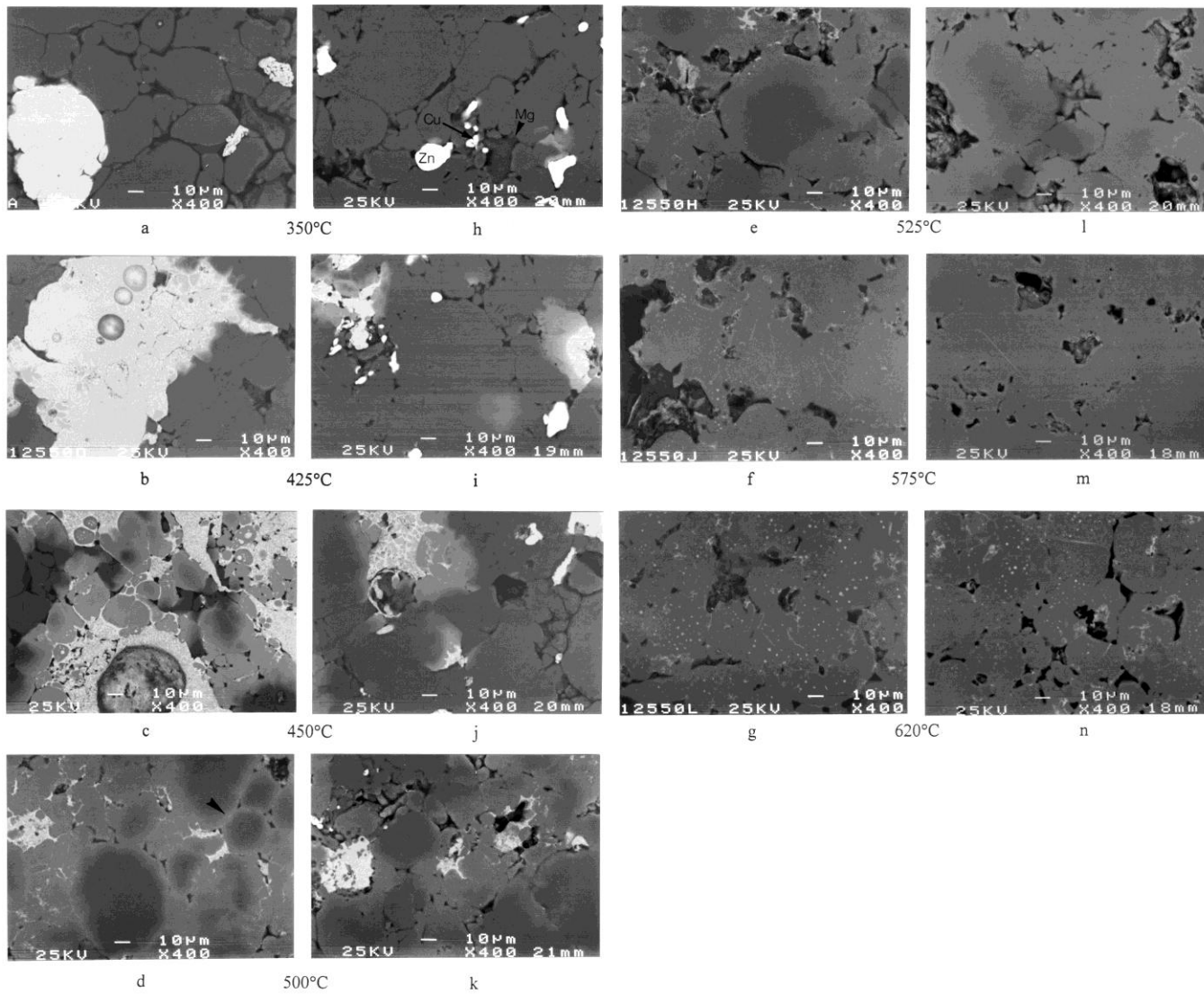
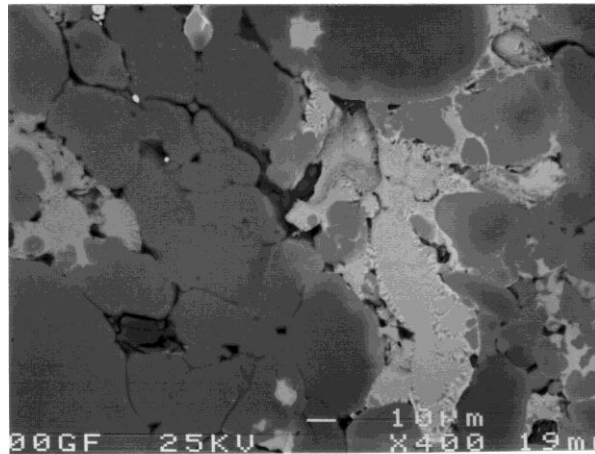
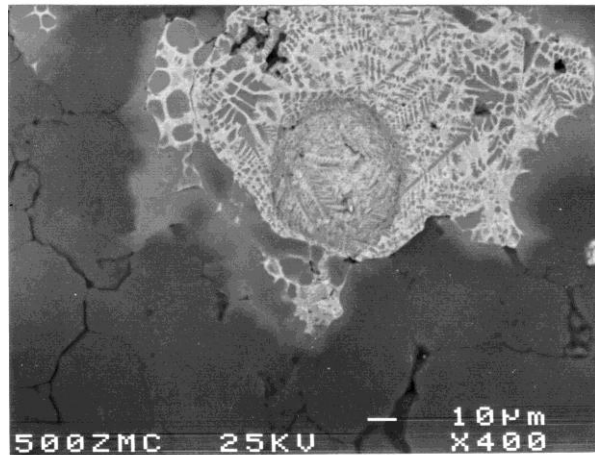


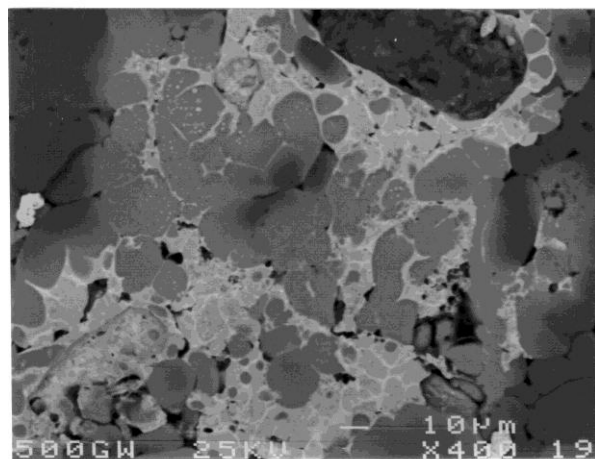
Figure 4.34 The effect of additive zinc size in Al-8Zn-2.5Mg-1Cu. (a-g) are for coarse additive zinc sizes, (h-n) are for fine additive zinc sizes. The volume of liquid phase generated where coarse zinc powders are used is greater than that from fine zinc powders. However, there are several advantages of using fine additives for sintering, due to the proximity of elemental powders with each other. Several of the additive powders are labelled in (h), and it is of note that these regions are more likely to form higher order eutectics at lower temperatures. Also note (d), which is exhibiting bright contrast (Zn rich) in prior particle boundaries which have now bonded (arrowed). The transient liquid phase has dispersed by 525°C in both coarse and fine cases, and the equilibrium liquid phase is evident in (g&n). (Backscattered SEM)



a



b



c

Figure 4.35 The microstructures of Al-8Zn-2.5Mg-1Cu for the three size ranges examined. Samples were water quenched from 500°C. For the range containing mostly fine zinc powders (zinc3) the liquid tends to act only locally, but has a good distribution in the sample. This is shown at (a). The range containing mostly coarse zinc powders (zinc 4) forms greater quantities of liquid phase but is poorly distributed. The very wide size range (zinc 5) showed optimum sintering, combining the advantages of a relatively large particle size widely distributed throughout the sample. These are shown at (b) and (c) respectively. (Backscattered SEM).

TABLE 4.3. The effect of varying zinc particle size ranges on quaternary alloys.

Additive Zn particle size range	Effect
Narrow range, mostly fine powders	Higher order eutectics, little liquid.
Narrow range, mostly coarse powders	Mostly binary eutectics at low temperatures, large quantity of liquid.
Combination of coarse and fine ranges	Higher order eutectics, large volume of widely distributed liquid.

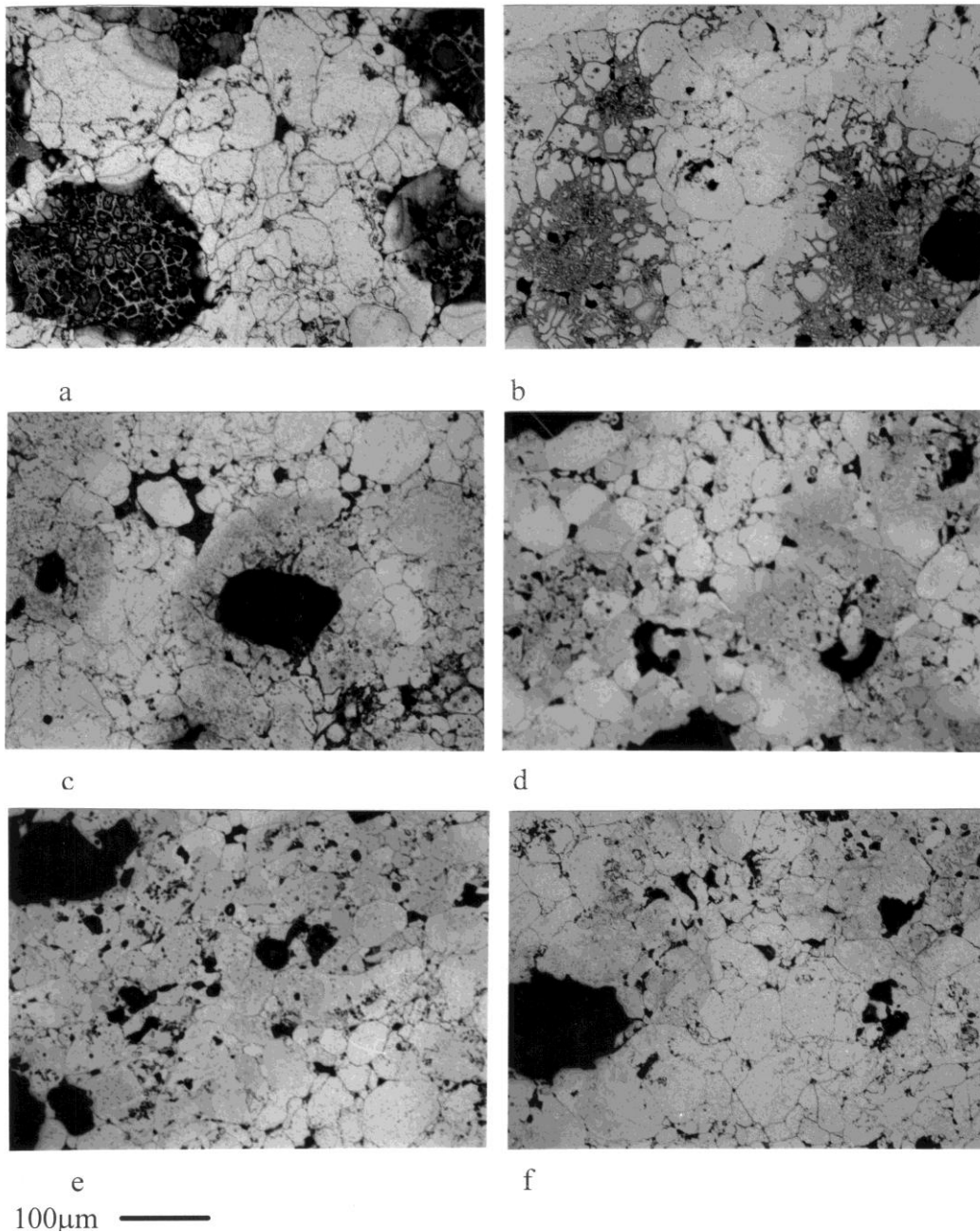


Figure 4.36 The effect of increasing magnesium content in Al-8Zn-xMg. (a) 0%Mg, (b) 0.2%Mg, (c) 0.5%Mg, (d) 1%Mg, (e) 1.5%Mg, (f) 2.5%Mg. With increasing Mg concentration, the diffusivity of Zn in Al is increased, minimising the effect of the liquid phase formed. Zinc 4 was used for all conditions. All samples were heated at 10°C/min. to 600°C, and quenched. Optical micrographs.

The addition of 0.5%Cu to Al-8Zn produced a dramatic change in the microstructural development. This is illustrated by Figures 4.38(a)&(b). The penetration of the liquid into the aluminium matrix appears to be substantially hastened. Above 0.5%Cu addition, there is no significant change in microstructural development. At higher copper contents, the liquid phase persisted for slightly longer times and the density decreased. Figure 4.38 shows the microstructures of Al-8Zn-xCu alloys at 600°C.

The contour maps (Figure 4.39) show the effect of changing the concentration of Cu and Mg on the density and hardness for a quaternary Al-8Zn-xMg-yCu alloy. Each map contains 31 data points, corresponding to the compositions in section 3.3, Table 3.3. Each data point on Figure 4.39a is the average of 3 densification results. Each data point on Figure 4.39b is the average of 15 hardness tests. These figures show that best densification is achieved at low copper and low magnesium levels. However, optimum as-sintered hardness values occur at high copper and/or high magnesium concentrations. That the contour lines are regularly spaced and parallel to the abscissa in Figure 4.39(a) indicates that expansion increases rapidly with copper additions at low copper levels and is virtually independent of the Mg concentration. At higher copper concentrations (ie.>~1%Cu), however, the contour lines are parallel to the ordinate. This indicates that dilation increases with Mg levels (more negative densification) and is almost independent of copper at concentrations $\geq 1.5\%$ Cu. In contrast, the hardness contour map exhibits the opposite effect. Hardness is increasingly dependent on copper but increases rapidly for all Cu concentrations at low Mg concentrations $< 0.5\%$. Above 0.5% Mg, hardness increases slowly with additions of both Mg and Cu. The contour lines are widely spaced in this region of the contour map, indicating that the hardness is changing only slowly.

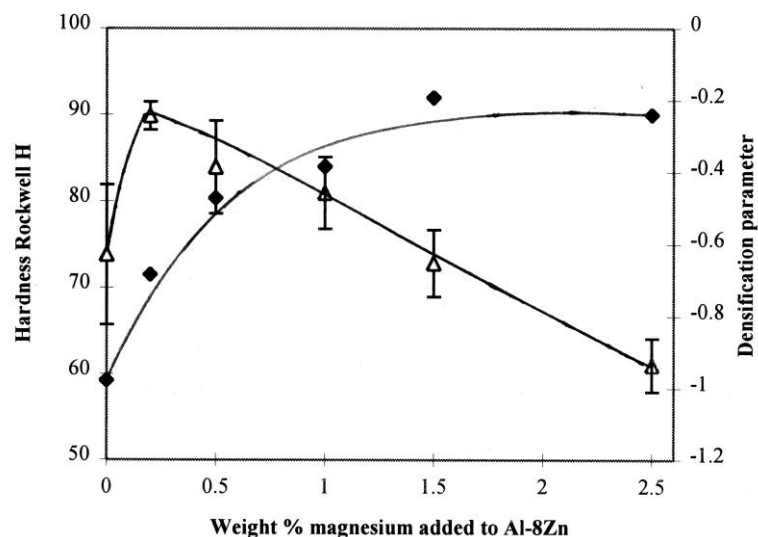


Figure 4.37 The effect of increasing additions of magnesium in Al-8Zn-xMg alloys on densification (open triangles) and hardness (diamonds). The densification increases rapidly with small additions of Mg, then linearly decreases with increasing Mg content. Hardness rises gradually and then remains constant at higher Mg additions. Error on hardness $\leq 8\%$.

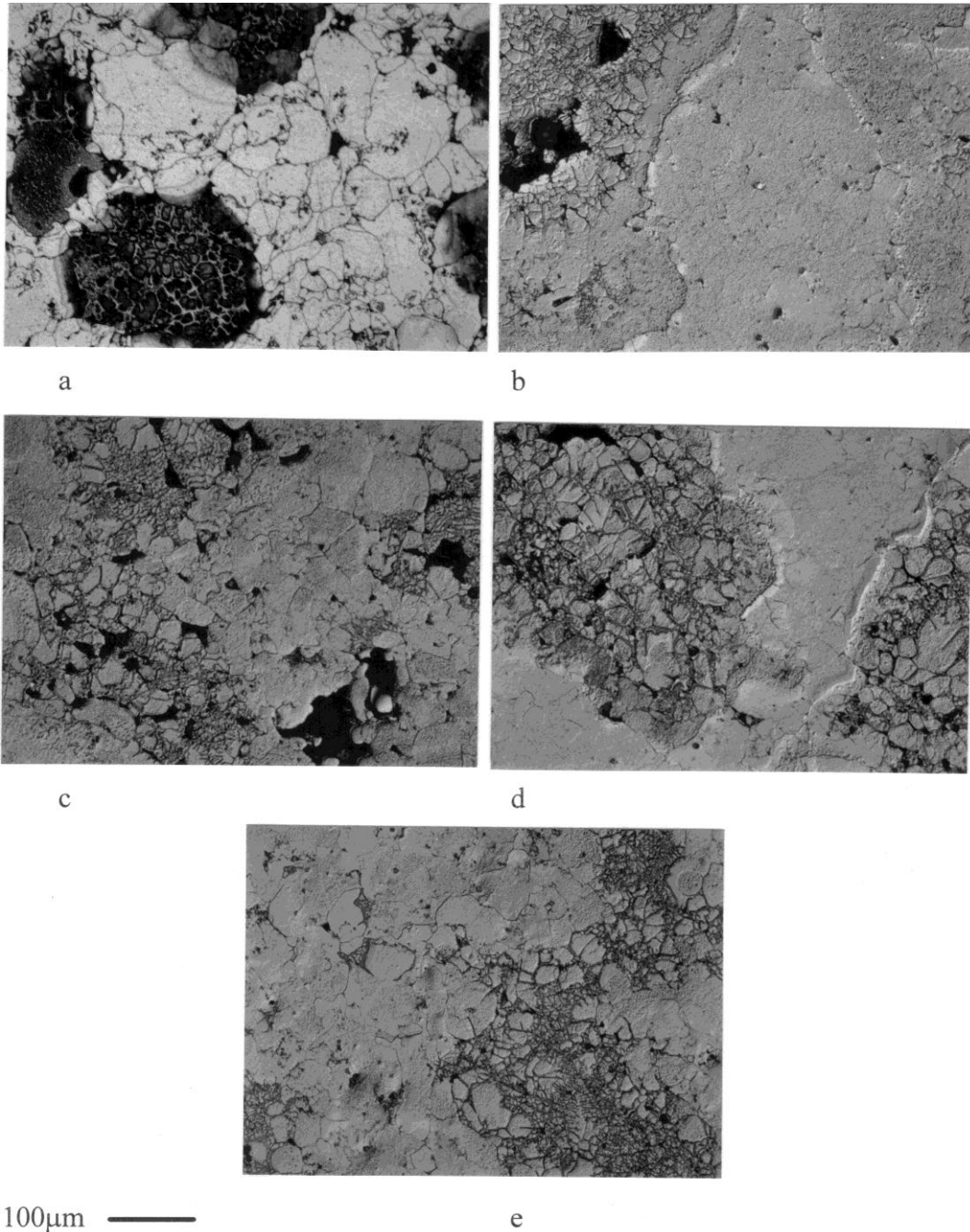
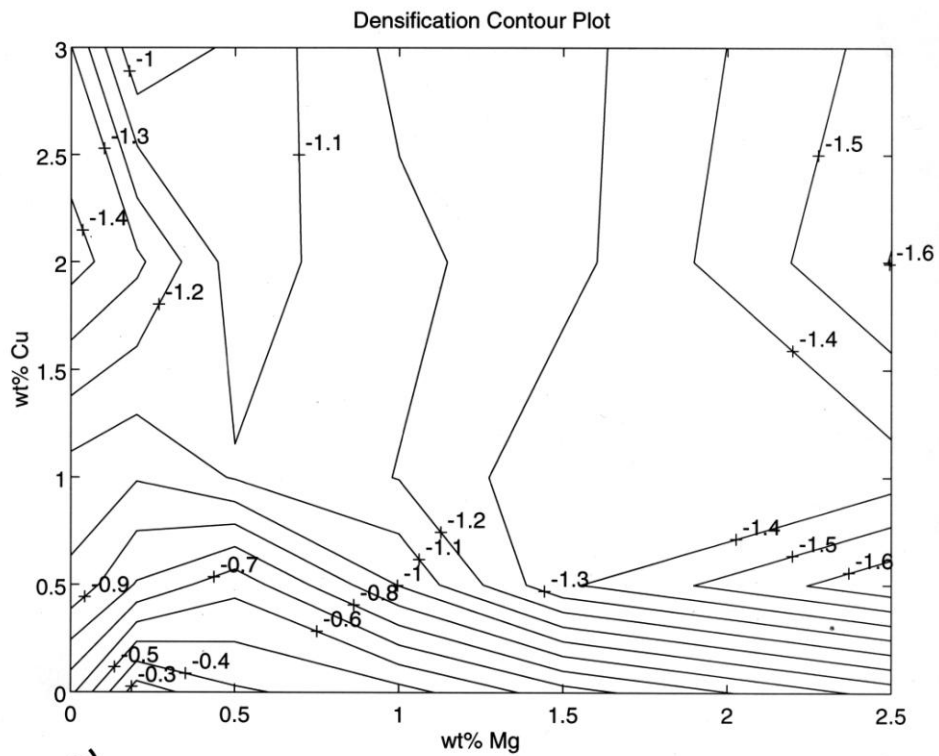
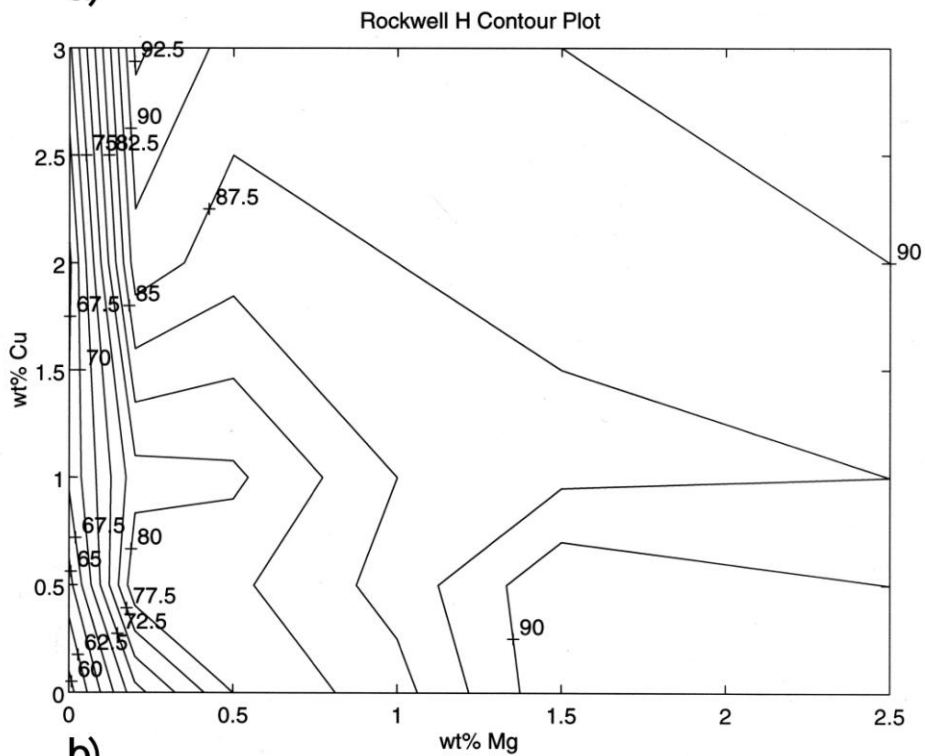


Figure 4.38 Optical micrographs of Al-8Zn-xCu alloys quenched as the samples reached 600°C. (a) 0%Cu, (b) 0.5%Cu, (c) 1%Cu, (d) 2%Cu, (e) 3%Cu. Zinc 4 was used for all conditions. There is a dramatic change in the morphological development with the addition of 0.5%Cu. Further additions of Cu increase the volume fraction of liquid present but have little effect on the sintering liquids.



a)



b)

Figure 4.39 Contour plots of Al-8Zn-xMg-yCu alloys showing the effect of Mg and Cu levels on (a) densification and (b) hardness (as sintered). Samples were sintered for 2 hours at 600°C.

4.7 The Effect of Gravity on Al-8Zn-2.5Mg-1Cu

Gravity effects the sintering of quaternary Al-Zn-Mg-Cu in the manner illustrated by Figure 4.40. Figure 4.40(a) shows the volume fraction liquid phase from top to bottom for multiple samples and Figure 4.40(b) shows typical microstructures for each region. The liquid volume increased from ~15% at the top of the sample to ~21% at the bottom. There was also a corresponding change in shape (Figure 4.40(c)). There is a contraction towards the middle of the sample, and the diameter of the top surface is greater than that of the bottom surface.

4.8 Effect of Cooling Rate

After sintering for 2 hours at 620°C, substantial additional shrinkage occurred when a quaternary alloy was cooled from 620°C to 200°C at 2°C/min. (Figure 4.41). By slow cooling, apparent densities of up to 98% have been achieved. Cooling slowly caused more densification than sintering for longer times at 620°C. XRD scans of samples quenched at 620°C+2hrs, 550°C, 375°C and 200°C (Figure 4.42) exhibit the phase changes as cooling occurred. At 620°C+2hrs the trace shows Al plus the remnants of the liquid phase, which has solidified as MgZn₂. As seen from the trace taken from a sample removed at 550°C during cooling, and Figure 4.43, an intermetallic phase forms. This intermetallic phase does not return to solution during solution treatment, even at relatively high temperatures (550°C) and long solution treatment times (5 hrs). This compound was identified by comparative XRD⁽¹¹⁸⁾ and analysis of ternary and pseudo-binary^(119,120) phase diagrams as Mg₃₂(AlZn)₄₉, (also written as Al₆Mg₁₁Zn₁₁ (τ)). This phase exists over a large composition range^(119,120) and is one of two phases in the ternary Al-Zn-Mg system which can solidify straight from the melt. The other phase is Mg₅Zn₂Al₂ (φ), which exists over a narrow composition range. The reaction sequence for the formation of the τ phase from molten eutectic is either L→Al+L→Al+L+Al₆Mg₁₁Zn₁₁ or L+MgZn₂→Al+Al₆Mg₁₁Zn₁₁⁽⁷³⁾. It is noteworthy that Mg₃₂(AlZn)₄₉ is isomorphous with Mg₃₂(AlCu)₄₉ which forms in the ternary Al-Cu-Mg system⁽⁷⁴⁾. Hence it is likely that there is some Cu replacing Zn in this compound, so the actual formula would be best written as Mg₃₂(Al[Zn,Cu])₄₉. It is apparent that this intermetallic phase has little effect on shrinkage in these compacts (Figure 4.41, at 550°C). As the compact passes the solvus at ~400°C, it appears that precipitates of MgZn₂ begin to come out of solution. Figure 4.44 shows that the precipitates that form tend to nucleate on free surfaces and grain boundaries. As the temperature decreases further, the amount of precipitation increases at the same time that shrinkage increases.

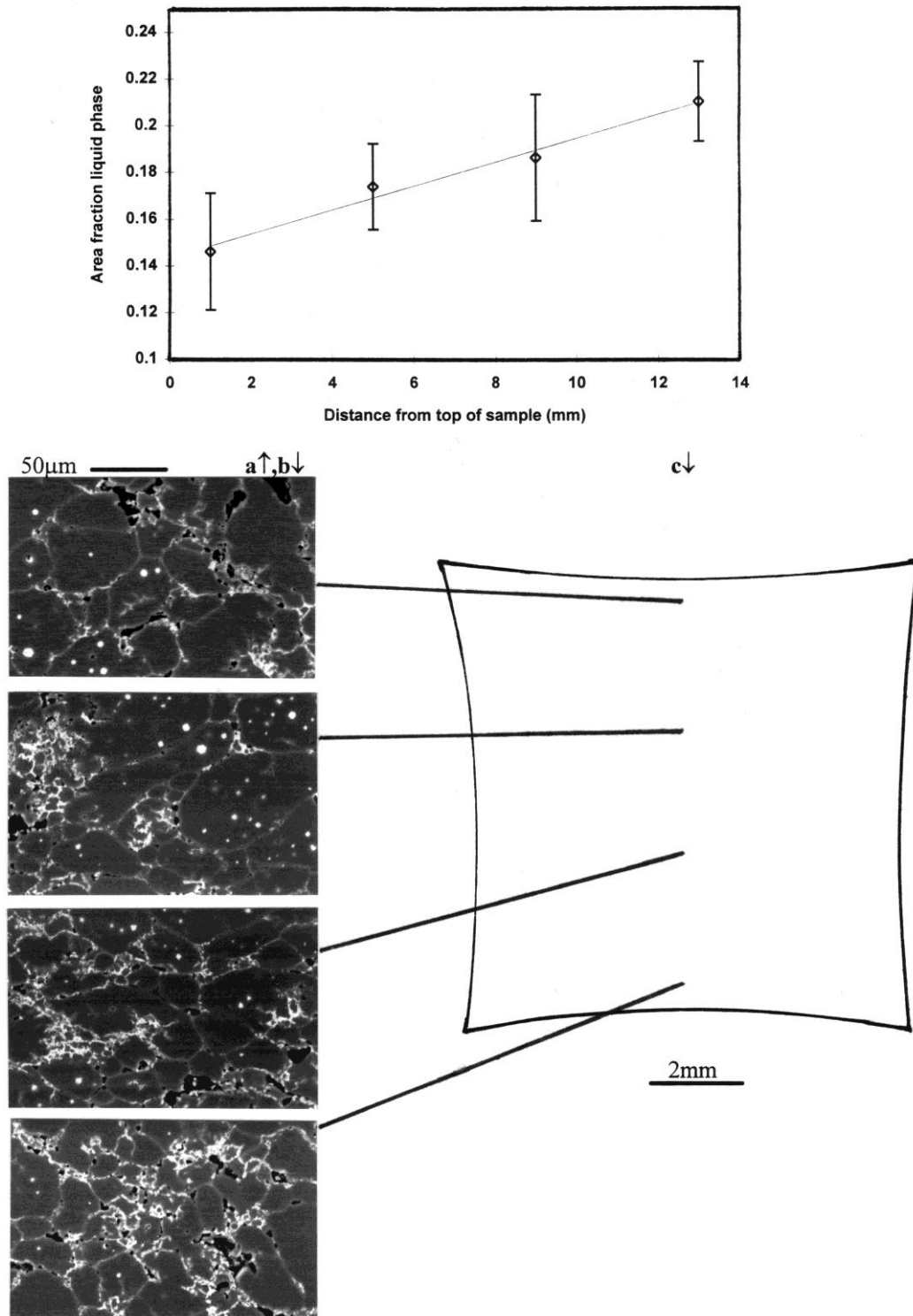


Figure 4.40 The effect of gravity on the liquid phase sintering of Al-8Zn-2.5Mg-1Cu, sintered for 2 hours at 620°C. (a) shows the area fraction of liquid phase as a function of distance from the top of the specimen. The fraction of liquid phase increases linearly towards the bottom of the sample. (b) shows representative backscatter SEM micrographs from the relevant regions of the sample examined. (c) shows the shape of the sectioned sample which was examined and the relative positions from which the micrographs were taken.

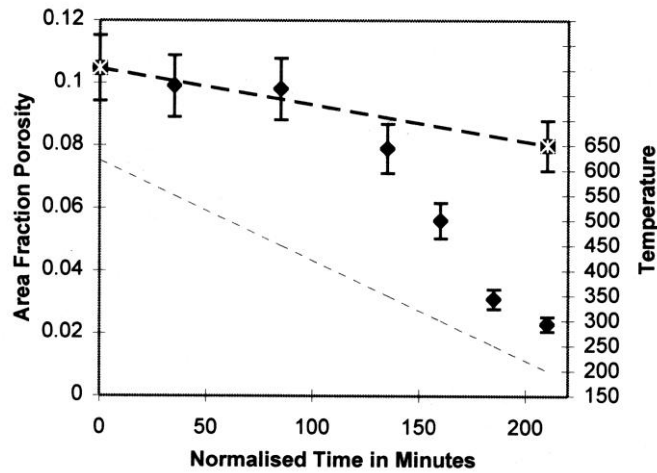


Figure 4.41 The effect of slow cooling ($2^{\circ}\text{C}/\text{min.}$) from 620°C to 200°C on area fraction porosity for a quaternary Al-8Zn-2.5Mg-1Cu alloy sintered 2 hours at 620°C (diamond markers). A large shrinkage occurs below 350°C ; this is attributed to precipitation. The asterisk/square symbol shows the area fraction porosity of a sample sintered at 620°C for 5.5 hours and water quenched. The faint (bottom) dashed line is the cooling cycle.

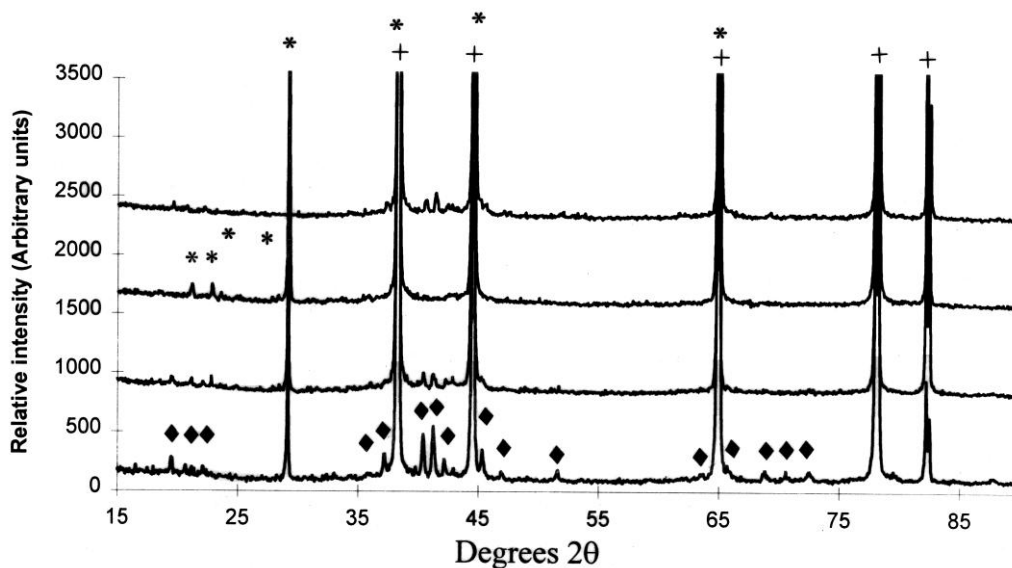


Figure 4.42 X-ray diffraction scans of slow cooled Al-8Zn-2.5Mg-1Cu samples at: $620^{\circ}\text{C}+2\text{hrs}$, 550°C , 375°C and 200°C (top to bottom, respectively). At $620^{\circ}\text{C}+2\text{hrs}$ there is Al + MgZn_2 present, this being representative of the solidified equilibrium liquid phase. At 550°C there is Al and an intermetallic phase. There is no change in the scan until 375°C where, there is evidence that precipitation of MgZn_2 has begun. The amount of precipitation then increases with reduced temperature. Diamonds identify MgZn_2 , plus symbols show Al, and asterisks the intermetallic phase.

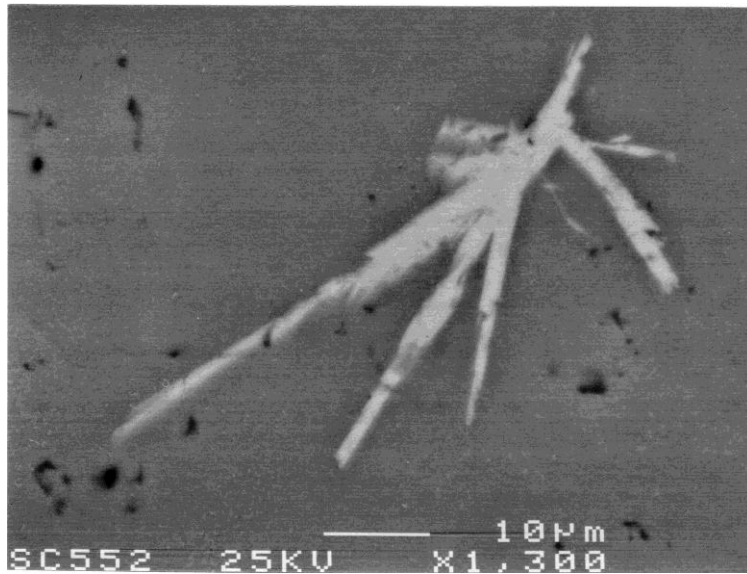


Figure 4.43 The intermetallic phase $Mg_{32}(AlZn)_{49}$ formed on slow cooling above $550^{\circ}C$. Backscattered SEM.

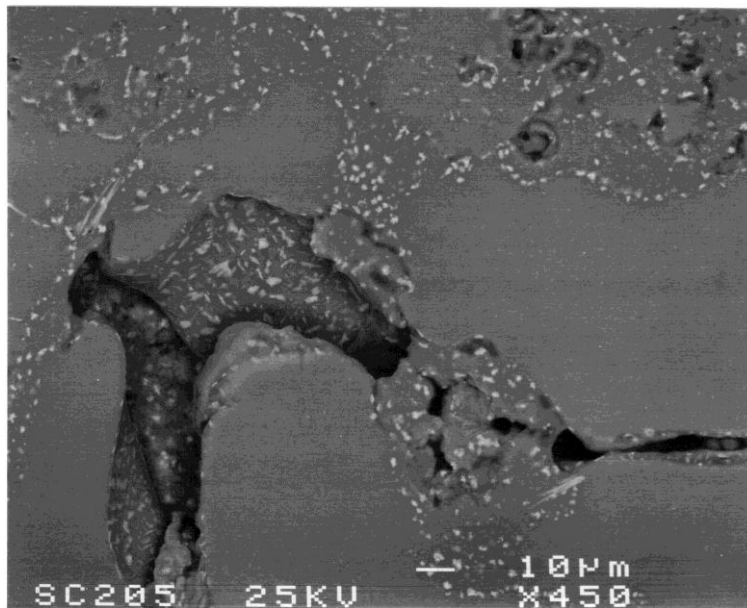


Figure 4.44 Precipitates formed during the slow cooling of Al-8Zn-2.5Mg-1Cu. Note the location of the precipitate phase, which forms preferentially on free surfaces and grain boundaries. Backscattered SEM of a sample slow cooled to $200^{\circ}C$ and water quenched.

4.9 Summary of Results

Additions of Zn or Mg in binary Al alloys leads to linearly decreasing sintered density with increasing concentration. Additions of Cu also lead to a linearly decreasing sintered density up to 3% Cu. Above 3% Cu, a sharp increase in sintered density occurs. Magnesium is highly transient in aluminium and the liquid phase that forms at the eutectic temperature (445°C) lasts for a relatively short period (2 minutes) for concentrations ≥ 6 wt%. At lower concentrations (eg. 2.5%) the reaction sequence is slower and there is liquid present up to 525°C. TEM of an Al-2.5Mg alloy exhibited regions of fine crystals which appear to be spinel, MgAl_2O_4 .

It is evident in all those systems examined which have a transient aspect to the sintering cycle that the additive particle size has a critical influence on microstructural development. This particle size effect was not evident in Al-Sn, which is a persistent system having unipolar solubility conditions. The use of a relatively coarse additive particle size in Al-Cu alloys can result in an increase in tensile properties. In the quaternary alloy studied, compacts exhibited a transient stage to the sintering cycle, and a persistent stage at the sintering temperature. A very wide particle size range in the quaternary system produces the most efficacious liquid phase. This particle size distribution results in higher order eutectics forming (which is generally a function of fine powders) and a large volume of widely distributed liquid.

Low concentrations of Mg (0.2%) in ternary and quaternary alloys improve the sintered density. Optimum hardness values (quaternary) are obtained at high copper and/or high Mg concentrations. Densification is essentially independent of Cu at high Mg levels, but densification is dependent on Mg at high Cu content and dependent on Cu at low Cu content.

Gravity has an effect on dimensional stability in the quaternary Al-8Zn-2.5Mg-1Cu alloy. Liquid volume fractions increase from ~ 0.15 to ~ 0.21 from the top to the bottom of the samples studied. There is a contraction towards the middle of the sample, and the diameter of the top surface is greater than that at the bottom.

By slow cooling quaternary alloy compacts from 620°C to 200°C, a substantial amount of densification can be induced. There is precipitation of MgZn_2 during cooling with a corresponding increase in shrinkage.

Chapter 5. Discussion

5.1 Introduction

This investigation into the sintering of aluminium alloys has identified several factors which effect sintering and microstructural development. Process variables including prior particle size, compact chemistry, compaction conditions and the sintering cycle are critical to the development of sintered properties. The presence of liquid phases and the duration for which they exist can be enhanced by manipulating selected variables. This chapter discusses the following:

1. the role of isothermal solidification in liquid phase sintering;
2. the wetting of Al particles by additive liquid phases;
3. the sintering of Al with Mg and the role of Mg in oxide disruption;
4. the effect of Zn, Cu and Mg concentration in binary Al alloys;
5. the effect of additive particle size on microstructural development in binary Al-Zn, Al-Cu, Al-Sn, and Fe-Cu alloys;
6. the effect of additive particle size on microstructural development in multicomponent Al alloys;
7. the effect of composition in multicomponent Al alloys on densification, mechanical properties and microstructural development;
8. the effect of gravity on dimensional stability in quaternary Al-Zn-Mg-Cu alloys;
9. the effect of cooling rate on the densification behaviour of quaternary alloys.

5.2 Isothermal Solidification

In addition to those detailed in section 2.5.3, there may be another mechanism contributing to sintering in systems having a transient aspect. This is commonly termed isothermal solidification and is a process used for joining temperature resistant materials. How isothermal solidification relates to transient bonding and joining processes is reviewed in section 2.5.5.1. The role of isothermal solidification in the sintering of powder metallurgy components has not previously been described. In a transient liquid phase sintering system the additive material is generally considered to simply pass into solution at the sintering temperature⁽⁹⁾. The following discussion relates this bonding phenomenon to transient liquid phase sintering.

Consider the transient end of a model system, where an additive 'B' has appreciable solubility in the base 'A' (Figure 5.1) and preferential diffusivity of B in A. C_{teq} is the equilibrium composition of a fully transient system, C_s the solidus composition, C_{peq} the equilibrium composition of a persistent system exhibiting some transient behaviour, and C_l the liquidus composition. Assuming an infinite (fast) heating rate, the composition of local sintering liquid regions will follow the dotted line shown, until the sample reaches equilibrium. If the heating rate was comparatively slow the line would slope

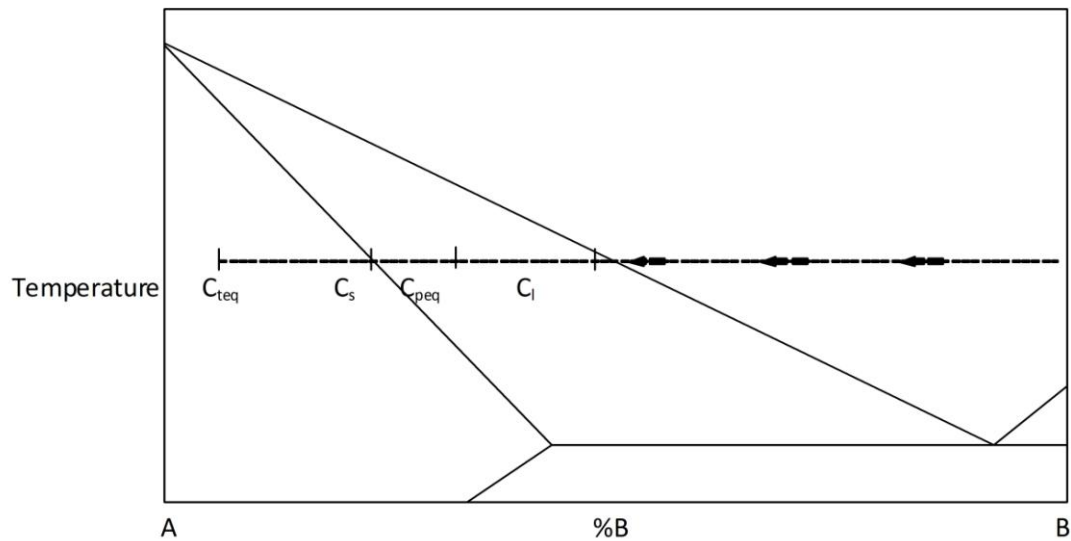


Figure 5.1 A representation of the transient end of a model sintering system. (See text for details).

downwards toward the additive end (B) due to time dependent homogenisation of the liquid. During the period up to the point at which C_1 is reached, the base material A is being constantly dissolved into the liquid, as it has a high solubility in the liquid. The liquid volume fraction will therefore increase until C_1 is reached. At this point the composition of the liquid will cease changing and the volume fraction (liquid) will decrease due to the onset of solidification. Because this solidification occurs at constant temperature, it is termed isothermal solidification. This is different to the solidification process which is more commonly observed during casting, where the temperature of the material is constantly decreasing.

Between the compositions C_1 and C_{peq} (or C_s) there is an increasing degree of undercooling, given by the difference between the liquidus at a given temperature and the temperature of sintering. In the range of compositions between C_1 and C_s material of A will be deposited according to conventional solidification processes (Figure 5.2⁽¹⁸⁾). The morphology of the solidifying material is dictated by the stability of the solid-liquid interface. If there is high interface stability, then the growth front may tend toward a planar interface; if there is a constitutionally unstable interface, then the growth front may exhibit an irregular or dendritic structure.

The major difference between conventional solidification and isothermal solidification processes is that in isothermal solidification solute rejection does not occur back into the melt, it occurs into the substrate. Thus the stability of the interfacial region is constantly changing. Hence it would be possible that in a transient liquid phase sintering situation, particle growth morphologies will be determined by the nature of reprecipitation of the base A as the liquid changes composition. Additionally, the

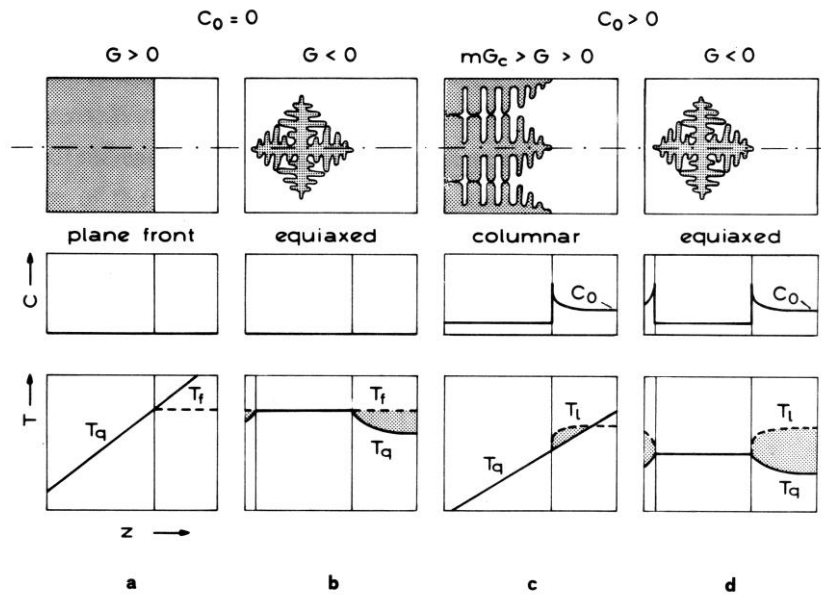


Figure 5.2 Concentration and temperature fields of dendrites. (From Kurz and Fisher⁽¹⁸⁾.) These diagrams illustrate the heat and mass diffusion fields existing along the dendrite axis, and correspond to various possible cases. In pure substances (a&b), there is no solute rejection and dendrites can form only in an undercooled melt. In (b) the heat rejection occurring during growth sets up a negative temperature gradient ahead of the interface. This leads to the establishment of the necessary conditions for the instability of thermal dendrites. In the case of alloys (c&d), dendrites can form irrespective of the temperature gradient if the interface is constitutionally unstable. If G is greater than zero (c), the latent heat is transported, together with the unidirectional heat flux, into the solid. To a first approximation, therefore, solute rejection alone needs to be considered in the case of directionally solidified dendrites. Equiaxed dendrites in alloys reject both solute and heat. (© Reproduced with permission of Trans Tech Publications.)

presence of the additive can also alter the stability of the solid-liquid interface and therefore dendrites may form. One of the consequences of forming dendrites in these situations would be that the fine dendrite arms may break off and be carried by the liquid (similar to grain-liquid mixture flow) into the melt, possibly coalescing with grains and other arms also floating in the melt. This would lead to grain growth in regions that may otherwise become pores, and hence densification could result to some degree.

The situation of planar growth in isothermal solidification of liquid-solid regions will cause bonding between particles and grains to occur in a different manner to that of non-planar growth. The influence of isothermal solidification as a bonding mechanism is largely dependent on the diffusion rate of the additive moving into the base, when this diffusion begins and the original width of the liquid seam. How isothermal solidification effects transient liquid phase sintering is represented in Figure 5.3. Figure 5.3 is a schematic representation of transient, partially transient and persistent liquid phase sintering processes.

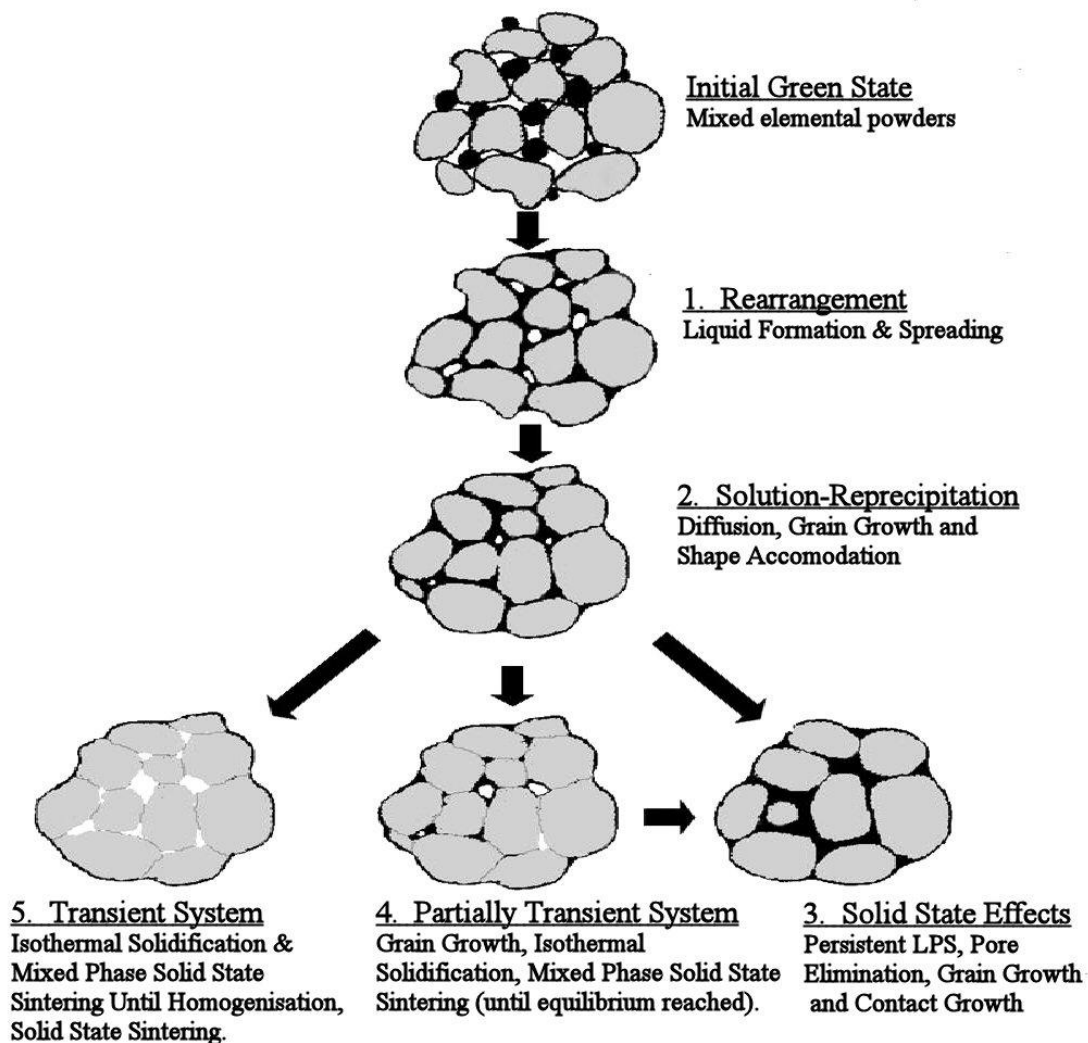


Figure 5.3 A schematic representation of persistent, transient and partially transient liquid phase sintering processes. Adapted from German⁽⁹⁾.

In sintering, the degree of bonding attributable to isothermal solidification is governed by the duration of stage 2 (solution-reprecipitation) represented in Figure 5.3. If stage 2 is of limited duration then isothermal solidification will dominate bonding. This occurs when there is a high diffusivity of the additive into the base resulting in a rapid transition to either stage 4 or 5. Stage 4 and 5 correspond to the equilibrium compositions C_{peq} and C_{teq} in Figure 5.1 respectively. Examples of this effect can be observed in Figures 4.15c&d, 4.19d&e, 4.28b&d and 4.34c,d&e. If stage 2 lasts for an appreciable period, then solution-reprecipitation mechanisms will show an increased contribution to bonding. An example of this effect can be seen in Figure 4.19a-e where the sample takes approximately 40 minutes to reach its equilibrium condition. It should be noted that during this period, isothermal solidification is still occurring, but its significance is reduced.

When isothermal solidification is occurring simultaneously to solution-precipitation, it may be possible that grain growth is accelerated. This is due to the increased rates of mass transfer from the liquid to the solid.

Isothermal solidification has a substantial effect on microstructural development. Before (and during) isothermal solidification extensive liquid networks exist. Upon completion of isothermal solidification the microstructure becomes a rigid skeleton. Examples of this can be seen by Figures 4.15c&d, 4.19d&e, 4.28b&d, also 4.34c,d&e.

The driving force for isothermal solidification as a bonding mechanism is governed by the chemical potential arising from concentration gradients occurring from the liquid into the solid base. In a planar S-L interface, the bonding liquid, being eutectic (eg. Al-Zn, Al-Cu) or peritectic (eg Fe-Cu) in nature, loses the additive element via diffusion into the base, reducing the width of the liquid seam between adjacent particles. Due to conservation of matter, these adjacent particles expand and grow. When isothermal solidification has ceased, further sintering via solid state mechanisms occurs. The material in the bond region has a composition similar to the base material, but rich in solute. Because the diffusivity of the additive in the base is faster than the self-diffusivity of the base there are similarities to solid state activated sintering. When the system becomes homogeneous conventional solid state mechanisms predominate. An example of this effect can be seen in Figure 4.15c&d. For the case where dendrites form from unstable interfaces, the above also happens as the last stage, but not before substantial grain/particle growth occurs (Ostwald ripening) (eg. Figure 4.19d&e). Dendrites that form and grow away from particle centres can impinge on each other and interlock, leaving a well-bonded region that is likely to be pore free and granular. Again, as the liquid disappears, adjacent regions expand and grow and hence bond as the liquid forming element passes into solution.

Isothermal solidification may therefore be considered to exhibit a substantial contributory effect to the processes that are occurring during the transient stage of sintering. These contributions may be evident in the form of enhanced grain growth and subsequent bonding.

5.3. Wetting

The major impediment to the sintering of Al is the oxide layer present on the surface of all aluminium particles^(74,81,84,86,89,92,94-105). The presence of oxide phases on the surface of aluminium generally should mean that no wetting and hence no sintering should occur. However, wetting and sintering is observed in Al systems. The wetting of aluminium by liquid phases in sintering processes is a phenomenon that has not been explained thoroughly. For a liquid phase to wet aluminium, the oxide layer must be disrupted during sintering. There are two mechanisms by which this oxide rupture may occur. The first of these is discussed below, and the second in section 5.4.

It has been observed in this work (considering only binary systems) that a zinc rich or copper rich liquid will wet aluminium particles with a relatively sharp dihedral angle (Figure 4.15c&4.19d). Tin however, spreads to great distances and exhibits a large volume fraction of liquid (Figure 4.26&4.27), although the dihedral angle is large (Figure 5.4). The major difference between the two situations is the solubility of Zn and Cu in Al.

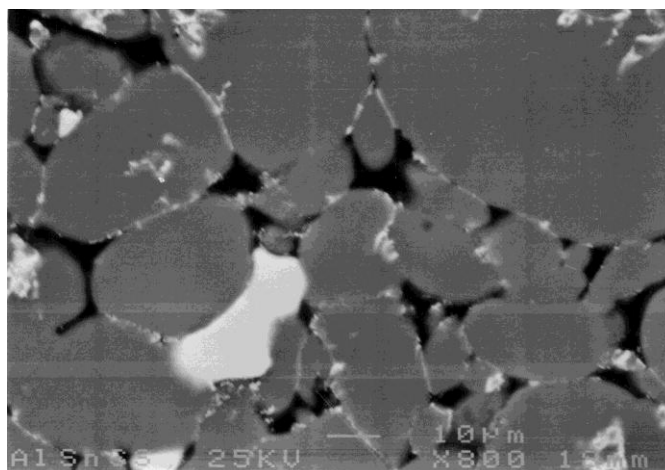


Figure 5.4 Backscattered SEM micrograph of aluminium sintered with tin exhibiting the poor wetting associated with this system.

For the persistent Al-Sn system, compaction ruptures oxide surfaces by shear and metal-metal contact occurs. This forms weak bonds between Al-Al and Al-Sn particles. Due to the solubility conditions (a high solubility of Al in liquid Sn, and a low solubility of Sn in solid Al) a large quantity of Al is dissolved in the liquid Sn above 575°C (Figure 4.26&4.27). This occurs where oxide surfaces have been ruptured. Wherever Sn has not formed metal-metal contact with Al, there is no dissolution and the liquid does not spread (Figure 5.4). German⁽⁹⁾ reports that during the spreading process a reaction occurs at the solid-liquid interface until the liquid approaches saturation with the solid component. Liquid phase spreading ceases when the liquid reaches its equilibrium composition. The spreading rate⁽⁹⁾ is governed by the mechanisms of spreading and not by the free energy decrease associated with wetting. The mechanism of spreading is controlled by the flow of the liquid over the solid surface. Therefore spreading kinetics depend on the surface energy of the solid. In the case of Al-Sn, this process is hampered due to the oxide. Only oxide regions which have been previously disrupted come into contact with the liquid phase. Due to the large amount of oxide rupture during compaction, however, the liquid phase will contact most particles. After the initial liquid penetration, further sintering is limited (Figure 5.4). This is due to the inability of liquid Sn to wet Al₂O₃ surfaces.

For the case where there is some transient aspect to the sintering process (Zn and Cu) there are competing factors dictating liquid flow and infiltration. These are the dissolution of Al in the liquid phase and the diffusion of the liquid forming additive into

the base. Hence there is mass transfer of elements in opposite directions. The process by which transient (Zn, Cu) liquid phases may wet Al is represented in Figure 5.5. For these transient systems the diffusion of the additive into the base results in a concentration gradient from the tip of the liquid seam to the interior of the particle. The composition of the solid region immediately adjacent to the liquid should therefore be close to the maximum solid solubility of the additive in the base at the sintering temperature. This diffusional process causes an expansion of the Al particles, placing a stress on the oxide film (Figure 5.5B). This may result in the rupture of the oxide layer in front of the liquid. As the oxide ruptures, the liquid wets the underlying metal. The means by which an oxide film can rupture under a tensile strain is shown in Figure 5.6⁽¹²¹⁾.

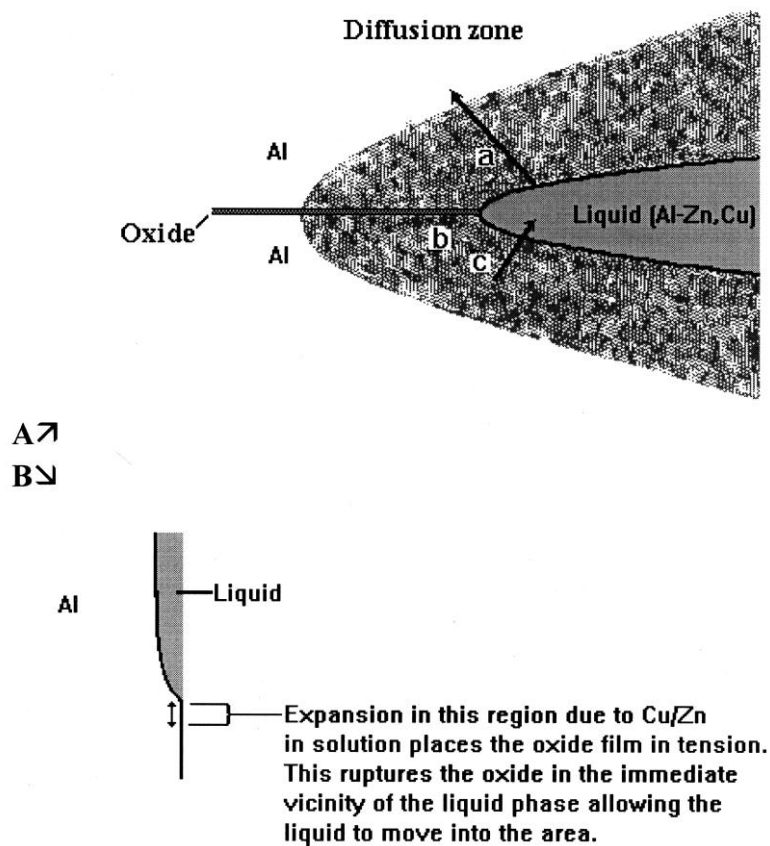


Figure 5.5 The process of liquid phase spreading in Al-(Zn,Cu) alloys. In Fig.(A) 'a' represents a diffusion gradient radiating outwards from the liquid phase; 'b' is the region of highest expansion due to this area containing almost the solubility limit of additive at the sintering temperature; in this region the oxide phase is placed in tension and ruptures (Fig.5.5B). 'c' represents the dissolution of Al which becomes part of the liquid phase.

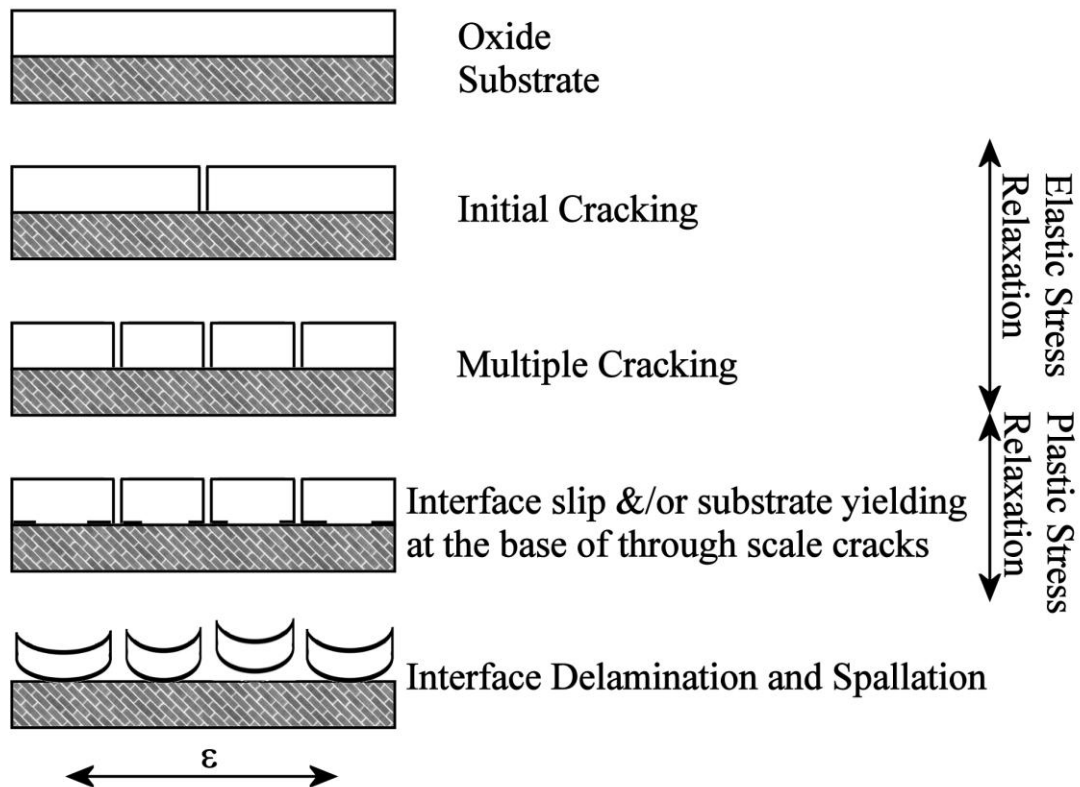


Figure 5.6 The means by which oxide films rupture under tensile strain. Adapted from Nagl and Evans⁽¹²¹⁾.

If this model is correct, the most efficacious sintering liquid for Al (ie. one with a sharp wetting angle and sufficient spreading) would be that which fulfilled the following criteria:

1. a high diffusivity of the additive in the base (to allow fast liquid penetration),
2. a relatively low solubility in the base at the sintering temperature (to maintain liquid volumes),
3. a high solubility of the base in the liquid phase to facilitate spreading.

This effect can be seen for the binary Al-Cu system, when compared to both the Al-Sn and Al-Zn systems. The three systems are compared in Table 5.1. The diffusivity of Cu in Al at 600°C is more than double that of either zinc or tin; yet the duration of the maximum liquid phase presence is extended when compared to Zn (Figures 4.15&4.19). This is due to the limited solid solubility (~3wt%) at 600°C of Cu in Al. The comparable solid solubility of Zn in Al under the same conditions is 17% at 600°C and 13% at 620°C.

These observations support the hypothesis that oxide break-up and subsequent wetting of the substrate is facilitated by the diffusion of the solute into the base ahead of the liquid seam.

Table 5.1. A comparison of observed wetting and spreading features for three binary Al alloys.

System	Solubility at the sintering temperature (additive in base) ⁽¹²⁰⁾	Diffusivity at the sintering temperature (cm ² /sec) (additive in base) ⁽¹²²⁾	Solubility at the sintering temperature (base in liquid) ⁽¹²⁰⁾	Dihedral angle (°)
Al-Sn	<0.1%	0.2440 at 600°C	59%	73±20°
Al-Zn	~16% at 600°C, 11% at 620°C	0.258 at 600°C	66% at 600°C, 76% at 620°C	7±1.5° at 620°C
Al-Cu	~3% at 600°C	0.63507 at 600°C	79%	11±4°

5.4 The Role of Mg in the Break Up of the Oxide Layer

Generally, in press and sinter operations in other non- aluminium systems, the atmosphere is used to reduce the oxide layer. However, this has only recently been found to be possible with Al⁽¹⁰³⁾. Nakao *et al.*⁽¹⁰³⁾ found that Mg₃N₂ vapour under reduced pressure (0.1 Torr) in a rare gas atmosphere results in the reduction of the oxide layer on Al particles. It has been postulated^(100,102) that the presence of elemental Mg in sintering operations may affect the oxide layer, but this has not been experimentally demonstrated. This current work suggest that magnesium, especially at low concentrations, has a disproportionate effect on sintering because it disrupts the passivating Al₂O₃ layer through the formation of a spinel phase. The following discussion proposes a mechanism by which this may occur.

It has been found⁽¹²³⁾ that very small additions of Mg can substantially alter densification in persistent liquid phase sintered aluminium alloys. Figures 4.37 and 4.39 support these findings. Figure 4.13 shows the spinel phase MgAl₂O₄ present in an Al-2.5Mg alloy. A possible reaction sequence for the formation of spinel is

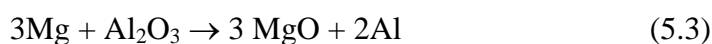


which is a partial reduction reaction to form cubic spinel and aluminium. This should be distinguished from reaction 5.2 which often occurs at higher temperatures via a solid state reaction between oxide materials⁽¹²⁴⁾



Reaction 5.1 is more likely to occur due to the greater free energy change⁽¹²⁵⁾ associated with the reaction.

Reaction 5.1 is observed at bonding interfaces in metal matrix composites and in studies of the oxidation behaviour of Al-Mg alloys⁽¹²⁵⁻¹³³⁾. However, it has been found⁽¹²⁵⁾ in studies of Al-Mg based composites that at some concentration between 4 and 8% Mg, that the complete reduction reaction (5.3) is dominant, as indicated by analysis of the equilibrium activity of Mg⁽¹²⁵⁾.



It is of interest that the free energy changes documented⁽¹²⁵⁾ for reactions 5.1 and 5.3 are very close at 2 and 4% Mg, with 5.1 being most favourable at 2% Mg, while 5.3 is the more favourable at 4 and 8% Mg. Reaction 5.3 can occur directly, or by way of reaction 5.1, (ie. $\text{MgAl}_2\text{O}_4 + 3\text{Mg} \rightarrow 4\text{MgO} + 2\text{Al}$ as a second step). McLeod and Gabriel⁽¹³²⁾ calculated the Mg concentration in equilibrium with reactions 5.1 and 5.3. This is shown in Figure 5.7. These figures suggest that the critical percentage of Mg facilitating reaction 5.1 is actually <1 wt%, and possibly <0.02% in the range of ~500°C to 660°C.

Therefore, in Al-Mg powder alloys, the presence of the observed spinel phase (Figure 4.13) indicates that when the oxide disrupting reaction occurs, the local Mg concentration may have been low in local regions, because of the preferential formation of spinel over MgO. If this were the case, then the oxide would not have been reduced through contact with the eutectic liquid (~36% Mg at 445°C) but by Mg in solution in the Al matrix. In studies of the oxidation behaviour of Al-Mg alloys⁽¹²⁷⁾, it has been noted that pure Al forms a continuous amorphous oxide film that acts as a diffusion barrier. At temperatures above 400°C, $\gamma\text{-Al}_2\text{O}_3$ nucleates at the oxide-metal interface to rupture the continuous oxide film. If the alloy contains Mg in solution, disruption of the oxide film by the formation of spinel domains is facilitated. Hence for spinel formation to occur in Al-Mg powder materials it would be required that the Mg should be in solution before reaction 5.1 occurs at the oxide-metal interfaces.

This mechanism for the reduction of the alumina layer is confirmed by Scamans and Butler⁽¹²⁶⁾ who conducted in-situ oxidation experiments of Al alloys. It was found that 50-75nm crystallites of spinel formed at the oxide-metal interface, nucleating on alumina grain boundaries with a density of greater than $10^{10}/\text{cm}^2$ at <475°C. Kovacs *et al.*⁽¹³⁴⁾ found that detectable Mg evaporation could be observed above 215°C in an Al alloy, and proposed that this would occur after Mg had diffused to the surface, through the alumina layer^(134,135). Hence it is likely that the oxide surface is actually ruptured at relatively low temperatures by the Mg, possibly allowing subsequent Mg evaporation. Magnesium vapour has been previously found to promote filler alloy flow during fluxless brazing of aluminium in vacuum or inert atmospheres⁽¹³⁵⁻¹³⁷⁾. It was found by Terril *et al.*⁽¹³⁷⁾ that the best candidate activator materials for fluxless brazing were Mg, Ca, Sr and Li. Magnesium had the highest vapour pressure of these materials, and it was noted that the minimum Mg concentration for vacuum brazing was ~0.3%Mg for an ideal solution of Mg in Al. It is of note that Mg vapours are documented^(135,138) as forming protective atmospheres preventing subsequent oxidation of substrate surfaces, and improve wetting under brazing conditions.

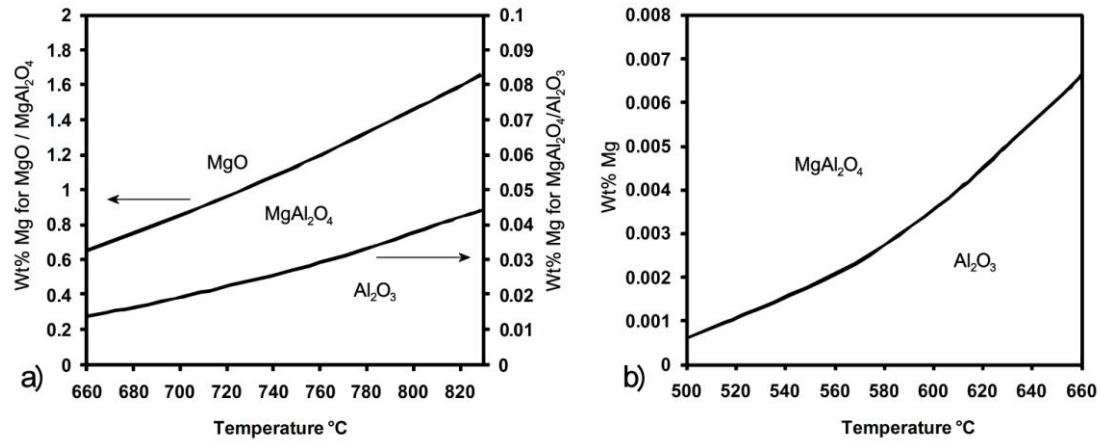


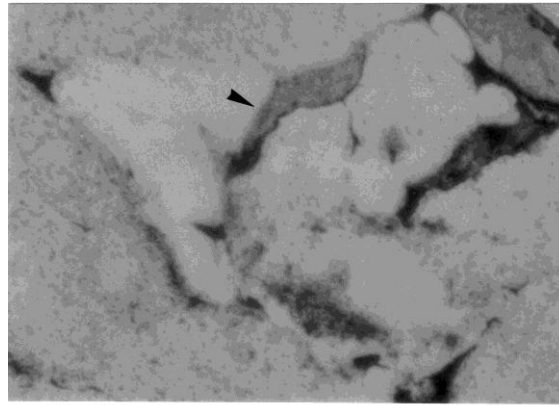
Figure 5.7 Thermodynamic stability of Al-Mg oxides in Al-Mg alloys; (a) liquid alloys, (b) solid state. (Adapted from McLeod and Gabriel⁽¹³²⁾).

Notable diffusion of magnesium in aluminium has been found to occur at relatively low temperatures in aluminium powder systems (Figure 5.8) (the diffusivity of Mg in Al between 300°C and 550°C is $\sim 1.2 \text{ cm}^2/\text{sec}$.⁽¹³⁹⁾). As a consequence, the Mg may have begun reducing the oxide layer via diffusion before the eutectic temperature is reached. As there is no evidence of the formation of MgO, and there is limited liquid phase present, it is conceivable that only solid state reduction occurs via the diffusion of Mg to oxide regions. This disruption of the oxide phase has been reported to effect consolidation in extruded 7000 series alloys⁽¹⁵⁴⁾ and is a possible cause for the enhanced sintering response in the presence of Mg. After the reduction reaction is completed, the Mg may work to form a protective atmosphere which prevents further oxidation.

It is proposed that the possible sequence of events in oxide disruption is as follows:

1. Local oxide regions are ruptured during compaction allowing metal-metal contact;
2. Where Mg is in direct contact with the oxide, it is possible that MgO may form via reaction 5.3⁽¹²⁵⁾, but no evidence of this was identified;
3. The Mg diffuses through the adjacent Al powder particles at relatively low temperatures and reduces the oxide at the metal-oxide interface, forming spinel;
4. Nearby Al particles (not directly in contact with Mg) are exposed to Mg and their oxide layers are subsequently disrupted.
5. Mg vapours may form and provide a protective atmosphere during the remainder of sintering.

This is presented schematically in Figure 5.9.



15 μ m —————

Figure 5.8 Diffusion zones around Mg particles (arrowed) at 350°C in a quaternary Al-Zn-Mg-Cu alloy. Optical micrograph. (In unetched samples containing Mg, diffusion zones are evident by the differences in polishing rate between the matrix Al and the solution strengthened Al adjacent to the Mg)

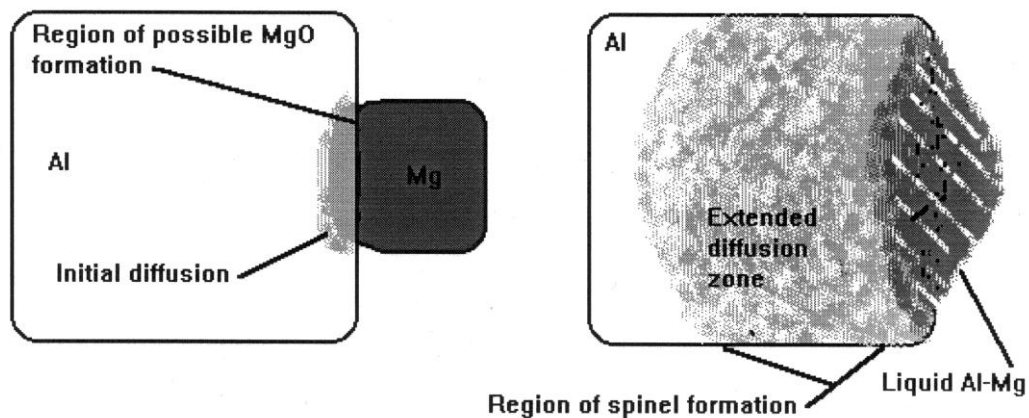


Figure 5.9 A representation of the processes involved in the reduction of the alumina layer by Mg during sintering of Al-Mg alloys.

In this way the magnesium, even if only at low concentrations, can chemically attack the aluminium oxide layer and disrupt it sufficiently to allow an improved sintering response.

5.5 *The Sintering of Al with Mg- Microstructural Development and Sintering Events*

For persistent compositions (eg. 14% Mg) the liquid phase is evident first at 445°C (Figure 4.7) and passes into solution 2 minutes later at 465°C (Figure 4.9). A limited amount of supersolidus liquid returns when the sample exceeds the solidus temperature (480°C), which can be observed by re-running high Mg concentration samples (after rapid cooling) in the DSC (Figure 4.6). Any liquid that was present

before the sample was cooled will re-melt at the eutectic temperature. This gives an indication of how much liquid was present at the equilibrium condition. The Al-Mg phase diagram indicates that there should have been approximately 30% liquid at the sintering temperature for Al-14Mg. As the second DSC run (Figure 4.6) exhibited a melting endotherm having 15% of the energy of the initial peak, it is possible that the oxidation of the Mg (as evidenced from TGA, eg. Figure 4.12) was consuming some of the equilibrium liquid phase. It is also possible that in the second run the Mg was diffusing into the Al up to the eutectic temperature, therefore reducing the amount of melt formed.

The liquid phase formation sequence for high Mg transient compositions (eg. 6%) was the same as for the persistent (14% Mg) system examined except that no supersolidus liquid phases formed.

Low Mg samples (2.5wt%) attained homogeneity more slowly, with some liquid still present at 525°C (Figure 4.10). Whereas higher concentration Mg alloys exhibited reaction of virtually all Mg particles at or about the eutectic temperature, lower Mg alloys showed a more gradual reaction. That is, the Mg particles reacted with the Al over a temperature range starting at the eutectic temperature (presumably where there was metal-metal contact from compaction) and gradually continuing through to 525°C. This variance may be due to the differences in the volume of Mg present; 2.5 wt% Mg occupies a volume fraction of 0.04, while 14 wt% Mg occupies a volume fraction of 0.2. Therefore in high Mg samples, there is widespread liquid formation, and Mg particles which do not have metal-metal contact are easily incorporated into the sintering liquid. This is not possible in low Mg alloys, as the liquid volume will not be great enough in local regions to incorporate the unreacted Mg.

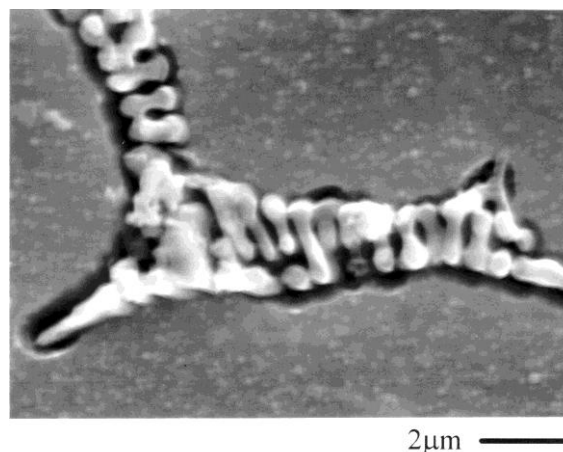


Figure 5.10 The eutectic liquid phase in an Al-14Mg alloy penetrating particle and grain boundaries at 455°C. (Backscattered SEM micrograph).

In the early stages of sintering when the liquid fraction is at a maximum, capillary effects and isothermal solidification (section 5.1) are the major sintering mechanisms. Some grain boundary attack does occur (eg. Figure 5.10, 4.7 and 4.8), but the local liquid is not present in sufficient quantities to cause particle disintegration. This attack does however provide excellent sites for grain boundary diffusion, hastening homogenisation.

TGA (Figure 4.12) of an Al-6Mg alloy (with 1% stearic acid) indicates that 3 events occur during the sintering cycle. When the melting point of the stearic acid is exceeded at 54°C, no weight loss is noted. This is not unexpected because no vaporisation has occurred. The first inflection, which begins at ~13 minutes (128°C) into the sintering cycle, corresponds to the onset of stearic acid vaporisation. This gives a weight loss of 0.625%. During the dewaxing cycle (20 minutes at 250°C) no significant weight loss is recorded. At 46 minutes (310°C) a second weight loss of 0.38% begins which continues until 61 minutes (460°C). It is possible that a metal stearate (possibly magnesium stearate) forms earlier in the sintering cycle and burns off at this higher temperature. Simultaneous mass spectrometry is required to confirm this. It is possible that magnesium stearate is similar in characteristics to lithium stearate, another common P/M lubricant, which is known to scavenge oxygen and water from powder compacts⁽¹¹²⁾. Hence the formation of magnesium stearate may be beneficial to sintering. At 500°C (65 minutes) a weight gain begins, probably due to the oxidation of the sample. This weight gain continues through to the end of sintering and is consistent with oxidation behaviour noted previously^(126,127).

5.6 The Effect of Increasing Chemical Additions on Mechanical Properties in Binary Alloys

Increasing the amount of additive elements in transient liquid phase sintered materials generally increases the amount of secondary porosity present^(57,58). The mechanical properties of a material continually decrease with increasing porosity levels⁽¹⁴⁰⁾. This is in contrast to the behaviour noted here in Figures 4.1, 4.4 and 4.5.

The sintered properties of the binary systems studied (Al-Zn, Al-Mg and Al-Cu) are directly influenced by the concentration of additive elements in three ways: firstly, increasing the additive concentration increases the number and size of secondary pores in the sintered material (due to compact expansion from homogenisation), which will decrease the sintered properties. Secondly, increasing additive concentration increases the volume of liquid phase which develops, resulting in improved bonding which will increase sintered properties. Finally, increasing additive concentration will increase the contribution of solid solution hardening to the final properties of the material.

It is apparent that increased alloying can improve the hardness of sintered aluminium despite the presence of greater volumes of porosity. This occurs because other hardening mechanisms play a dominant role.

5.7 The Particle Size Effect

5.7.1 Introduction

Small additive particles are generally considered^(9,141) to improve sintering because they have a high surface/volume ratio (and hence provide a higher driving force for sintering), are better distributed in a compact and leave smaller pores in the final sintered material. However, preliminary work indicated that the reverse may be true in the Al-Zn system⁽³⁵⁾. It was suggested that the unusual relationship with particle size may have been due to the non-ideal solubility ratio between the additive and the base (see section 2.8.2.5). This previous work may have been compromised by the presence of impurities in the zinc. This is tested here using pure zinc powders. In addition, the relationship between particle size and solubility was further investigated using other systems. The Al-Cu system has some similar characteristics to Al-Zn, except the solubility of Cu in Al is not as large as zinc in aluminium. The effect was also tested in Fe-Cu, because it is a non aluminium system with a similar solubility relationship to Al-Zn and it is the basis for widely used commercial alloys. Al-Sn was used as a control because it is an ideal persistent system.

Zinc has a lower melting point than aluminium, no intermediate phases form and there is complete solubility in the liquid phase. However, the mutual solid solubilities are non ideal: zinc is highly soluble in aluminium (83.1 wt% max.) whereas aluminium has a low solid solubility in zinc (1.2 wt% max.). The Al-Cu system is dissimilar to Al-Zn; the solid solubility of Cu in Al (5.6 wt%) is not as large as Zn in Al, the melting point of Cu (1085°C) is much higher than that of Al (660°C) and a number of intermetallic phases form. Fe-Cu exhibits characteristics similar to Al-Zn, having the same type of solubility ratio (the max. solubility of Cu in Fe is 13 wt%) and the melting point of the additive is substantially less than that of the base. Tin has a lower melting point than aluminium, there is mutual solid insolubility and complete solubility in the liquid phase. There are no intermediate compounds. The relevant phase diagrams are shown in Figure 5.11.

5.7.2 Sintering mechanisms and microstructural development for Al-Zn

5.7.2 (a) Fine particles

Where fine additive particles were used, little liquid phase formed due to its highly transient nature (Figure 4.15e-h). Once the zinc reacts with the aluminium matrix, diffusion is rapid (Figure 4.15f). As a result, the final microstructure is virtually

unsintered (Figure 4.15h). The boundaries present in this micrograph are prior particle boundaries, not grain boundaries. The grain size of the elemental Al powder is less than $10\mu\text{m}$ ⁽³⁵⁾. Due to the limited liquid quantity, only solid state sintering mechanisms were observed, although DSC (Figure 4.16) indicated zinc melt formation. The dominant sintering mechanisms were isothermal solidification and solid state sintering. Additionally, the high vapour pressure of Zn at the sintering temperature may contribute to pore rounding and some sintering at longer times⁽³⁾. This occurs by evaporation and condensation of the vapour phase (see also section 2.5.1.).

5.7.2 (b) Coarse particles

The dominant sintering mechanisms in Al-Zn where coarse particles were used are generally consistent with those noted in other transient sintering systems^(11,29,37,66) although the high vapour pressure of zinc adds additional factors. Persistent liquid phase sintering mechanisms such as Ostwald ripening, coalescence, directional particle growth and contact flattening are expected to contribute only minimally to sintering. When coarse particles are used, the effect of the liquid phase is increased (Figure 4.17). Due to its limited duration, however, its effect on persistent liquid phase sintering mechanisms, which require longer times to be effective, is reduced.

In the microstructural development of Al-Zn compacts, the zinc melts at 420°C , but there is no reaction between the zinc and aluminium until higher temperatures are reached ($\geq 525^\circ\text{C}$) (Figure 4.15a). Once reaction has begun, aluminium is dissolved in the liquid, increasing the liquid volume. Additionally, as part of this process, grains at the edge of melt pools are broken off by grain boundary attack and float into the melt. Hence both pore elimination by liquid flow and by grain-liquid mixture flow occur. These mechanisms have a limited role in the sintering process because they exist only on a limited scale, but do assist the spread of liquid phase and are the precursor to grain boundary attack. At 580°C , penetration of particle and grain boundaries by the liquid phase begins, which reaches a maximum spreading and volume fraction at 620°C (Figures 4.15c&4.17). When this occurs, the effective particle size in the liquid rich regions is decreased (Figure 4.15c) allowing high mobility of these particles. Over the following 10 minutes, the liquid phase passes into solution and bonding and grain growth via isothermal solidification (section 5.1) dominates. This results in a well-sintered structure (Figure 4.15d). Additionally, solid state sintering via diffusive processes continue to aid sintering when sintering times are extended. The effect of the zinc vapour phase may also be contributing to bonding, but it would seem that its effect is largely deleterious. Zinc vapour porosity generated during the sintering process impedes densification and tends to remain in the sintered material. However, the vapour phase could be expected to aid pore rounding.

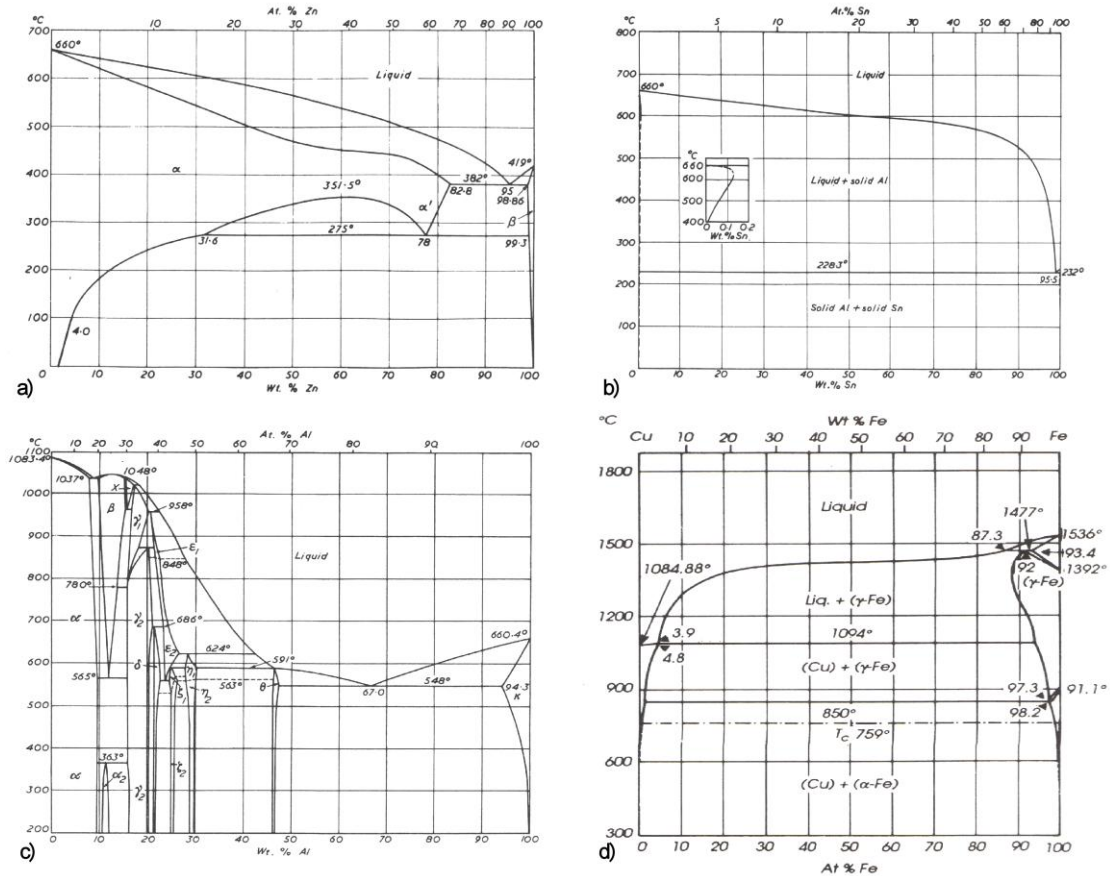


Figure 5.11 The phase diagrams of the binary systems examined to assess the effect of additive particle size. (a) Al-Zn, (b) Al-Sn, (c) Al-Cu, (d) Fe-Cu.⁽¹²⁰⁾²

5.7.3 Sintering mechanisms and microstructural development for Al-Cu

5.7.3 (a) Fine particles

Where fine copper particles were used, limited liquid phase was present and, as in the Al-Zn system, did not appear to contribute greatly to bonding (Figure 4.19g-l). At 550°C (2°C above the eutectic temperature) some diffusion is occurring as can be seen by the formation of an intermetallic phase around some copper particles (Figure 4.19g, arrowed). By 575°C (Figure 4.19h) all fine copper particles have reacted and the amount of liquid phase is at a maximum. This liquid decreases gradually in volume and after 10 minutes at 600°C (Figure 4.19j) the compact appears to have reached its equilibrium condition. While the liquid phase is present, pore elimination by liquid flow and a degree of coalescence must be occurring before isothermal solidification takes over as the dominant bonding mechanism. As this system is partially transient, the persistent liquid that exists will continue to aid sintering by contributing to additional coalescence and Ostwald ripening.

² The original reference for this figure was ASM Handbook, *Alloy Phase Diagrams*, 10th ed., Vol.3, ASM International, Materials Park Ohio, 1992.

5.7.3 (b) Coarse particles

Mechanisms occurring in this system appear to have many similarities to those in the Al-Zn system (except for the vapour phase). However, as the duration for which the liquid phase existed was extended, and the system was only partly transient, persistent liquid phase sintering mechanisms had a greater effect.

Initially, large pools of eutectic liquid form, although no sintering is apparent (Figure 4.19b). As more Al dissolves in the liquid, grains and fine particles float into the liquid pools (Figure 4.19c). Soon after, the liquid begins to penetrate particle and grain boundaries and a substantial amount of liquid flow begins, which continues until 40 minutes after the sintering temperature has been reached. Additionally the grains and fine particles that have floated into melt pools grow via Ostwald ripening and isothermal solidification (Figure 4.19d). It is of particular note that regions adjacent to prior liquid pool sites exhibit a larger grain size than those at distances further away (Figure 5.12). This appears to be due primarily to these regions being surrounded by liquid for most of the sintering cycle. The variation in grain size in the final sintered material is the result. Isothermal solidification may have a critical contribution to this grain growth, possibly being responsible for the unusual grain morphology noted in Figure 4.19d (arrowed). This is explained in more detail in section 5.1. Ostwald ripening and coalescence dominate during the liquid presence (see Figure 4.19d). This effect of Ostwald ripening can be seen by the large change in grain size evident in the final sintered material (Figure 5.12). A large degree of rearrangement and shape accommodation were facilitated during the period in which the non-equilibrium liquid phase was present. Little liquid remains at equilibrium and this is mostly concentrated at prior particle sites (Figure 4.19f, arrowed).

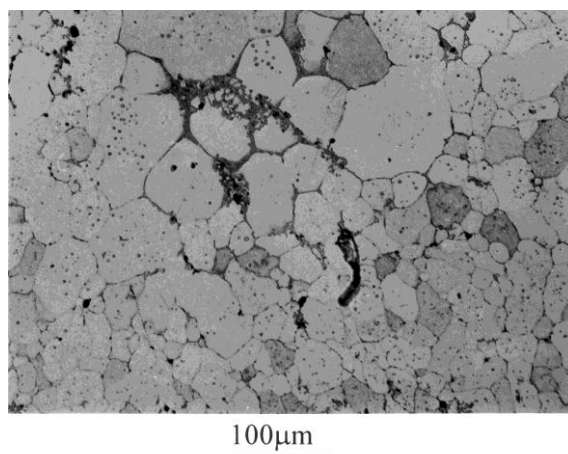
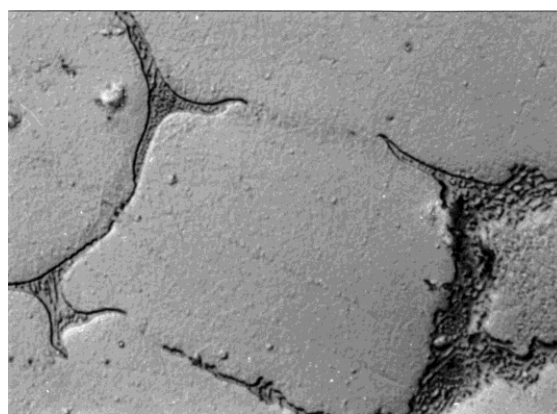


Figure 5.12 Al-5.5Cu (particle size 75-106 μ m) sintered 40 minutes at 600°. Note the variation in grain size due to activated Ostwald ripening and isothermal solidification where greatest quantities of liquid still exist.

One of the particularly interesting aspects in the morphological development of this system is the change in grain size during sintering, and the variability in grain size

when the compact has reached compositional equilibrium. Apart from Ostwald ripening, chemically induced interface migration (CIIM) may also be occurring and may contribute to this effect. Unusual neck growth and bulge's in prior particle boundaries may be the result of DIGM (see Figure 5.13). From Figure 5.13, it should be noted that etching has revealed the region in the wake of the migrating boundary to be solute rich. This is consistent with effects reported elsewhere^(11,43,48). As noted in section 2.5.5.3(a) experiments on the Mo-Ni system by Kaysser⁽¹¹⁾ showed that a saturated solid solution formed behind migrating boundaries. This type of boundary migration occurs when the solid solution left in the wake of the boundary has a lower free enthalpy than the material in front of the boundary. When the boundary migrates at constant velocity, a steady state concentration profile develops. Additionally, the unusual microstructures noted in the Al-Cu system (Figure 5.14) are typical^(11,43,48) of systems exhibiting DIGM. However, these microstructural effects may be partially a consequence of isothermal solidification, or a combination of the two.



15μm

Figure 5.13 Unusual neck growth in the form of a bulge on a prior particle boundary. Note the region in the wake of the migrating boundary has etched to reveal a region of differing composition. This is consistent with DIGM.

The role of isothermal solidification in this system and others containing Cu, is unusual. The irregular dendrite-arm like structures that form (Figure 4.19d) may influence the dominant sintering mechanisms to the effect that the absolute role of the persistent liquid phase sintering mechanisms is ambiguous. This is because the structures that form are not consistent with those formed during normal sintering processes (eg. Figure 2.13) and hence cannot be compared. Grain growth is at times highly irregular, liquid seams are not stable (Figure 5.14), and coalescence via the liquid phase is questionable. Similar microstructural features have been noted during isothermal solidification (section 5.1) in a study of Ni-11P braze drops on a Fe-20Cr substrate⁽¹⁴²⁾. Reported features corresponded to the second stage of isothermal solidification where growth of the substrate was occurring as material passed into solution. This growth occurred in the form of acicular crystals and resulted in an

irregular growth front. It is of note that Rhee and Yoon⁽⁴⁸⁾ document that the effect of CIIM resulted in corrugated interfaces and comments that CIIM should effect solidification fronts in this way.

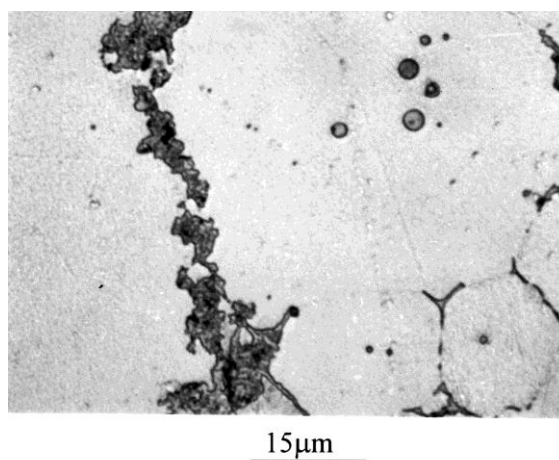


Figure 5.14 Irregular interface morphology along a liquid seam in an Al-Cu alloy sintered 40 minutes at 600°C. This kind of microstructural feature is common in systems exhibiting CIIM^(43,48). The liquid spheres are also indicative of CIIM⁽⁴⁵⁾.

Unusual effects in the sintering of Al-Cu have also been observed by Savitskii⁽⁴⁹⁾. Abnormally high rates of grain growth were observed, and occurred where no solution reprecipitation processes should occur. Savitskii also notes that similar effects occur in the ternary Sn-Pb-Cd system. The unusually large amount of grain growth in Al-Cu (eg. Figure 5.12) was attributed⁽⁴⁹⁾ to activated recrystallisation. This activated recrystallisation was thought to be a response to DIGM occurring in the material. The diffusion coefficient in the moving grain boundary was determined to be ~1000 times higher than in a stationary boundary, and approached mass transfer rates similar to that in liquid phases.

A possible mechanism and explanation for the contribution of CIIM to liquid phase sintering follows. It is known that CIIM processes occur in Al-Cu alloys⁽⁴⁵⁾. (See also Figures 5.13, 5.14). During sintering, grain growth is excessive in the Al-Cu alloys examined here (Figure 5.12). Kaysser⁽¹¹⁾ notes that in many sintering systems, diffusion controlled Ostwald Ripening is the rate controlling step for sintering. As the diffusion coefficient in the moving boundary is excessively large⁽⁴⁹⁾, activated Ostwald Ripening is likely to be occurring, as is activated solid state sintering. Due to much of the liquid phase existing on grain boundaries at the equilibrium condition, an increase in grain size will result in liquid segregating to the pore space, possibly improving connectivity. Additionally, the excessively large grain size will mean that there is a greater amount of liquid involved in the sintering of the solid particles, which should result in improved densification⁽⁹⁾. Hence it is likely that a combination of factors lead to the improvement in sintering in Al-Cu. These are summarised below:

1. CIIM and the associated interfacial instability results in excessive grain growth both during the isothermal solidification stage and during persistent liquid phase sintering at the equilibrium condition.
2. DIGM causes activated sintering due to rates of mass transfer approaching that for liquid phases.
3. The increase in grain size via points 1 and 2 above causes the liquid phase to segregate to the prior particle boundaries at longer sintering times as a consequence of grain growth, resulting in a greater effect of the liquid phase. This should result in enhanced bonding and densification⁽⁹⁾.

5.7.4 Sintering mechanisms and microstructural development for Fe-Cu

5.7.4 (a) Fine particles

Where iron was sintered with fine copper powders (Figure 4.28e-h), a limited amount of liquid phase was present and the effect of the liquid phase was minimal. At 1100°C (Figure 4.28f) the liquid volume is at its maximum and flow along particle and grain boundaries occurs. Because the iron does not have the stable oxide film as aluminium does, the liquid flows readily along particle surfaces. Particle disintegration is the dominant sintering mechanism and diffusion is rapid (Figure 4.28f). Ostwald ripening and coalescence would be expected to contribute to bonding during the period that the liquid phase is present, and isothermal solidification is the dominant bonding mechanism as the liquid phase passes into solution. After 15 minutes at 1150°C, virtually all the copper has passed into solution (Figure 4.28h) and solid state sintering dominates until the end of the sintering cycle.

5.7.4 (b) Coarse particles

In the sintering of this system, there are no major differences between this work and that previously detailed in the literature⁽²³⁾ (section 2.7) for coarse copper powders (~100µm). Essentially the same mechanisms dominated sintering as those for Al-Zn (except the effect of the vapour phase). After the melting point of copper had been exceeded (1087°C) the liquid phase flowed extensively, to the effect that the remaining pores were generally confined to prior copper particle sites (Figure 4.28c). Again, particle disintegration played a major role by decreasing the effective particle size to allow greater mobility. The large decrease in porosity resulting from the liquid phase presence suggests that pore elimination by liquid flow dominates during the initial stages of sintering when the liquid phase is penetrating the compact. Particle disintegration occurs simultaneously. Once the liquid begins to pass into solution isothermal solidification dominates as the bonding mechanism. Subsequent sintering via the liquid is of limited duration and solid state sintering takes over once the material is single phase.

5.7.5 Sintering mechanisms and microstructural development for Al-Sn

The operative sintering mechanisms for Al-Sn are consistent with those documented^(9,11,23) for other unipolar systems; that is, Ostwald ripening, coalescence, and contact flattening. Additionally, pore elimination by liquid flow and grain-liquid mixture flow is observed.

There is no significant difference in the final sintered microstructures of aluminium sintered with coarse and fine tin powders (Figure 4.26&4.27). The only notable difference during the morphological development was that where fine powders were used, the liquid phase reached its maximum volume fraction slightly faster and at lower temperature. A large amount of liquid phase forms, due to the high solubility of aluminium in liquid tin at the sintering temperature; this accounts for the substantial increase in liquid fraction at 30 minutes (Figure 4.26). The diffusion of the additive into the base is virtually non-existent due to the low solid solubility of tin in aluminium⁽¹⁴³⁾. Hence the liquid that forms is entirely persistent and the additive powder size is insignificant. This can be expected for all systems where there is no solid solubility of the additive in the base but where the liquids are miscible.

5.7.6 The Relationship Between Solubility and Particle Size

For the Al-Zn, Al-Cu and Fe-Cu systems (Figures 4.15, 4.19 and 4.28), it is apparent that the additive particle size effects the quantity of liquid phase that forms; ie. coarse particles generate proportionally greater quantities of liquid for the same weight fraction of solute than fine particles do. This may be due to the high solubility of the additive in the base. Where fine additive particles are used, the base adjacent to the additive is never saturated. That is, all the additive is absorbed by the base and the alloy approaches equilibrium before substantial quantities of additive rich liquid can form. For coarse additive particles, however, the base becomes locally saturated before homogenisation is achieved. Hence the additive forms a liquid which flows among particles and aids sintering. Absorption of the additive and subsequent homogenisation of the alloy occurs after the liquid has affected sintering.

If the particle size effect is due to the attainment of local saturation, then both high and low heating rates should reduce the effect. Low heating rates would allow homogenisation to occur before liquid flow for even the coarsest zinc particles. At high heating rates, the liquid fraction forming from fine particles would be enhanced because the opportunity for diffusion to occur before melting and subsequent reaction with the aluminium is minimised. Because the reaction is delayed to higher temperatures, the equilibrium solubility limit is smaller and therefore local saturation can occur more easily. This would increase the quantity of liquid that forms from both fine and coarse particles. Both these effects are observed here (Figure 4.18).

As a consequence of this delayed reaction where coarse zinc particles were used, a lesser degree of grain boundary penetration and a greater degree of interparticle liquid flow occurred (compare Figures 4.18a and 4.15c, which are at a similar stage of

microstructural development). This imparts a positive aspect to sintering, as the liquid phase that forms travels further and increases connectivity between prior aluminium particles.

That the particle size effect occurred in a system such as Al-Cu which has close to ideal solubility conditions^(9,141), suggests that there may be other contributing factors besides solubility ratio. In this system, the diffusion rate of Cu into Al is faster than the reverse. The diffusivity, D , of Cu into Al at 600°C is 0.63507 cm²/sec⁽¹²²⁾ and Al into Cu is 0.07823 cm²/sec⁽¹³⁹⁾. The faster diffusivity of the additive in the base (the Kirkendall effect) would serve to enhance the homogenisation rate. This reduces the amount of free copper available to form a liquid phase. Coarser particles therefore provide more liquid and enhanced sintering. In the Fe-Cu system, as in the Al-Cu system, the diffusion of Cu into Fe is faster than the reverse. The diffusivity, D , of Cu into Fe at 1080°C (~5°C below the melting point of Cu) is 1.7534 cm²/sec and Fe into Cu is 1.3342cm²/sec.⁽¹³⁹⁾

5.7.7 The Effect of Additive Particle Size on Mechanical properties (Al-4Cu)

Densification measurements of Al-4Cu specimens showed that for the three size ranges examined (copper 2,3 & 4 (<45µm, <100µm &<150µm, respectively)), densification decreased with increasing mean particle size (Figure 4.21a). However, for these three size ranges the tensile properties passed through a maximum and decreased again for the largest mean particle size (Figure 4.20a-b). For the three cropped particle sizes (copper 1,2&5) densification remained constant with increasing particle size (Figure 4.21b). This is due to the competing effects causing expansion and contraction. The expansion due to the liquid may be countered by the shrinkage, meaning that the net dimensional change is due mostly to diffusion of Cu into Al. This effect is not observed with the ranges examined because individual copper particles are contributing differently to the sintering process, depending on their particle size and hence the amount of liquid that develops in their immediate vicinity. Tensile testing of Al-Cu specimens showed that despite the lack of change in densification where coarse powder sizes were used, the increased liquid volumes meant that the tensile properties passed through a maximum and then decreased again where the pore size became excessively large (Figures 4.20c&d, Figure 4.25).

It appears likely that there is a critical secondary pore size which overrides the positive aspect of the increased liquid volumes generated by coarser additive particles. From the results presented here, it is apparent that where starting additive particles have a size greater than ~100µm, then the resultant pores are detrimental to mechanical properties.

Fractography (Figure 4.23) showed major differences in surface topography due to the proximity of large pores where coarse particles were used (see also Figure 4.22). That

is, the cracks pass between the nearest adjacent pores and where fine particles were used the pores are uniformly distributed and this distance is small. Therefore the fracture proceeds in a planar manner. Where coarse powders were used the pores are not generally situated in a planar manner and hence the fracture follows the positions of these pores with angles of fracture surfaces between pores of approximately 45°. It appears that there are two major influences on sintered properties; the pore size, which

is increasingly detrimental as pore size increases, and enhanced bonding from greater liquid volumes. It is an unfortunate consequence that these two aspects are counteractive, but it is likely that by using a faster heating rate to increase liquid volume fractions for finer powders (section 4.4.1), that equivalent volume fractions of liquid could be achieved while maintaining a finer pore size. This theory was tested by maximising the heating rate by placing Al-4Cu(<45µm) compacts into a furnace at 600°C with no dewaxing cycle and sintering for 40 minutes. Densification was improved by using this process, being -0.32 compared to -0.49 at 10°C/min. The tensile results from these samples (section 4.4.2) showed increases of ~25% in the UTS, ~20% in the proof stress and ~50% in the elongation to failure. These findings are consistent with those presented in literature⁽⁵²⁾ for transient liquid phase sintering systems where a fine additive particle size can be beneficial if the appropriate variables are manipulated. Additionally it is noteworthy that the samples sintered with coarse powders have a rough exterior surface and poor dimensional stability. These features were not observed where fine Cu powders were added. Hence the Al-Cu system is optimised by using a fine Cu particle size with the maximum possible heating rate.

5.7.8 Summary of the particle size effect in binary systems

These observations are in contrast to previous work on Al-Zn⁽⁴⁹⁾ and the conclusions drawn from that work⁽⁹⁾. Savitskii showed that Al-Zn had poor sintering characteristics except at high temperatures and high zinc concentrations. However, only fine zinc powder sizes were used (<50µm), the microstructural development was not reported and the process variables, except aluminium particle size and sintering temperature, were not manipulated. Others⁽⁹¹⁾ also showed elemental zinc to be an ineffective sintering aid, although the particle size was not specified. Observations of Fe-Ti⁽⁵³⁾ and Cu-Sn⁽⁵²⁾ indicate that finer additive powder sizes can be beneficial, despite reduced liquid formation. That the additional liquid which here forms from coarse particles improves sintering is evident in Figures 4.15, 4.19&28. While the pores in the final sintered material are large where coarse particles are used, the distance between the pores is also large. In addition, the intrapore regions are well bonded. Where fine additive powders are used, the microstructures appear comparatively unsintered: bonding between particles is poor or nonexistent and connectivity is low (compare Figures 4.19e&k). The increased bonding where coarse

additive particles were used is attributed to enhanced liquid phase sintering resulting from increased liquid volumes.

5.8 The Role of Ternary Additions of Mg and Cu on the Particle Size Effect

5.8.1 Microstructural Evolution and Sintering Mechanisms

The sintering mechanisms in the ternary systems are similar to the equivalent binary systems. Major differences in morphological development during the isothermal solidification step were caused by the addition of copper, which appeared to promote unstable interfaces, as discussed in section 5.7.3.

5.8.1.1 Sintering mechanisms and microstructural development for Al-8Zn-2Mg

The particle size dominated the effect of the sintering liquids that formed in this system. The major difference to the binary Al-Zn system was that additions of Mg increased the rate of diffusion of Zn into Al (Figure 4.36) (discussed further in section 5.10.1). This resulted in the particle size effect being magnified. The sintering liquids that formed passed into solution faster than the equivalent binary case (Figure 4.31) even though the volume of liquid forming additives was almost doubled. The sintering mechanisms present were the same as for Al-Zn although the compacts became homogeneous faster.

5.8.1.2 Sintering mechanisms and microstructural development for Al-8Zn-1Cu

The particle size effect was again evident in this system (where Zn particle size as opposed to Cu particle size was altered) (Figure 4.32) and again there were few observable differences in sintering mechanisms compared to the binary Al-Zn system (section 5.7.2). Copper additions to the binary Al-Zn system appear to increase the volume of the liquid phase which forms (by increasing the quantity of liquid forming elements and decreasing the solidus temperature), for both coarse and fine zinc powders, providing more sintering liquid than for the binary Al-Zn case. The addition of 1% Cu also causes the system to become persistent, whereas the binary Al-8Zn alloy is completely transient. Copper thereby enhances sintering for both coarse and fine zinc particles, although the zinc particle size effect is still evident. Liquid is present over an increased period for both coarse and fine Zn powders.

With additions of copper, the morphological development of the partially sintered microstructures (coarse Zn powders) is different during the isothermal solidification step (Figure 5.15a). For the binary Al-Zn system, the microstructures observed during isothermal solidification are cellular (Figure 4.15c). For the ternary Al-8Zn-1Cu system, the microstructures are duplex cellular-dendritic in nature (Figure 5.15a). The interfacial instability due to the presence of Cu results in the isothermal solidification front being dendritic instead of planar. The existence of these fine dendrite arms may be advantageous in providing good bonding between particles and grains, as the arms will impinge on each-other as grain growth occurs. Also, arms that break off and move in the liquid seams have high mobility. These fine particles are able to coalesce

by either normal sintering mechanisms, or during the isothermal solidification step as the liquid phase diminishes and fine particles grow. This duplex microstructure also occurs in the other ternary systems containing copper (Al-8Zn-3Cu, Al-4.5Cu-1.6Mg, (eg. Figure 5.15b)).

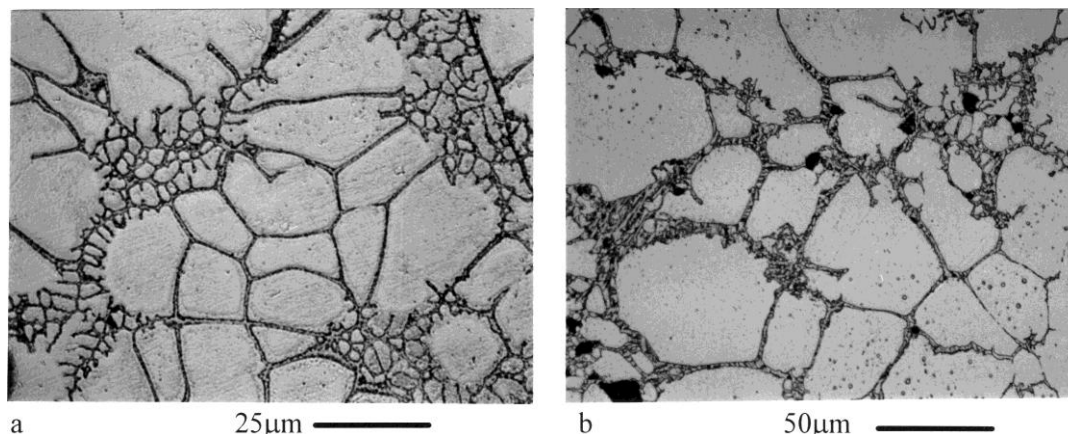


Figure 5.15 Duplex cellular dendritic microstructures developed in ternary Al alloys containing copper. It is apparent that copper in these alloys promotes an unstable interface and in many cases, the isothermal solidification front is dendritic in nature. (a) is of an Al-8Zn-1Cu alloy quenched from 600°C, and (b) is an Al-4.5Cu-1.6Mg alloy quenched after 2 minutes at 600°C. Optical micrographs.

5.8.1.3 Sintering mechanisms and microstructural development for Al-8Zn-3Cu

For the system Al-8Zn-3Cu (copper particle size altered as opposed to zinc) the particle size effect was again noted (Figure 4.33). The major difference to the binary Al-Zn system was that the liquid duration was increased enhancing persistent liquid phase sintering mechanisms. As in the Al-8Zn-1Cu system, isothermal solidification produced a duplex cellular-dendritic microstructure as the penultimate sintering step.

5.8.1.4 Sintering mechanisms and microstructural development for Al-4.5Cu-1.6Mg

Additions of Mg to the Al-Cu system had little effect on the mechanisms and microstructural development when compared to the binary Al-Cu case. It is apparent that the effect of Mg on the diffusion of Zn in Al does not occur for the diffusion of Cu in Al. The isothermal solidification step again produced a duplex microstructure (Figure 5.15b).

5.8.2 Summary of Ternary Sintering Systems

The addition of Mg to an Al-Zn alloy increases the rate of diffusion of Zn into Al. This limits the duration for which liquid is present, and increases the magnitude of the particle size effect. The addition of Mg to an Al-Cu alloy has little influence on microstructural development and the particle size effect. Mg does not appear to increase the diffusivity of Cu in Al as it does with Zn.

The addition of copper to Al-Zn increased liquid volumes and promoted the formation of duplex cellular-dendritic microstructures during the isothermal solidification step. This is thought to be due to copper promoting unstable solid-liquid interfaces resulting in dendritic regions developing as the additive passes into solution. These microstructural observations correlate to apparent interfacial instability developed during the sintering of binary Al-Cu (Figures 4.19d&5.15). The addition of 1% Cu to Al-8Zn enhances the sintering processes. This may be by a mechanism similar to that occurring in the binary Al-Cu system (section 5.7.3).

5.9 The Particle Size Effect in Quaternary Al-8Zn-2.5Mg-1Cu

5.9.1 Microstructural Evolution and Sintering Mechanisms for Quaternary AlZnMgCu

The dominant sintering mechanisms in this system can be divided into two major forms; those which occur during the transient stage of the sintering process (350°C up to 575°C), and those which occur during the persistent stage of sintering (600°C to 620°C+2hours). The microstructural development of this alloy sintered with coarse and fine additive particles is shown in Figure 4.34. It should be noted that the particle size effect only influences sintering during the transient stage and has a minimal effect on the final microstructure (compare Figures 4.34g&n). However, the particle size effect is important in this system because of the implication it has on the use of fine additive particles with a high heating rate. That is, where fine additive particles are used with a high heating rate, there should be an improvement in the sintered material consistent with those discussed in sections 5.7.6 and 5.7.7. The transient and persistent stages relate to the sintering cycle as shown by Figure 5.16 which should be considered in conjunction with Figure 4.34.

5.9.1.1 The transient stage of the sintering cycle

Dominant mechanisms occurring during the transient stage are generally consistent with those observed in the binary Al-Zn system (section 5.7.2), and are largely influenced by additive particle sizes. However, competing effects occur which are discussed below.

5.9.1.1(a) Fine additive zinc particles

Due to the better distribution of additive powders where fine Zn was used, there is a greater probability that additive powder particles will be near enough to each other to form higher order eutectics at lower temperatures. This is evident from the DSC curves which show a small peak at ~340°C (Figure 4.30) and from Figure 4.29 which shows two eutectic phases formed before 350°C. This indicates that higher order eutectic liquids can form at relatively low temperatures, initiating sintering at temperatures well below that for coarse additive particles.

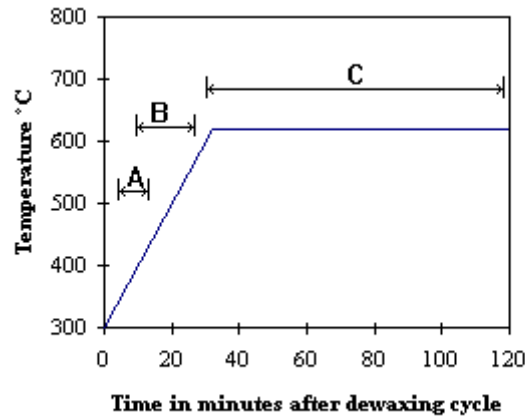


Figure 5.16 A plot of the sintering cycle exhibiting the onset and duration of the transient and persistent liquid phases as a function of the sintering cycle for quaternary Al-8Zn-2.5Mg-1Cu. Region A is the transient liquid phase sintering stage for fine Zn particles, region B the transient stage for coarse Zn particles, and region C the persistent stage for both coarse and fine Zn particles. Solid state sintering occurs between the end of the transient region and the start of the persistent region.

By 425°C, the liquids are beginning to spread, although fast diffusion of the additive in the base limits the effect of the liquid. At 450°C, the liquid volume fraction is at a maximum, although much of the additives have already passed into solution. This means that the liquid phases act only locally (ie. in the immediate vicinity of the additive particle) (Figure 4.34j). It is of interest to compare the microstructure formed with fine particles to that from the coarser additive powders at the same temperature (Figure 4.34c). Although the distribution of the liquid phases is improved for the case where fine additives were used, the volume of liquid phase developed is reduced in comparison to that for coarse additive powders. By 500°C (Figure 4.34k) much of the additives have passed into solution, although some liquid remains due to the later reaction of some additive (possibly Cu) particles. Predominant mechanisms for the transient stage of sintering are consistent with those of coalescence, particle disintegration, pore elimination by grain-liquid mixture flow and isothermal solidification. The material is almost homogeneous by 525°C and any sintering that occurs between this temperature and 600°C (approximately where the liquid phase returns) is by solid state mechanisms.

5.9.1.1(b) Coarse additive zinc particles

For coarse additive zinc particles, there is limited reaction between the additives and the aluminium before 425°C, where reaction of Zn with the other elements begins. By 450°C, the liquid spreads widely, disintegrating particles causing high mobility of the solid phase in the liquid (Figure 4.34c). During the transient stage of sintering, the dominant mechanisms appear consistent with particle disintegration, coalescence and pore elimination by grain-liquid mixture flow (Figure 4.34c). By 500°C, the liquid

phase is diminishing and isothermal solidification dominates. Regions which have bonded by isothermal solidification can be seen in Figure 4.34d (arrowed). By 525°C, the liquid phase is beginning to disappear, with limited liquid remaining. The liquid that remains is due to the later reaction between unreacted Cu particles and the Al. The compact becomes homogeneous by 575°C and the liquid phase has completely disappeared.

5.9.1.1(c) Analysis of the transient stage of the sintering cycle

The presence of Cu resulted in the formation of lower temperature eutectics where fine zinc particles were used (due to proximity effects) and a later liquid phase presence (Al-Cu binary eutectic) where coarse Zn particles were used. Liquid is therefore present over an increased period for both coarse and fine Zn powders. Additionally, it is apparent that liquid phases containing copper contribute to improved sintering (section 5.7.3, 5.10.2).

The major difference between using coarse and fine additive powders in ternary and quaternary alloys is that fine additive powders allow the formation of many binary, ternary and quaternary eutectic liquid phases, whereas binary eutectics form predominantly from coarse powders (Figure 4.34). The system has to be considered in terms of all of these phases. Higher order eutectics have been reported previously to wet aluminium powders better than the binary eutectics⁽⁹¹⁾, and their presence may therefore be advantageous. However, as discussed in section 5.4, the presence of Mg in the sintering of Al provides a means of oxide disruption, improving wetting. Therefore, it is likely that higher order eutectics containing Mg are not the means by which the wetting is improved; rather the presence of Mg in solution in Al facilitates the improvement. Additionally, as discussed in section 5.7.3, copper may improve sintering by chemically induced interface migration (CIIM).

5.9.1.2 The persistent stage of the sintering cycle

For both coarse and fine additive Zn sizes there is the reappearance of a liquid phase at ~600°C (presumably the equilibrium liquid phase as DSC indicates the solidus is at ~585°C). This exists first on grain boundaries and then spreads by capillary action. The similarity between the microstructures produced for both coarse and fine Zn compacts at 620°C (Figure 4.34g&n, respectively) should be noted. This occurs because the compacts have passed into the two phase α +L region where persistent liquid phase sintering can commence.

Although the persistent liquid phase appears to dominate densification, the sintering that has occurred previously via the transient liquid phase is also important. Sintered regions are generally well bonded and relatively pore free and hence require minimum further bonding. The secondary porosity that occurs during the transient stage (prior additive particle sites) is generally closed porosity, which would usually cause

problems in a persistent sintering system (eg. Al-Sn) because closed pores are surrounded by solid. However, due to the reappearance of the liquid phase along grain boundaries (supersolidus liquid phase sintering), it is a problem that can be overcome. Liquid can move freely by maintaining a complete capillary unaffected by oxide surfaces. The ability for grain boundary attack and disintegration is crucial. This can occur because of the high solubility of the additives in the matrix aluminium. Mechanisms occurring during the persistent phase of sintering are consistent with those outlined for other supersolidus sintering systems (section 2.5.4). As in supersolidus sintering where prealloyed powders are used^(9,17,39,40,50,144,145), the grain boundary attack that is evident is different to that which occurs by solution-precipitation (section 2.5.3.2(f)). This is because the liquid is not penetrating the grain boundary, rather the grain boundary liquefies, (due to the equilibrium $\alpha+L$ condition), facilitating mass transfer paths for sintering.

The role of the vapour phase again must be considered deleterious. Zinc vapour phase porosity is generally observed (Figure 5.17) in enclosed liquid pools where the vapour cannot escape. These liquid pools appear in the interior of particles and may be the result of liquification in prior grain boundary triple points, an effect of the reappearing (supersolidus) liquid phase (Figure 5.18) or regions left behind as liquid seams close during grain growth. Vapour phase bubbles subsequently form inside these liquid pools and appear to have no preferred location. That is, they will just as likely be formed centrally as at the top or the bottom of the liquid. The effect of vapour bubbles has only previously been documented in studies performed under microgravity conditions on W-Ni alloys⁽³⁴⁾. A possible explanation for the similarity between bubble formation under microgravity (W-Ni) and terrestrially (Al-Zn-X) is discussed below.

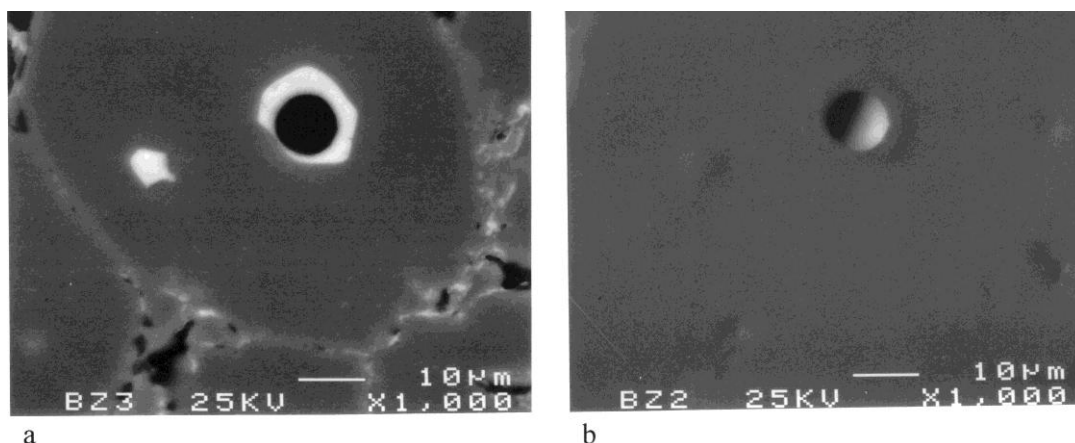


Figure 5.17 Zinc vapour phase porosity in enclosed liquid pools in a quaternary Al alloy. (a)Backscattered compositional, (b)backscattered topographical SEM.

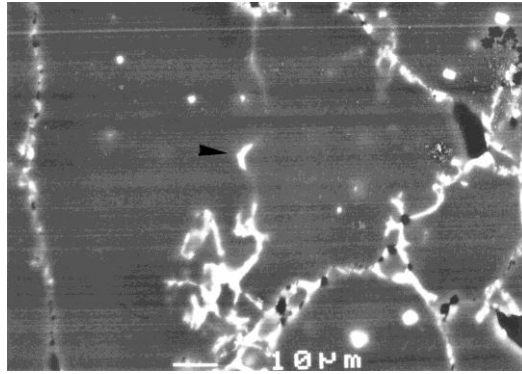


Figure 5.18 Prior grain or particle boundary triple points closing and entrapping liquid phase (arrowed). (Backscattered SEM).

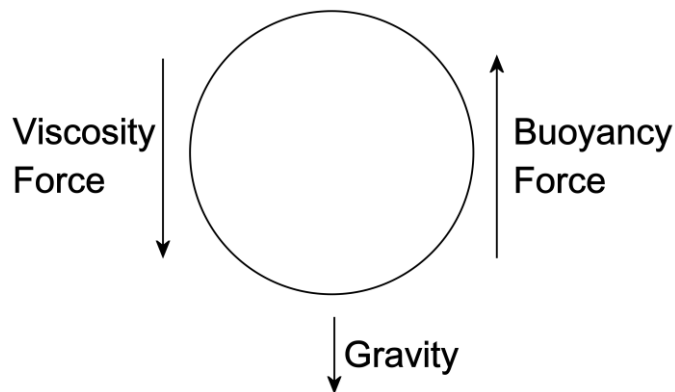


Figure 5.19 A diagrammatical analysis of the forces operating on a gas bubble rising in a liquid.

By analysing the forces operating on a vapour bubble in a liquid (Figure 5.19) it is possible to determine whether or not a zinc vapour bubble will segregate to the top of a zinc rich liquid by bouyancy, or remain stationary in the liquid due to viscous forces. By conducting this analysis, it should firstly be determinable whether or not the bubble is stationary or mobile. From this, the origins of this phenomenon should be determinable. Consider first the buoyancy force (5.4):

$$F_b = \rho_f V g \quad (5.4),$$

the effect of gravity,

$$mg = \rho_o V \quad (5.5),$$

and the viscosity force (Stokes' equation),

$$F_v = 6\pi r \eta_i v \quad (5.6),$$

where ρ_f is the density of the fluid, ρ_o the density of the bubble, V is the volume of the bubble, m is the mass of the bubble, g is gravity, r is the radius of the bubble, η_i is the fluid viscosity, and v the velocity of the bubble relative to the fluid⁽¹⁴⁶⁾. The terminal velocity (where $F_b = F_v$ and bubble motion ceases) is given by:

$$v_t = (\rho_o - \rho_f) V g / 6\pi r \eta_i \quad (5.7).$$

The density of the bubble is simply,

$$\rho_o = m / V \quad (5.8)$$

The fluid viscosity, η_i is given by⁽¹⁴⁷⁾;

$$\eta_i = \eta_o e^{Q/RT} \quad (5.9)$$

where η_o and Q are constants⁽¹⁴⁷⁾.

To determine the density of the vapour bubble, the number of moles of zinc within the gas bubble can be calculated from the ideal gas law⁽¹⁴⁶⁾:

$$PV = nRT \quad (5.10)$$

where P is the pressure of Zn vapour at 620°C (2217 Pa⁽¹²²⁾), V the volume, n the number of moles, R is the universal gas constant, and T the temperature in degrees Kelvin.

For a typical 10 μ m bubble the number of moles of Zn gas in the bubble is 1.563x10⁻¹⁶ moles. The mass of zinc vapour is thus 1.02 x10⁻¹⁷ kg. Substituting into equation 5.8, the density of the bubble, $\rho_o = 1.95 \times 10^{-2}$ kg/m³. The density of the fluid is determined using proportions of the fluid densities of the additive elements⁽¹⁴⁷⁾, assuming a liquid composition of 14% Al, 20.5% Mg, 53% Zn, and 12% Cu as reported by Muhlburger and Paschen⁽⁹¹⁾. This gives a density of 5130 kg/m³ but it should be noted that the density of liquid Zn is 6500 kg/m³ and the true density of the liquid regions will be more likely to be somewhere between these two values. For this analysis however, the density of the liquid will be taken as the least value, 5130 kg/m³ so the analysis applies to all situations. Using equation 5.9, the viscosity η_i is 2.285*10⁻³ Pa•s. Therefore, the terminal velocity (equation 5.7) where the force of buoyancy equals the force of viscosity is 122 μ m/sec. Following the same procedure for a 10 μ m argon bubble in liquid nickel, the terminal velocity is 105 μ m/sec. For the condition where $F_v < F_b$ (ie. buoyancy causes the bubble to rise), the velocity of the moving bubble (relative to the fluid) will always be proportionately less than the terminal velocity. Hence it is unlikely that the viscous force would equal the buoyancy force meaning that it is unlikely that bubbles in these liquid metals will be stationary in terrestrial conditions.

However, in alloys containing Zn, the bubbles do not appear to be escaping as they do in W-Ni alloys (terrestrial). In W-Ni alloys on Earth, the argon bubbles introduced from the sintering atmosphere disappear and are not replaced by others. Under microgravity conditions where buoyancy forces are absent, Ar bubbles do not escape, and hence influence sintering. In Al-Zn-X alloys Zn vaporises profusely and much of the Zn escapes from the sample. This is observed by TGA and density measurements and can be as much as ~0.5% over a two hour sintering cycle at 620°C. However, bubble formation is still widespread after 2 hours. Hence Zn bubbles in liquid pools are constantly being formed because of high vapour pressure. Surface tension causes a compression of the bubble surface equally in all directions resulting in a spherical shape. Viscosity effects will slow bubble motion but do not stop it. It is most likely that the bubbles that form, if they reach an aluminium surface, may disperse via diffusion into the solid or the liquid, or continue to grow until they displace all liquid

present in the pool in which they formed. Hence the pools can continue to form in new regions and bubbles are continually generated inside them. The appearance of Zn vapour pores appears to be a continual process, not a static one. Therefore bubbles will appear to have a random orientation or location in liquid pools and do not all segregate to the top, as could be expected if bubble formation was a singular event.

5.9.1.3 The Role of Additive Particle Size Ranges in Al-8Zn-2.5Mg-1Cu

Two major effects occur when using a range of zinc particle sizes in the quaternary Al-Zn-Mg-Cu alloy as opposed to discrete size fractions. Firstly, it is apparent that the temperature at which the maximum volume of liquid phase occurs increases with increasing mean particle size. Secondly coarser particles contribute to increased quantities of liquid. As a result, a greater degree of particle and grain mobility is facilitated. That is, where a fine range was used, the sintering liquid tends to only act locally (ie. in the immediate vicinity of prior additive powders)(Figure 4.35a), whereas for the coarse and medium ranges (Figure 4.35b&c, respectively) the liquid acted globally (ie. throughout the sample). However, the range exhibiting the most efficacious liquid phase (widespreading liquid acting globally) developed from the broad particle size range (zinc 5). This size range combined the global advantages of having some coarse additive powders with the localised effect of the fine additive powders. The effects of particle size ranges are summarised in Table 4.3.

5.10 Effect of Composition in Quaternary Al-8Zn-xMg-yCu Alloys

5.10.1 The Role of Increasing Additions of Mg

The effect of magnesium on liquid phase sintering in aluminium alloys differs between ternary alloys containing zinc as the major additive phase and those containing copper as the major additive phase. When Mg is added to Al-Zn and Al-Zn-Cu systems, the liquid phase persists for a much shorter period than without it, even though the amount of liquid forming additives is increased (8 wt% Zn has an equivalent volume to 1.7 wt% Mg). It appears that the presence of magnesium increases the transient nature of the zinc rich liquid phase, reducing its duration. It is possible that this is due to enhanced diffusivity of the Zn in Al. This effect has been documented previously⁽¹³⁹⁾ and would explain the decreasing liquid phase duration with increased Mg content (Figure 4.36). Additionally, oxide disruption allows the reaction between the additive and base to occur at lower temperature. The combination of a lack of significant lower temperature endotherms in the quaternary alloy and the small eutectic endotherm for Al-Mg at ~450°C, indicate that Mg may be in solid solution before the Al-Mg eutectic temperature is reached (Figure 4.30). Figure 4.11 supports this hypothesis for an Al-0.2 Mg alloy, which has been held at temperatures below the eutectic to simulate the dewaxing cycle. The decreasing energy of melt formation indicates that Mg does partially pass into solution well before any liquid phases are formed. This Mg in solution allows oxide disruption (section 5.4) and also the enhanced diffusivity of Zn in Al to be effective (Figure 4.36).

The liquid phase does not appear to be influenced when Mg is added to the binary Al-Cu alloy; that is, Mg does not noticeably influence the diffusivity of Cu in Al in the same way that it does Zn. The necessary experimental data for the corresponding diffusivities are not available in the literature.

5.10.2 The Role of Increasing Additions of Cu

Cu content in Al-8Zn-xCu (Figure 4.38) showed a major effect on microstructural development. From Figure 4.38, it can be seen that copper is effecting the microstructures which form, but only between 0 and 0.5% Cu. There is a more widespread liquid phase, indicating that there is a benefit to be gained by using 0.5% Cu; this does not continue to affect microstructural development above 0.5% Cu. With Cu additions greater than 0.5% there is an increase in the volume of liquid phase, due to both decreased solubility of the additive in the base and the reduced solidus temperature. There is little difference between the microstructures formed with 0.5% Cu and with 3% Cu. Therefore it appears likely that Cu has an activating effect on the sintering of Al-Zn alloys. It has been observed here that copper promotes unstable interfaces in Al-Zn alloys (section 5.8.1.2), and instigates CIIM in binary Al-Cu alloys (section 5.7.3). Hence it may be possible that the improvement in sintering that occurs with copper additions is due to CIIM. However, analytical TEM is required to confirm this.

Increasing Cu content in Al-8Zn-xCu alloys shows a gradual decrease in densification up to approximately 2% Cu (Y-axis, 0% Mg, Figure 4.39a) at which point the densification begins to slowly increase. It is apparent that at compositions above 2% Cu, sufficient persistent liquid phase is present to allow some shrinkage to occur.

5.10.3 The Combined Role of Additions of Mg and Cu

For the quaternary alloys, the contour plots (Figure 4.39) show that least expansion is achieved at low Cu and low Mg levels. This is thought to be due to both copper and magnesium's solubility in Al causing expansion via the Kirkendall effect. It may be expected that densification would decrease (become more negative) with increased Cu additions until the system became persistent. As the measure of shrinkage is (usually) directly related to the volume fraction of liquid⁽⁹⁾, an increased volume of liquid phase increases density. This effect can be noted above approximately 1%Cu with the most rapid increase occurring at higher Mg levels where most liquid is present. Note should be made of the fact that for all compositions $\geq 1.5\%Cu$ increasing Mg content causes an increase in density followed by a gradual expansion towards higher Mg levels. Below $\sim 1\%Cu$, the density changes slowly up to approximately 1%Mg, above which the density decreases rapidly.

The increase in density at low Mg concentrations and the trough that exists in the lower composition range (up to 0.5 Cu and up to 1 Mg) may be due to both the break-

up of the oxide phase by the presence of Mg (discussed in section 5.4) and to the improved sintering response where 0.5%Cu is added to Al-Zn alloys (section 5.10.2). For alloys containing no copper (Figure 4.37, the abscissa of Figure 4.39), the increase in density at low Mg levels becomes more notable. The effect of solution hardening is also readily observable. The reduction in density compensates for the increase in solution strengthening with higher Mg levels, resulting in no change in hardness above 1%Mg.

At high Cu levels (2.5-3%Cu) and low Mg levels (up to 0.5%) the break-up of the oxide works synergistically with the persistent liquid, resulting in an increase in density in this region. This combined with solid solution strengthening results in the sharp increase in hardness noted in this region; at 3%Cu, between 0 and 0.2Mg the hardness rises from 72RH to 93 RH. At 0%Cu the corresponding increase is from 60RH to 67RH (Figure 4.39). The densification increase is the same for both (0.3) although the sintered density for Al₈Zn_{0.2}Mg₃Cu is -1 and for the Al₈Zn_{0.2}Mg is -0.3. The magnitude of the hardness increase has tripled, exhibiting the synergistic effect of combining a copper rich persistent liquid with the chemical disruption of the oxide layer (section 5.4).

5.11 The influence of gravity on quaternary Al-8Zn-2.5Mg-1Cu

Previous studies on the effect of gravity have centred on heavy metal systems^(21,32,33), where the solid phase was of a higher density than the liquid, resulting in a settling effect of solid phase particles. In the Al-8Zn-2.5Mg-1Cu alloy, however, the reverse is observed where the liquid tends to segregate to the bottom of samples. This is due to the density of the liquid being between 5.1g/cm³ (multicomponent liquid) and 6.5 g/cm³ (pure Zn liquid) (section 5.9.1.2) and the density of the solid being > ~2g/cm³ and <~3g/cm³ (this value being dependent on the local composition of the solid, which may not be homogeneous). Figure 4.40a shows that the liquid volume increased from ~15% to ~21% from top to bottom of the specimens examined with representative backscattered SEM micrographs shown in Figure 4.40b. The volume fraction of the liquid phase is directly related to the volume shrinkage⁽⁹⁾ and hence in this system the samples were of higher apparent densities towards their base. Figure 4.40c exhibits the shape change associated with these differences in liquid volume fraction. This effect has also been noted in Fe-Cu⁽¹⁴⁸⁾ and could be expected to have a role in all systems where the liquid phase has a higher density than the solid phase (eg. Al-Sn, Al-Cu).

5.12 The Effect of Slow Cooling

After examination of samples of the quaternary Al-8Zn-2.5Mg-1Cu alloy quenched from 620°C+2hrs, it appeared possible that the vapour bubbles present in quaternary alloys (section 5.9.1.2) may be impeding densification. This may have been the result of freezing of the material around the bubble space upon quenching. Hence a means of removing the bubble space via the cooling rate may be successful in increasing density. After slow cooling, pores resulting from the vapour phase were not observed. However, it is apparent that substantial shrinkage occurred when the samples were cooled from 620°C to 200°C at 2°C/min. (Figure 4.41) resulting in densities of up to 98%. This increase could not solely be attributed to removing vapour phase porosity. Examination of samples having undergone the entire cycle showed substantial precipitation. Mondolfo *et al*⁽¹⁴⁹⁾ found that precipitation in an Al-6Zn-2Mg alloy caused a 6% volume contraction. Hence a possible explanation for this shrinkage effect is precipitation, which will remove solute elements from solution thereby causing shrinkage. This is the reverse of the expansion which occurs during sintering due to diffusion (the Kirkendall effect). In addition, the precipitate forms preferentially on particle boundaries, pore surfaces and regions of the matrix which are relatively disordered (Figure 4.44). This will also aid shrinkage by filling the void space. Since precipitation is expected to occur below the solvus, it is notable that the shrinkage rate increases below 400°C. XRD (Figure 4.42) shows that the shrinkage occurring corresponds to the precipitation of MgZn₂, and that increasing precipitation results in increased shrinkage. Although hardness values were very high (>90HRE), the tensile strengths are comparatively low (~250MPa and <1% strain in the T6 condition). This may be due to the intermetallic phase Mg₃₂(AlZn)₄₉ that has been observed to form at high temperatures (Fig.4.43) and does not return to solution, even during solution treatment. Others have found that impurities which lower interfacial energy will selectively segregate to interfaces and these species often result in embrittlement⁽¹⁵²⁾. However it should be noted also that increases in density via precipitation may be lost upon solution treatment.

Chapter 6 Conclusions

This thesis has investigated the sintering of aluminium using both transient and persistent liquid phases. The role of these liquid phases has been examined and the following conclusions drawn.

1. Besides the conventional sintering mechanisms which usually occur, a further bonding mechanism has been identified during these studies. Isothermal solidification has been found to contribute substantially to particle growth and bonding in systems exhibiting transient liquid phase sintering behaviour. Additionally, unusual microstructures may develop during the isothermal solidification step, particularly where Cu is present. This may be due to Cu promoting unstable growth interfaces during isothermal solidification.
2. The means by which liquid phases wet aluminium in the absence of a reducing agent has been examined. The wetting characteristics of the liquid phase appear to be largely governed by the solubility of the base in the liquid phase, the solubility of the additive elements in the base and the diffusivity of the additive in the base. The most desirable wetting liquid for aluminium surfaces is that which has a high diffusivity of the additive in the base to allow fast liquid penetration, but a relatively low solubility in the base at the sintering temperature to maintain liquid volume. The Al-Cu system exhibits these factors, and may explain why additions of Cu to Al alloys improve sintering.
3. Additions of Mg as low as 0.2wt% in Al facilitate the disruption of the alumina layer on Al particles. This occurs via the partial reduction of the alumina to MgAl_2O_4 .
4. Additions of Zn and Mg in binary Al alloys lead to linearly decreasing densities with increased additions up to 14wt%. Additions of Cu also lead to a linearly decreasing sintered density up to 3%Cu. Above 3%Cu, a sharp increase in sintered density occurs. The sintered properties of these materials appears to be influenced by the concentration of additive elements in three ways: firstly, increasing the additive concentration increases the number and size of secondary pores in the sintered material, decreasing the mechanical properties. Secondly, increasing liquid forming additives increases the volume of liquid phase developed, improving bonding and therefore improving sintered properties. Finally, increasing additive concentration increases the influence of solid solution strengthening, improving sintered strength.
5. Additive particle size has a critical influence on microstructural development in all those systems examined which have a transient aspect to the sintering cycle. The systems showing this effect were Al-Zn, Al-Cu, Fe-Cu, Al-Zn-Mg, Al-Zn-Cu, Al-Cu-Mg, and Al-Zn-Mg-Cu.

6. Additive particle size was unimportant in the Al-Sn system which is an ideal, persistent system having unipolar solubility conditions.

7. The effect of additive particle size on mechanical properties was examined in the Al-4Cu system. There are competing effects governing the mechanical properties in these alloys, these being secondary pore size and the degree of bonding. Coarser additive particle sizes generate greater quantities of liquid phase, but leave large secondary pores. The tensile properties therefore pass through a maximum at an intermediate additive particle size (75-106 μm). However, optimisation of this system occurs when a fine additive particle size and a very fast heating rate are utilised. This results in a greater quantity of liquid phase and a finer secondary pore size.

8. In the quaternary Al-8Zn-2.5Mg-1Cu alloy studied, compacts exhibited a transient stage to the sintering cycle and a persistent (supersolidus) stage at the sintering temperature. A very wide particle size range in the quaternary system produces the most efficacious liquid phase. This particle size distribution results in higher order eutectics forming (being a function of fine additive powders) and a large volume of widely distributed liquid (being a function of coarser additive powders).

9. Low concentrations of Mg in ternary and quaternary alloys improve sintered density due to the disruption of alumina surfaces on aluminium particles. Optimum mechanical properties for the quaternary systems examined occur at high copper and/or high Mg concentrations.

10. The addition of Mg to an Al-Zn alloy increases the rate of diffusion of Zn into Al. This impedes liquid duration, and increases the magnitude of the particle size effect. The addition of Cu to Al-Zn increased liquid volumes and promoted the formation of duplex cellular-dendritic microstructures during isothermal solidification. Additions of copper $\geq 0.5\%$ influence the sintering processes by promoting chemically induced interface migration (CIIM), which increases mass transfer rates. This may be responsible for the unusual morphology noted in Al-8Zn-1Cu during the isothermal solidification stage of sintering. Additionally, it appears that CIIM may cause excessive grain growth during sintering in alloys containing Cu.

11. Gravity has an effect on dimensional stability in the quaternary Al-8Zn-2.5Mg-1Cu alloy. Liquid fractions increase from $\sim 15\%$ to $\sim 21\%$ from the top to the bottom of the samples studied. There is a contraction towards the middle of the sample, and the diameter of the top surface is greater than that of the bottom surface.

12. A substantial amount of densification is induced when quaternary Al-8Zn-2.5Mg-1Cu alloys are cooled at $2^\circ\text{C}/\text{minute}$. During the cooling cycle there is precipitation of MgZn_2 which occurs preferentially on free surfaces and grain boundaries. This

precipitation results in apparent densities of 98%. In the T6 condition the hardness of these alloys is very high (>90HRE) but the tensile properties exhibit a moderate UTS (~250MPa) and <1% strain at break.

13. In alloys containing Zn, Zn vapour phase porosity is evident and is considered deleterious. In the quaternary Al-8Zn-2.5Mg-1Cu system, fine liquid pools are generated and vapour pores which form inside these cannot escape. These vapour bubbles form dynamically and hence have no preferred location or orientation. Microstructures generated are consistent with those reported to form under microgravity conditions.

Chapter 7 References

1. German, R.M, *Powder Metallurgy Science*, 2nd ed. MPIF, New Jersey, 1994.
2. Metals Handbook, Ninth Edition, Vol.7, *Powder Metallurgy*, American Society For Metals, 1993.
3. Lenel, F.V, *Powder Metallurgy Principles and Applications*, MPIF, Princeton, New Jersey, 1980.
4. Thummler, F., and Oberacker, R., *Introduction to Powder Metallurgy*, The Institute of Materials Series on Powder Metallurgy, I. Jenkins and J.V. Woods (eds.), Institute of Materials, London, 1993.
5. Bufferd, A.S, Complex Superalloy Shapes, *Powder Metallurgy for High Performance Applications*, J.J Burke and V. Weiss (eds), Syracuse Press, Syracuse, N.Y, 1972, pp 303-316.
6. Vonazountas, J., and Davies, T.J., Compaction Pressure Density Relationships in Iron Based P/M compacts. Proceedings of the 1992 Powder Metallurgy World Congress, *Advances in Powder Metallurgy and Particulate Materials, Compaction and Other Consolidation Processes*, 1992, Vol.2, pp. 99-113.
7. Kaysser, W.A and Petzow, G., Recent Conceptions in Liquid Phase Sintering, *Proceeding Sintering Theory and Practice Conference*, The Metals Society, London U.K, 1984, pp. 10.1-10.6.
8. Bickerdike, R.L., Selected Government Research Reports, Vol.9, *Powder Metallurgy*, Report #8, An Aluminium Alloy Made By Powder Metallurgy, His Majesty's Stationary Office, 1951.
9. German, R.M, *Liquid Phase Sintering*, Plenum Press, New York, 1985.
10. Courtney, T.H, Densification and Structural Development in Liquid Phase Sintering, *Metallurgical Transactions A*, vol. 15A, June 1984, pp. 1065-1074.
11. Kaysser, W.A, Liquid Phase Sintering, *Powder Metallurgy-An Overview.*, The Institute of Metals Series on Powder Metallurgy, 1991, pp.183-197.
12. Kingery, W.D, Bowen, H.K, and Uhlman, D.R, *Introduction to Ceramics*, 2nd ed., Wiley, New York, 1976.
13. Kingery, W.D., and Berg, M., Study of the Initial Stages of Sintering Solids by Viscous Flow, Evaporation-Condensation and Self Diffusion, *Journal of Applied Physics*, Vol.26, 1955, pp.1205-1212.
14. Richerson, D.W, *Modern Ceramic Engineering, Properties, Processing, and use in Design.*, Vol.1, Marcel Dekker, New York, 1982.
15. Price, G.H.S, Smithells, C.J, and Williams, S., Sintered Alloys Part 1. Copper-Nickel-Tungsten Alloys Sintered With a Liquid Phase Present., *The Journal of the Institute of Metals*, Vol.62, no.1, 1938, pp.239-264.
16. Hu, C. and Baker, T.N, Microstructure of Al-Fe Alloys Sintered Via In-Situ Microfusion Process, *Materials Science and Technology*, Jan. 1993, vol.9., pp.48-56.
17. Huppman, W.J, Sintering to High Density, *The International Journal of Powder Metallurgy and Powder Technology*, Vol.21, no.3, 1985, pp. 184-185.

18. Kurz, W., and Fisher, D.J., *Fundamentals of Solidification*, Trans Tech Publications, Rockport, MA, 1984.
19. Murr, L., *Interfacial Phenomena in Metals and Alloys*, Advanced Book Program, Addison-Wesley Publishing Co., Reading, Massachusetts, 1975.
20. Petzow, G., and Huppman, W.J., Liquid Phase Sintering-Densification and Microstructural Development, *Zeitschrift Fur Metallkunde*, vol. 67, 1976, pp.579 - 590.
21. Mani, S.S, and German, R.M, Kinetics of Gravity Induced Distortion in Liquid Phase Sintering, Proceedings of the 1990 P.M. Conference and Exhibition. *Advances in Powder Metallurgy*, vol.1., 1990.
22. Kingery, W.D., Densification During Sintering in the Presence of a Liquid Phase. 1. Theory. *Journal of Applied Physics*. Vol.30, no.3, March 1959.
23. Kaysser, W.A and Petzow, G., Present State of Liquid Phase Sintering., *Powder Metallurgy*, Vol.28, no.3, 1985 pp.145-150.
24. Raj, R., Morphology and Stability of the Glass Phase in Glass Ceramic Systems., *Journal of the American Ceramic Society*, vol.64, no.5, may 1981, pp.245-248.
25. Svoboda, J., Riedel, H., and Gaebel, R., A Model For Liquid Phase Sintering, *Acta Materialia*, Vol.44, #8, 1996, pp.3215-3226.
26. Yoon, D.N, and Huppman, W.J., Chemically Driven Growth of Tungsten Grains During Sintering in Liquid Nickel., *Acta Metallurgica*, vol.27, no.6., 1979, pp.973 -977.
27. Kang, S.-J.L., and Azou, P., Trapping of Pores and Liquid Pockets During Liquid Phase Sintering., *Powder Metallurgy*, Vol.28., no.2, 1985, pp.90-92.
28. Park, H., Cho, S., and Yoon, D. Pore Filling Processes in Liquid Phase Sintering, *Metallurgical Transactions A.*, vol 15A, June 1984, pp.1075-1080.
29. Huppman, W.J, Riegger, H., Kaysser, W.A, Smolej, V., and Pejovnik, S., The Elementary Mechanisms of Liquid Phase Sintering, I Rearrangement, *Zeitschrift fur Metallkunde*, #70, 1979, pp.707-713.
30. Zukas, E.G., Rogers, P.S.Z., and Rogers, R.S., Spheroid Growth By Coalescence During Liquid Phase Sintering, *Zeitschrift Fur Metallkunde.*, vol.67., 1976, pp.591-595.
31. Yoon, D.N., and Huppman, W.J., Chemically Driven Growth of Tungsten Grains During Sintering in Liquid Nickel, *Acta Metallurgica*, vol.27, 1979, p.693.
32. Yang, S.C., Mani, S.S, and German, R.M, Grain Growth Behaviour in Liquid Phase Sintered Heavy Alloys, Proceedings of the 1990 P.M. Conference and Exhibition, *Advances in Powder Metallurgy*, vol.1., 1990, pp. 469-482.
33. Kipphut, C.M., German, R.M., Bose, A., Kishi, T., The Gravitational Effects of Liquid Phase Sintering, Proceedings of the 1989 Powder Metallurgy Conference and Exhibition, *Advances in Powder Metallurgy*, vol.2., 1989, pp.415-429.
34. Liu, Y., Iacocca, R.G., Johnson, J.L, German, R.M., and Kohara, S., Microstructural Anomalies in a W-Ni Alloy Liquid Phase Sintered Under

- Microgravity Conditions, *Metallurgical and Materials Transactions A*, Vol.26A, 1995, pp. 2484-2486.
35. Lumley, R.N, *The Transient Liquid Phase Sintering of Aluminium With Zinc*, Postgraduate Honours Thesis, University of Queensland, 1993.
 36. Kehl, W., and Fischmeister, H.F., Liquid Phase Sintering of Al-Cu Compacts., *Powder Metallurgy*, no.3, 1980, pp.113-119.
 37. Kaysser, W.A., Huppman, W.J., and Petzow, G., Analysis of Dimensional Changes During Sintering of Iron-Copper, *Powder Metallurgy*, Vol. 23, 1980, pp.86-91.
 38. German, R.M., Supersolidus Liquid Phase Sintering Part 1: Process Review, *The International Journal of Powder Metallurgy*, Vol.26, #1, 1990, pp.23-34.
 39. Tandon, R and German, R.M., Particle Fragmentation During Supersolidus Sintering, *The International Journal of Powder Metallurgy*, Vol.33, #1, 1997, pp.54-60.
 40. Tandon, R., and German, R.M., Supersolidus -Transient Liquid Phase Sintering Using Superalloy Powders, *The International Journal of Powder Metallurgy*, Vol.30, #4, 1994, pp.435-443.
 41. Belhadjanida, A., Johnson, J.L., Tandon, R., and German, R.M., Advances in Liquid Phase Sintering, *Journal of Materials Synthesis and Processing*, Vol.1, #4, 1993, pp.275-285.
 42. German, R.M., Supersolidus Liquid Phase Sintering of Prealloyed Powders, *Metallurgical and Materials Transactions A*, Vol.28A, 1997, pp.1553-1567.
 43. Yoon, D.Y., Theories and Observations of Chemically Induced Interface Migration, *International Materials Reviews*, Vol. 40, 1995, pp.149-179.
 44. Zieba, P. and Pawlowski, A., Diffusional Penetration During Diffusion Induced Grain Boundary Migration Process in an Al-Zn Couple., *Journal of Materials Science*, 29, 1994, pp.6231-6240.
 45. Kuo, M., and Fournelle, R.A., Diffusion Induced Grain Boundary Migration (DIGM) and Liquid Film Migration (LFM) in an Al-2.07wt%Cu Alloy, *Acta Metallurgica and Materialia*, Vol.39, #11, 1991, pp.2835-2845.
 46. Lawcock, R.L., and Davies, T.J., Effect of Carbon on Dimensional and Microstructural Characteristics of Fe-Cu Compacts During Sintering, *Powder Metallurgy*, Vol.33, #2, 1990, pp.147-150.
 47. Baik, Y.J., Kim, J.K., and Yoon, D.K., The Effect of Elastic Anisotropy on the Migration of Intergranular Liquid Films and the Precipitation of a Liquid Phase in a Co-Cu Alloy, *Acta Metallurgica and Materialia*, Vol.41., #8, 1993, pp.2385-2393.
 48. Rhee and D.N. Yoon, The Instability of Solid-Liquid Interface in Mo-Ni Alloy Induced By Diffusional Coherency Strain, *Acta Metallurgica*, 1987, Vol.35, pp.1447-1451.

49. Savitskii, A.P., *Liquid Phase Sintering of the Systems with Interacting Components*, Russian Academy of Sciences, Siberian Branch, Institute of Strength Physics and Materials Science., Translated by M.V. Kokunova, 1993.
50. German, R.M., Advances in High Alloy Sintering Using Supersolidus Liquids, Conference Proceedings, PM²TEC97, Chicago, Illinois, July 1997.
51. Puckert, F.J., Kaysser, W.A., and Petzow, G., Transient Liquid Phase Sintering of Ni-Cu, *Zeitschrift Fur Metallkunde*, 74, #11, 1983, pp.737-743.
52. Acharya, N.N., and Mukunda, P.G, Sintering in Copper-Tin System Part 3: Influence of Variables, *International Journal of Powder Metallurgy*, Vol.31, 1995 pp.81-88.
53. German, R.M., and Dunlap, J.W., Processing of Iron-Titanium Powder Mixtures by Transient Liquid Phase Sintering., *Metallurgical Transactions A.*, Vol. 17A, 1986, pp.205-213.
54. Richerson, D.W, *Modern Ceramic Engineering, Properties, Processing, and use in Design*, vol2. Marcel Dekker, New York, 1992.
55. Huppman, W.J., and Dalal, K., *Metallographic Atlas of Powder Metallurgy*, Verlag Schmid GMBH, Freiburg, West Germany, 1986.
56. Langford, G., and Cunningham, R.E., Steel Casting by Diffusional Solidification, *Metallurgical Transactions B*, Vol.9B, 1978, pp.5-19.
57. Danninger, H., Homogenisation and Pore Formation During Sintering With Transient Liquid Phase, *Powder Metallurgy International*, Vol.20, #1, 1988, pp.21-25.
58. Danninger, H., Secondary Porosity in Sintered Steels and its Effects on Product Quality and Consistency, *Powder Metallurgy*, Vol.30, #2, 1987, pp.103-109.
59. Duvall, D.S., Owczarski, W.A., and Paulonis, D.F., Transient Liquid Phase Bonding: A New Method for Joining Heat Resistant Alloys, *Welding Journal*, Vol.53, 1974, pp.203-214.
60. Tuah-Poku, I., Dollar, M., and Massalski, T.B., A study of the Transient Liquid Phase Bonding Process Applied to a Ag/Cu/Ag Sandwich Joint., *Metallurgical Transactions A.*, Vol.19A, 1988, pp.675-686.
61. Zhou, Y., Gale, W.F., and North, T.H., Modelling of Transient Liquid Phase Bonding, *International Materials Reviews*, Vol.40, 1995, pp.181-196.
62. Niemann, J.T., Garrett, R.A., Eutectic Bonding of Boron-Aluminium Structural Components, *Welding Journal*, Research Supplement, Vol.53., 1974, pp.175-184
63. Wells, R.R., Microstructural Control of Thin Film Diffusion-Brazed Titanium, *Welding Journal*, Research Supplement, Vol.55, pp.20-27.
64. Nakagawa, H., Lee, C.H., and North, T.H., Modelling of Base Metal Dissolution During Transient Liquid Phase Brazing., *Metallurgical Transactions A.*, Vol.22A, 1991, pp.543-555.
65. Courtney, T.H., Microstructural Evolution During Liquid Phase Sintering, Part 2., Microstructural Coarsening, *Metallurgical Transactions A.*, vol.8A, May 1977, pp.685-689.

66. Magee, B.E and Lund, J, Mechanisms of Liquid Phase Sintering in Iron-Copper Powder Compacts., *Zeitschrift Fur Metallkunde.*, vol. 67, no.9, 1976, pp.596-610.
67. Lee, D.J., and German, R.M., Sintering Behaviour of Fe-Al Powder Mixes., *The International Journal of Powder Metallurgy and Powder Technology*, vol.21, no.1, pp.9-21.
68. Wanibe, Y., Yokoyana, H., and Itoh, T., Expansion During Liquid Phase Sintering of Iron-Copper Compacts, *Powder Metallurgy*, Vol.33, #1, 1990, pp.65-69.
69. Jamil, S.J., and Chadwick, G.A., Investigation and Analysis of Liquid Phase Sintering of Fe-Cu and Fe-Cu-C Compacts, *Powder Metallurgy*, Vol.28, #2, 1985, p.65.
70. Griffo, A. and German, R.M., Dimensional Control in the Sintering of Iron-Copper-Carbon Via Particle Surface Area, *The International Journal of Powder Metallurgy*, Vol.30, #4, 1994, pp.399-407.
71. Griffo, A., German, R.M., and Nayar, H.S., Powder Selection and Sintering Pathways for Zero Dimensional Change in Fe-2Cu-0.8C, *Advances in Powder Metallurgy and Particulate Materials*, Vol.3, APMI, MPIF, Princeton, N.J., p.301-316.
72. Froes, F.H., Kim, Y-W., Krishnamurthy, S., Sundaresan, R., Current Status of P/M, *Technology of Light Metals.*, *Powder Metallurgy, an Overview.*, The Institute of Metals Series on Powder Metallurgy., 1991, pp.220-255.
73. *Light Alloys, Metallurgy of the Light Metals*, 2nd ed., by I.J. Polmear, Metallurgy and Materials Science Series, Edward Arnold, London, 1989.
74. Dudas, J.H., and Dean, W.A., The Production of Precision Aluminium P/M Parts., *International Journal of Powder Metallurgy*, no.5., Vol.2., 1969, pp21-36.
75. Daver, E.M., Ulrich, W.J, and Patel, K.B, Aluminium P/M Parts-Materials, Production and Properties, *Key Engineering Materials*, Vol.29-31(1989), pp.401 - 428.
76. Generous, J.D., Aluminium Business Machine Parts., *Modern Developments in Powder Metallurgy*, no.13., Ferrous and Nonferrous Materials., American Powdered Metal Company pp.501-510.
77. Dudas, J.H., and Brondyke, K.J., Aluminium P/M Parts- Their Properties and Performance., *SAE Transactions*, 700141, 1970, Vol.79., pp573-579.
78. Miura, S., Youich, H., Mitsuaki, S., Starting Powder For Producing Sintered Aluminium Alloy, *European Patent Application 0466120A1*, 1992.
79. Timofeev, N.S and Savitskii, A.P, Volumetric Changes in Powder Bodies in Liquid Phase Sintering of the Aluminium-Magnesium System, *Poroshkovaya Metallurgiya*, no.3(327), pp.20-25, 1990.
80. Bocchini, G.F, Zocchi, R., Current Status of Sintered Aluminium and some Comparisons with Sintered Iron, *Metal Powder Report*, 1980, p.193.

81. Sundaresan, R., and Ramakrishnan, P., Liquid Phase Sintering of Aluminium Base Alloys., *International Journal of Powder Metallurgy and Powder Technology*, 1978, vol.14, no.1, pp.9-16.
82. Sercombe, T.B., and Schaffer, G.B., Sintering of a Non-Conventional Aluminium Powder Alloy, Proceedings of PM²TEC'97, Chicago, Illinois, 1997.
83. Schaffer, G.B., and Huo, S.H., High Strength Sintered Aluminium Alloys, *Advances in Powder Metallurgy and Particulate Materials*, Vol. 14, Proceedings of PM²TEC96, Washington D.C, 1996, pp.27-39.
84. Neubing, H.C and Jangg, G., Sintering of Aluminium Parts: The State of the Art., *Metal Powder Report*, Vol.41(5) May 1987, pp. 354-358.
85. Savitskii, A.P., and Martsunova, L.S., Effect of Solid State Solubility on the Volume Change Experienced by Aluminium During Liquid Phase Sintering, *Theory and Technology of Sintering, Thermal and Chemicothermal Treatment Processes*, pp.333-337, 1977.
86. Kehl, W., and Fischmeister, H.F., Observations of Dimensional Changes During Sintering of Al-Cu Compacts., *Sintering Theory and Practice*, Proceedings of the 5th Round Table Conference on Sintering, Portoroy, Yugoslavia, 7-10 Sept. 1981. *Materials Science Monographs*, vol.14, p.269-274.
87. Farzin-Nia, F., and Davies, B.L., Production of Al-Cu and Al-Cu-Si Alloys by P/M. Methods., *Powder Metallurgy*, vol.25, no.4, 1982.
88. Esper, F.J., and Lueze, G., The Influence of the Powder Particle Size on the Properties of Al. P/M Parts, *Powder Metallurgy International*, vol.3, no.3, 1971, pp.123-126.
89. Watanabe, T., and Yamada, K., Effects of Copper Adding Methods on the Strength of Sintered Aluminium-Copper Alloys., *Report of the Castings Research Laboratory*, Waseda University, no.19, 1968.
90. Savitskii, A.P., Burtsev, N.N., and Martsunova, L.S. Volume Changes Experienced by Al-Zn Compacts During Liquid Phase Sintering, *Theory and Technology of Sintering, Thermal, and Chemicothermal Treatment Processes*, 1983, pp.760-764.
91. Muhlburger, M., and Paschen, P., Flussigphasensintern von AlZnMgCu Legierungen (Liquid Phase Sintering of AlZnMgCu Alloys), *Zeitschrift fur Metallkunde*, vol.84, no.5, 1993, pp.346-350.
92. Amato, I., Corso, S., and Sgambettera, E. Sintering Procedures for Aluminium P.M Parts and Metallographic Examination During the Process, *Powder Metallurgy*, no.3, 1976, pp.171-175.
93. Kempf, L.W., Properties of Compressed and Heated Aluminium Alloy Powder Mixtures, *Powder Metallurgy*, Conference Proceedings of the 1940 and 1941 Conferences on Powder Metallurgy, J. Wulff (ed.), ASM, 1942, pp.314-316.
94. Vassilew, V., Mitin, B., Serow, M., and Bach, H., Microstructural Transformations in an Al-5Cu Alloy During Liquid Phase Sintering., *Zeitschrift Fur Metallkunde*, Vol.80, #10, 1989 pp.745-748.

95. Davis, S.J., Miodownik, A.P., and Watts, J.F., Degassing and Surface Analysis of Gas Atomised Alloy Powders, *Journal of Materials Science.*, 30, 1995, pp.3811-3819.
96. Danninger, H., Sintered Aluminium Camshaft Belt Pulleys, *Metal Powder Report*, June 1993, pp.46-52.
97. Miura, S., Machida, Y., Hirose, Y., and Yoshimura, R., The Effects of Varied Alloying Methods on the Properties of Sintered Aluminium Alloys, *Proceedings of the 1993 Powder Metallurgy World Congress*, Japan Society of Powder and Powder Metallurgy, 1993, pp.571-574.
98. Kehl, W., and Fischmeister, H.F., Liquid Phase Sintering of Al-Cu Compacts, *Powder Metallurgy*, #3, 1980, pp.113-119.
99. Griffith, W.M., Kim, Y.W., and Froes, F.H., Powder Metallurgy Processing of Aluminium Alloy 7091, *Rapidly Solidified Aluminium Alloys*, M.E. Fine and E.A. Starke, eds., ASTM, 1986, pp.283-303.
100. Aichen, T., A Study of the Air Sintering of Aluminium Powder and its Mechanism, *Journal of Central South, Institute of Mining and Metallurgy*, #8, Sept. 1988, pp.127-132.
101. Foss, J.E., DeFranco, D., The Northstar Cam Bearing Caps: A New Application for Aluminium P.M, SAE Technical Paper Series, International Congress and Exposition, 1994, #940429
102. Shibli, I.A., and Davies, D.E., Effect of Oxidation on Sintering Characteristics of Aluminium Powder and Effect of Some Minor Metallic Additions., *Powder Metallurgy*, Vol.30, #2, pp.97-101.
103. Nakao, Y., Sugaya, K., Seya, S., and Sakima, T., Process for Producing Aluminium Sintering, *United States Patent #5525292*, 1996.
104. Estrada, J.L., Duszcyk, J., and Korevarr, B.M., Gas Entrapment and Evolution in Prealloyed Aluminium Powders, *Journal of Materials Science*, 26, 1991, pp1431-1442.
105. Munir, Z.A., Surface Oxides and Sintering of Metals, *Powder Metallurgy*, 1981, #4, pp.177-180.
106. Dudas, J.H, Stevens, R.H., and Gildersleeve, B.K., Metallography and Structure Interpretation of Aluminium P/M Parts, *The International Journal of Powder Metallurgy and Powder Technology*, Vol.10, #4, 1994, pp.285-293.
107. Jha, A.K., Prasad, S.V., and Upadhyaya, G.S., Mechanical Behaviour of Sintered 6061 Aluminium Alloy and its Composites Containing Soft or Hard Particles, *Zeitschrift Fur Metallkunde*, Vol.81., 1990, pp.457-462.
108. Jha, A.K. and Upadhyaya, G.S., Properties of Sintered 2014 Aluminium Composite Containing WC, *Journal of Materials Science Letters*, Vol.2, 1983, pp.801-804.
109. Borhani, G.H., Srivastava, V.K., Pathak, J.P., and Ramachandra, C., Properties of Commercial Aluminium-Mica Composites Prepared By P/M Route, *Powder Metallurgy*, Vol.36, #1, 1993, pp.67-70.

110. Laffin, C.L., and Lopez, H.F, Compacting and Sinterability of Aluminium-Copper-Graphite Powder Mixtures, *Advances in Powder Metallurgy*, Vol.6, Proceeding of the 1991 Powder Metallurgy Conference and Exhibition, pp.227-235.
111. Dwyer, J., and Nayar, H., Comparative Studies of P/M Lubricants Under Different Atmospheres Using TGA Techniques, *Advances in Powder Metallurgy*, vol.1., Metal Powder Industries Federation, Princeton, N.J, 1990.
112. Goetzel, C.G, *Treatise on Powder Metallurgy, Technology of Metal Powders and Their Products*, vol.1., Interscience, New York 1949.
113. Kehl, W., Bugajska, M., and Fischmeister, H.F., Internal or Die Wall Lubrication For Compaction of Al Powders ?, *Powder Metallurgy*, Vol.26, #4, 1983, pp.221-227.
114. Abou El Khair, M.S., Taha, M., El-Mahallaway, N., Mazen, A.A., and Moussa, I., Cold Compaction of Al-Zn Powder Composite Materials, *Key Engineering Materials, Metal Matrix Composites*, Vol.79-80, 1993, pp.165-174.
115. Renowden, M., and Pourtalet, P., Experimental Studies on Lubricant Removal, *Advances in Powder Metallurgy*, vol.1., Proceedings of the 1990 Powder Metallurgy Conference, Pittsburgh, Pennsylvania, Metal Powder Industries Federation, Princeton, N.J., 1990, pp.261-278.
116. Merck Reagents, *Drying in the Laboratory*, Darmstadt, Federal Republic of Germany, pp.39-43.
117. Metallic Materials-Rockwell Hardness Test, *Australian Standard AS1815-1991*, Published by Standards Australia.
118. Powder Diffraction File, 1996, PDF-2 Database Sets 1-46, Vol. PDF2-46, Dataware Technologies Inc., International Centre for Diffraction Data, Pennsylvania, USA.
119. Villars, P., Prince, A., and Okamoto, H., *Handbook of Ternary Alloy Phase Diagrams*, Vol.4, Al-Ge-Ga to Au-Te-Tl, ASM International, 1995.
120. Smithells Metals Reference Book, Seventh Edition, E.A. Brandes and G.B. Brook eds., Butterworth Heinemann, Oxford, UK., 11-35, 11-51, 11-57, 11.229, 1992.
121. Nagl, M.M., and Evans, W.T., Review: The Mechanical Failure of Oxide Scales Under Tensile or Compressive Load, *Journal of Materials Science*, 28, 1993, pp.6247-6260.
122. Lide (ed.), *CRC Handbook of Chemistry and Physics*, 75th ed. CRC Press, Inc. (1995).
123. Sercombe, T.B., PhD thesis, University of Queensland, 1998.
124. Budnikov, P.P, and Ginstling, A.M., *Principles of Solid State Chemistry, Reactions in Solids*, Translated by Kenneth Shaw, Maclaren and Sons Ltd, London, 1968.

125. Levi, C.G., Abbaschian, G.J., and Mehrabian, R., Interface Interactions During Fabrication of Aluminium Alloy-Alumina Fiber Composites, *Metallurgical Transactions A*, Vol.9A, May 1978, pp.697-711.
126. Scamans, G.M., and Butler, E.P., In-Situ Observations of Crystalline Oxide Formation During Aluminium and Aluminium Alloy Oxidation, *Metallurgical Transactions A*, Vol.6A, Nov.1975, pp.2055-2063.
127. Kim, D.H, Yoon, E.P., and Kim, J.S., Oxidation of an Aluminium-0.4wt% Magnesium Alloy., *Journal of Materials Science Letters*, 15, 1996, pp.1429-1431.
128. Breval, E., Aghajanian, M.K., and Luszcz, S.J., Microstructure and Composition of Alumina/Aluminium Composites Made By Directed Oxidation of Aluminium., *Journal of the American Ceramic Society*, 73, 9, 1990, pp.2610-2614.
129. Molins, R., Bartout, J.D, and Bienvenu, Y., Microstructural and Analytical Characterisation of Al₂O₃-(Al-Mg) Composite Interfaces. *Materials Science and Engineering*, A135, 1991, pp.111-117.
130. Homeny, J., and Buckley, M.M., Transmission Electron Microscopy Study of an Aluminium Oxide Fiber / Aluminium Magnesium Alloy Metal Matrix Composite Interface., *Materials Letters*, Vol.10, #9, 10, 1991, p.421.
131. Munitz, A, Metzger, M., and Mehrabian, R., The Interface Phase in Al-Mg / Al₂O₃ Composites, *Metallurgical Transactions A*, Vol.10A, Oct.1979, pp.1491-1497.
132. McLeod, A.D., and Gabryel, C.M., Kinetics of the Growth of Spinel, MgAl₂O₄ on Alumina Particulate in Aluminium Alloys Containing Mg, *Metallurgical Transactions A*, Vol.23A, April 1992, pp.1279-1283.
133. Lea, C., and Molinari, C., Magnesium Diffusion, Surface Segregation and Oxidation in Al-Mg Alloys, *Journal of Materials Science*, 19, 1984, pp.2336-2352.
134. Kovacs, I., Lendvai, J., and Ungar, T., Investigation of Magnesium Loss During Heat Treatments in an Al-Mg-Si Alloy, *Materials Science and Engineering*, 21, 1975, p.169.
135. Mc Gurran, B., and Nicholas, M.G., A Study of Aluminium Brazes Using Hot Stage Scanning Electron Microscopy, *Journal of Materials Science*, 19, 1984, pp. 2713-2718.
136. Winterbottom, W.L., Process Control Criteria for Brazing Aluminium Under Vacuum, *Welding Journal*, 63, #10, Oct.1984, pp.33-39.
137. Terril, J.R., Cochran, C.N., Stokes, J.J., and Haupin, W.E., Understanding the Mechanisms of Aluminium Brazing, *Welding Journal*, Vol.50, 1971, pp.833-838.
138. Kobashi, M., Kumo, S., Choh, T., and Shimizu, T., The Effect of Surface Active Elements on the Wetting Behaviour of Iron by Molten Aluminium Alloy, *ISIJ International*, Vol.35, #5, 1995, pp.488-493.

139. Mehrer (ed.), *Landolt-Bornstein Numerical Data and Functional Relationships in Science and Technology*, Vol.3, 26, 1991.
140. Carceres, C.H., and Selling, B.I., Casting Defects and the Tensile Properties of an Al-Si-Mg Alloy, *Materials Science and Engineering A220*, 1996, pp.109-116.
141. Huppman, W.J., The Elementary Mechanisms of Liquid Phase Sintering, II Solution-Reprecipitation, *Zeitschrift fur Metallkunde*, #70, 1979, pp.792-797.
142. Ambrose, J.C., and Nicholas, M.G., Wetting and Spreading of Nickel Phosphorus Brazes: Detailed Real-Time Observations of Spreading in Iron-Chromium Substrates, *Materials Science and Technology*, June, 1996, Vol.12, pp.72-80.
143. Mc Alister, A.J., and Kahan, D.J., The Al-Sn (Aluminium-Tin) System, *Bulletin of Alloy Phase Diagrams*, 4,4, 1983, pp.410-414.
144. Liu, Y., Tandon, R., and German, R.M., Modelling of Supersolidus Liquid Phase Sintering: Part 1 Capillary Force, *Metallurgical and Materials Transactions A.*, Vol.26A, 1995, pp.2415-2422.
145. Liu, Y., Tandon, R., and German, R.M., Modelling of Supersolidus Liquid Phase Sintering: Part 2, Densification, *Metallurgical and Materials Transactions A.*, Vol.26A, 1995, pp.2423-2430.
146. D.C Giancoli, *General Physics*, Prentice Hall International, Englewood Cliffs, New Jersey, 1984.
147. Smithells, C.J., *Smithells Reference Book*, 7th ed., E.A. Brandes and G.B. Brook eds., Butterworth-Heinemann Ltd., 1992.
148. Courtney, T.H., Gravitational Effects on Microstructural Development in Liquid Phase Sintered Materials, *Scripta Materialia* 35, 1996, pp.567-571.
149. Mondolfo, L.F., Gjostein, N.A., and Lovinson, D.W., Structural Changes in an Al-Mg-Zn Alloy, *Journal of Metals*, Transactions AIME, Oct. 1956, pp. 1378-1385.
150. Lea, C., Muddle, B.C., and Edmonds, D.V., Segregation to Interphase Boundaries in Liquid Phase Sintered Tungsten Alloys, *Metallurgical Transactions A*, Vol.14A, 1983, pp.667-677.
151. Courtney, T.H. and Lee J.K., An Analysis For Estimating the Probability of Particle Coalescence in Liquid Phase Sintering Systems, *Metallurgical Transactions A*, Vol.11A, 1980, pp.943-947.
152. Takajo, S., Kaysser, W.A., and Petzow, G., Particle Growth by Coalescence During Liquid Phase Sintering of Fe-Cu, *Acta Metallurgica*, Vol.32, 1984, 115-122.
153. Kaysser, W.A, Takajo, S., and Petzow, G., Low Energy Grain Boundaries in Liquid Phase Sintered Cu-Ag, *Zeitschrift fur Metallkunde*, 1982, 73, 579-580.
154. Couper, M.J., Nauer, M., Baumann, R., and Singer, R.F., On the Break-Up and Redistribution of Oxides Following Powder Degassing and Consolidation of Elevated Temperature PM-Aluminium Alloys, in: "*PM Aerospace Materials*",

Proceedings International Conference on PM Aerospace Materials, MPR,
Lucerne, 1987, pp.1-10.